EXPERIMENTAL STUDY, MODELLING AND CONTROLLER DESIGN FOR AN RCCI ENGINE

By

Naga Nithin Teja Kondipati

A THESIS

Submitted in partial fulfillment of the requirements for the degree of

MASTER OF SCIENCE

In Mechanical Engineering - Engineering Mechanics

MICHIGAN TECHNOLOGICAL UNIVERSITY

2016

This thesis has been approved in partial fulfillment of the requirements for the Degree of MASTER OF SCIENCE in Mechanical Engineering - Engineering Mechanics.

Department of Mechanical Engineering - Engineering Mechanics

Thesis Advisor: *Dr. Mahdi Shahbakhti*

Committee Member: *Dr. Bo Chen*

Committee Member: *Dr. David D. Wanless*

Department Chair: *Dr. William Predebon*

Dedication

To my loving parents, brother and my awesome friends

who didn't hesitate to criticize my work at every stage - without which I would neither be who I am nor would this work be what it is today.

Contents

List of Figures

List of Tables

Acknowledgments

Firstly, I would like to thank my family who always encouraged and supported me from the starting with my decision of pursuing MS in US. I also thank them for supporting me mentally in times of distress and boosting me with confidence.

Next, I am heartily thankful to my advisor, Dr. Mahdi Shahbakhti , for joining me in his EML engine research team and giving me an opportunity to work on modeling and control of advanced combustion engines. I also thank him for providing an opportunity to work in the Ford project which further enhanced my knowledge on modeling.

I am also thankful to Dr. Bo Chen and Dr. David D. Wanless for accepting to be part of my defense committee members.

I want to thank Dr. Mehran Bidarvatan for introducing me to this project and also for his constant support and guidance in developing dynamic control model for this engine.

I also want to acknowledge my friends Jayant Kumar Arora, Kaushik Kannan and my colleague Dr. Hamit Solmaz for their support and contribution in collecting experimental data for this work.

Last but not the least, I want to thank my roommates at 2007F (Mahi,Sachin,Ippili) and 2002C (Pandavas) at MTU, Bachelor friends from RGUKT (Bharu,Sudheer,Vineel,Naveen and others) and school mates from JNV (Anil,Navya,Ram and Mouni) who regularly provided entertainment, motivation and helped me in overcoming the hurdles to successfully complete this thesis.

List of Abbreviations

Acronyms

aBDC	After Bottom Dead Center
aTDC	After Top Dead Center
BD	Burn Duration
BMEP	Break Mean Effective Pressure
BSFC	Break Specific Fuel Consumption
bTDC	before Top Dead Center
BTE	Break Thermal Efficiency
CA50	Crank Angle at which 50% fuel is burnt
CA10	Crank Angle at which 10% fuel is burnt
CAD	Crank Angle Degree
CDC	Conventional Diesel Combustion
CFD	Computational Fluid Dynamics
CN	Cetane Number
CI	Compression Ignition
CO	Carbon Monoxide
COM	Control Oriented Model
COV	Coefficient of Variation
DI	Direct Injection

DPF	Diesel Particulate Filter
EGR	Exhaust Gas Recirculation
EGT	Exhaust Gas Temperature
EML	Energy Mechatronics Lab
EPA	Environment Protection Agency
EOC	End of combustion
EVC	Exhaust Valve Closing
EVO	Exhaust Valve Opening
FMEP	Friction Mean Effective Pressure
FPGA	Field Programmable Gate Array
GDI	Gasoline Direct Injection
GHG	Green House Gases
HC	Hydro Carbon
HCCI	Homogeneous Charge Compression Ignition
HEV	Hybrid Electric Vehicle
HRR	Heat Release Rate
HTHR	High Temperature Heat Release
ICEs	Internal Combustion Engines
ID	Ignition Delay
IMEP	Indicated Mean Effective Pressure
IP	Indicated Power

ISFC	Indicated Specific Fuel Consumption
ITE	Indicated Thermal Efficiency
IVC	Inlet Valve Closing
IVO	Inlet Valve Opening
LCOM	Linear Control Oriented Model
LHV	Lower Heating Value
LNT	Lean NOx Traps
LTHR	Low Temperature Heat Release
LTC	Low Temperature Combustion
MABx	Micro Autobox
MAP	Manifold Absolute pressure
MFB	Mass Fraction Burnt
MIMO	Multi-input Multi-output
MKIM	Modified Knock Integral Model
MPRR	Maximum Pressure Rise Rate
MSE	Mean Square Error
MVM	Mean Value Model
NCOM	Nonlinear Control Oriented Model
NHTSA	National Highway Traffic Safety Administration
PCCI	Premixed Charge Compression Ignition
PFI	Port Fuel Injector

PI	Proportional Integral
PID	Proportional Integral Derivative
PM	Particulate Matter
PPCI	Partially Premixed Compression Ignition
PPRR	Peak Pressure Rise Rate
PR	Premixed ratio
PRF	Primary Reference Fuel
PSI	Pounds Per square Inch
RCCI	Reactivity Controlled Compression Ignition
RGF	Residual Gas Fraction
RPM	Revolutions Per Minute
SCR	Selective Catalytic Reduction
SOI	Start of Injection
SOC	Start of Combustion
SI	Spark Ignition
SISO	Single Input Single Output
TDC	Top Dead Centre
VVA	Variable Valve Actuation

Symbols

a	Crank radius(mm) in Chapter2
A_c	Surface area of in-cylinder(m^2)

AFR	Air Fuel Ratio (-)
B	Bore diameter(mm)
c_v	Specific heat capacity at constant volume ($\frac{kJ}{kg.K}$)
CA50	Crank angle for 50% fuel burnt (CAD aTDC)
cyc	cycle
ΔT	Temperature Increase due to the Combustion Process (K)
η	Efficiency (%)
F/A	Fuel-Air Ratio
$FMEP$	Friction Mean Effective Pressure (kPa)
h_c	Convective heat transfer coefficient ($\frac{W}{m^2K}$)
K_i	Integral control gain in PI control
k_p	Gain of thermocouple
K_p	Proportional Control Gain in PI Control
l	Length of connecting rod(mm)
λ	AFR over stoichiometric AFR (-)
LHV	Low Heating Value (kJ/kg)
m	Mass (g)
N	Engine speed (rpm)
n	Polytropic coefficient(-)
ON	Octane Number (-)
P_{in}	Intake pressure (kPa)

P_{max}	Maximum peak pressure(kPa)
P_{mot}	Motoring pressure(kPa)
p	Pressure (kPa)
ϕ	Fuel equivalence ratio (-)
Q	Amount of energy released(kJ)
Q_w	Heat loss from in-cylinder gas to surrounding walls (kJ)
r_c	Compression ratio(-)
R	Gas constant ($\frac{kJ}{kgK}$)
RGF	Residual Gas Fraction (-)
RPM	Revolutions Per Minute(-)
σ	Standard deviation
S_p	Mean piston speed(m/s)
SOC	Start Of Combustion Moment (CAD aTDC)
SOI	Start of Injection (CAD bTDC)
T	In-cylinder temperature(K) at every CAD
T_{in}	Intake temperature (^oC)
T_g	In-cylinder gas temperature(K)
T_w	Surrounding wall temperature(K)
t	Time (sec)
τ	Time Constant (sec)
θ	Crank Angle (°)

V	Volume (m^3)
V_d	Clearance volume(m^3)
V_d	Engine displacement volume (m^3)
W	Work (kJ)
x_b	Mass fraction burnt(-)
X_{rg}	Residual gas fraction (-)

Subscripts

a	Air
ave	Average
c	Compression
$comb$	Combustion
d	Displacement but duration in Chapter4
DI	Direct injection
e	Expansion
eoc (or) EOC	End of Combustion
evc	Exhaust Valve Closure
evo	Exhaust Valve Opening
exh	Exhaust Gas
$fuel$	Fuel
ht	Heat Transfer
i	Engine cycle Index

ig	Ignition
in	intake
iso	iso-octane
ivc	Intake Valve Closing
ivo	Intake Valve Opening
k	Ratio of specific heats in Chapter5
m	Manifold
mix	Mixture
$nhep$	n-heptane
PFI	Port-fuel injection
r	Residual
rg	Residual Gas
soc (or) SOC	Start of Combustion
st	Stoichiometric
t	Total
$therm, ind$	Indicated thermal
w	Cylinder walls

Abstract

Low Temperature Combustion (LTC) has got widespread attention over the past two decades in the field of Automotive Research and Development due to it's potential for achieving higher efficiencies with near-zero engine out NOx and soot emissions. Among all the LTC strategies Reactivity controlled compression ignition (RCCI) has shown the most promising results due to it's precise control over combustion phasing and heat release rate. However, RCCI being a dual-fuel stratified combustion, precise control over the injection timing of direct injected fuel and in-cylinder fuel reactivity of the mixture needs to be controlled effectively in order to achieve gross indicated thermal efficiencies as high as around 60% [1].

This thesis focuses on developing real-time, model-based controller for controlling combustion phasing of an RCCI Engine. Optimum combustion phasing can be achieved by varying mixture reactivity and injection timing of higher reactive fuel. An experimental study was performed to study the effects of these variables on combustion phasing. Next,a mean-value and dynamic control-oriented model (COM) was developed to predict combustion phasing during steady-state and transient operating conditions. The validation results have shown that the COM was able to capture the experimental trends with minimal error. Next, for implementing in real time, a PI controller was developed using the COM to track the desired combustion phasing by adjusting duel-fuel premixed ratio and start of injection timing. The PI controller is then implemented on the engine plant. The validation results proved that the designed controller can follow the desired combustion phasing with an average error of 2 crank angle degrees and rise time of 3 engine cycles.

Chapter 1

Introduction

In 2012, the United States (US) President Barack Obama and his administration finalized the announcement made in 2011 that by the Model Year 2025 average fuel economy of 54.5 miles per gallon(mpg) should be achieved for every passenger car and light-duty truck from the current average fuel economy of 35.5 mpg [2]. In addition to this, the US Environment Protection Agency (EPA) along with the US Department of Transportation's National Highway Traffic Safety Administration (NHTSA) has set emission regulations to cut 6 billion metric tons of Green House Gases (GHG) over the life-span of the vehicles sold in model years 2012-2025. In order to achieve 54.5 mpg they projected to reduce CO_2 emissions from current 243 g/mi to 163 g/mi for combined cars and trucks by 2025 [3]. Currently all the major automakers are striving for developing innovative technologies to increase the fuel economy and also reduce emissions to meet these standards.

Internal Combustion Engines(ICE's) have experienced a remarkable evolution with the improvement in latest technologies, sensors and onboard computing power over the past few years [4]. Industries and research laboratories are continuously working towards increasing the efficiency of the ICE's to compensate for fuel price and increasing consumption of fossil fuels. It is well known that diesel engines always provide higher efficiency than it's counterpart SI engines due to their higher compression ratios and throttle-less operation. They are also widely used for transportation and power generation applications. Due to higher intake percentage of air and high in-cylinder temperatures, most of the hydrocarbons present in the fuel get oxidized to CO_2 and H_2O. But due to it's heterogeneous combustion of air/fuel mixture and high local in-cylinder temperatures, diesel engines have higher output of NOx and particulate matter(PM) which are harmful for the environment and human health [5]. In order to reduce these emissions they require complex and costly exhaust aftertreatment systems. Diesel particulate filters (DPFs) can be used for trapping PM, but they require frequent active or passive regeneration in order to oxidize the trapped PM [6] . Active regeneration needs some extra fuel to be injected either into the exhaust or into the cylinder. Selective Catalytic Reduction (SCR) systems and Lean NOx traps (LNTs) are the main devices for reducing NOx emissions. SCR systems require a reducing agent like ammonia or urea in order to reduce NOx emissions and release them into the atmosphere as N_2. However in an SCR system a secondary fuel is being consumed in order to reduce NOx and at the same time urea is also

an expensive fuel. This system also adds burden to the vehicle as it needs separate storage system. Even though SCR is currently being used for heavy duty vehicles to control emissions, it faces problems with cold start and idling operation of engine. This is due to their dependency on temperatures where they work effectively only after 300°C [6]. Similarly, LNTs trap the exhaust NOx to be stored on a catalyst surface and during the period of rich engine operation the stored NOx get reduced to N_2. Even though these systems can effectively reduce the NOx, they require precious metal adsorbent which makes them expensive and requires extra usage of fuel at frequent periods [6, 7].

1.1 Motivation towards LTC Engines

As mentioned above, after-treatment systems are getting complex and expensive to extract the advantage of high efficiency from the diesel engines, the engine research community has focused on in-cylinder technologies to improve the fuel economy and reduce the emissions. The main goal is to identify a technology that would provide both high efficiency and also reduce the NOx and PM emissions. Advanced combustion techniques like increased injection pressure, charge dilution with exhaust-gas recirculation (EGR), modified piston-bowl geometries have been implemented but they still require exhaust after-treatment systems. So combustion development researchers have concentrated on alternative strategies of CI combustion. This has led

to in depth investigation on reducing flame temperatures in order to reduce NOx and operate in leaner equivalence ratios to avoid PM which finally showed a path towards Low-temperature Combustion (LTC) phenomenon.

All the LTC engines have common techniques of premixing the part of the fuel with air and making it homogeneous before entering the in-cylinder. This has resulted in achieving low combustion temperatures and long ignition delay. Reduction in flame temperatures inhibits the NOx production as it needs higher activation energy to promote NO formation reactions [8] and also provide diesel like efficiencies due to reduced heat transfer losses. Also longer ignition delay can be utilized to avoid rich regions inside the combustion chamber since more time will be available for the fuel to combine with air. This reduces PM emissions. Ignition delay can be further delayed with increasing dilution, either by increasing intake pressure or by EGR. This will further reduce peak temperatures which helps in reducing NOx formation and also reduce PM due to reduction in peak equivalence ratios [9]. But with higher dilution, the mixture gets leaner and the exhaust temperature decreases which can impact the oxidation of HC and CO and thereby increasing their emissions and reduction in combustion efficiency . The probability for misfire also increases with dilution [10].

Different LTC strategies are classified depending on the degree of premixing of air-fuel charge before the intake and the control of charge stratification inside the cylinder. Fig. 1.1 shows the comparison between Conventional Diesel Combustion (CDC) and

different LTC strategies in terms of the operating regions with respect to local equivalence ratio and local charge temperature [10] and their respective emission zones.

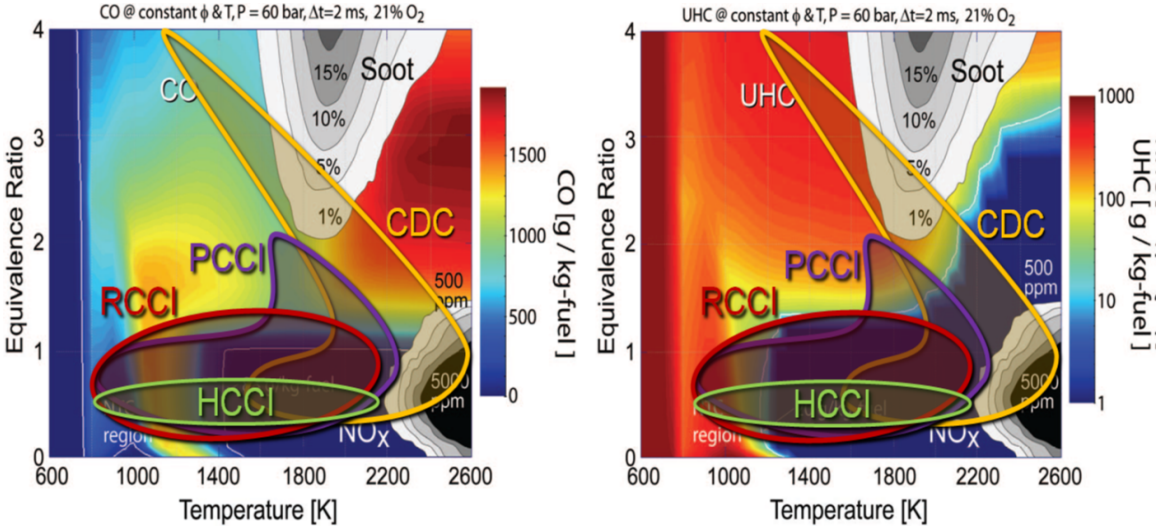

Figure 1.1: Contour plots showing soot, NOx, HC and CO emissions with overlaying different LTC regions [10].

It can be seen that CDC encounters both high local equivalence ratios and high local temperature zones which causes diesel combustion to produce both high soot and NOx emissions. Whereas on the other hand the LTC strategies, operate in the regions of low temperature ($1000 < T_{comb} < 2000$) and low equivalence regions ($0.5 < \phi < 1.5$) without encountering soot and NOx islands. However, it can be seen that they are falling in the regions of higher CO and HC concentrations. From the above observations it can be inferred that in order to meet the current emission standards, LTC strategies offer a good potential for reducing both NOx and PM emissions without complex aftertreatment systems. The operating regions can be controlled to maintain equivalence ratios closer to stoichiometric and in-cylinder temperatures to be in the range of 1400-2000K [10, 11]. This is why most of the current research studies

are being concentrated on developing these LTC strategies in order to achieve higher efficiencies with reduced NOx and PM emissions.

1.2 LTC Strategies

As said above, different LTC strategies are classified depending on the homogeneity of the mixture and stratification of charge inside the cylinder. Homogeneous Charge Compression Ignition (HCCI) is among the first studied LTC strategies. In HCCI, a combined homogeneous mixture of fuel and air is prepared before entering the cylinder and is compressed until auto ignition that results in volumetric heat release with a very short combustion duration. This has resulted in achieving higher efficiency and also ultra-low NOx and PM emissions. The shorter combustion duration and nearly constant-volume combustion has resulted in higher peak cylinder pressures and peak pressure rise rate (PPRR) which leads to knock. This limits HCCI to expand over high operating loads. The two major problems associated with HCCI are: (1) Lack of direct combustion phasing control similar to injection timing in diesel engines and spark timing in SI engines, and (2) Lack of control over heat release rate(HRR) as with fuel injection rate in diesel engines and turbulent flame propagation in SI engines [12]. Current research is concentrated on controlling the combustion phasing and also to increase the ignition delay while controlling HRR and PPRR. Various control strategies have been implemented such as control of combustion phasing [13,

14, 15], engine load [14, 16], exhaust gas temperature [19], multiple fuel injections [20], fuel stratification [21] in order to make HCCI operate over a wide range of speed and load.

In order to improve the control over combustion phasing and heat release rate, another strategy called Premixed Charge Compression Ignition (PCCI) which is a hybrid between HCCI and conventional diesel combustion has been proposed. This allows the coupling between the amount of fuel injected and combustion events. Ignition Delay (ID) can be increased by using excessive EGR rates, higher injection pressure and reducing compression ratios [12]. This strategy is also referred to as Partially Premixed Compression Ignition (PPCI) if the direct injection of fuel happens late in the compression stroke which prepares a partially premixed mixture of fuel and air. Kalghatgi et al. [22] conducted experiments using both diesel and gasoline for various Start of Injection (SOI) timings, EGR rates and loads. They observed that gasoline provided lower PM emissions than diesel at all SOIs. Also, they introduced the concept of duel fuel injection i.e., early pilot injection and retarded main injection. With this duel injection of gasoline, higher loads upto 17 bar IMEP were achieved with an extra advantage of control over combustion phasing through SOI. Later, researchers from Lund University [23, 24] found that even though diesel PPC can overcome the NOx-soot regions, they require higher EGR rates. Due to diesel's high boiling point or low volatility, early injections are quite challenging with larger quantities of fuel.

Gasoline PPC studies were done by Dempsey [7] and found that even though ID of gasoline allowed control over combustion event but the richness of the mixture made NOx emissions to be higher. Also, combustion efficiency was depleted at low load conditions. Later slowly as time passed by, researchers started investigating LTC strategies using different fuel blends such as n-butane and a blend of n-heptane and iso-octane; indolene and n-heptane etc. Bessonette et al. [25] has found that the best fuel for HCCI operation may have auto-ignition qualities between those of diesel fuel and gasoline. Gasoline's resistance to auto-ignition can be utilized for getting more ignition delay but at low load it can difficult to achieve combustion. In contrary, diesel has better auto-ignition properties, but requires high levels of EGR to get required combustion phasing at higher loads. Kokjohn et al. [26] has performed computational studies on HCCI combustion with different PRF(Primary reference fuels consisting of mixture of diesel and gasoline) blends. They observed that in order to operate at higher loads, the fuel reactivity i.e. cetane number of the mixture need to decreased in order to phase the combustion properly to get higher thermal efficiency. Similarly, Inagaki et al. [27] investigated the effect of varying fuel reactivity in PCCI combustion by using two separate injections of iso-octane through port fuel and direct injection of n-heptane fuel around 40°BTDC. With this operation, they could able to broaden their operating range(2-12 bar IMEP) by controlling the mixing ratio between n-heptane and iso-octane. From the above observations, it can be seen that in order to expand the operating regions for LTC strategies different

fuel blends were required at different operating conditions i.e at higher loads a lower cetane number mixture is preferred and at lower loads a high cetane number mixture is required. So a strategy which requires port injection of low reactivity fuel and direct injection of a higher reactive fuel in order to vary the fuel reactivity. This strategy was named as Reactivity Controlled Compression Ignition(RCCI) by Kockjohn et al. [9]. Fig. 1.2 shows the timeline of different LTC strategies evolved with their advantages and limitations.

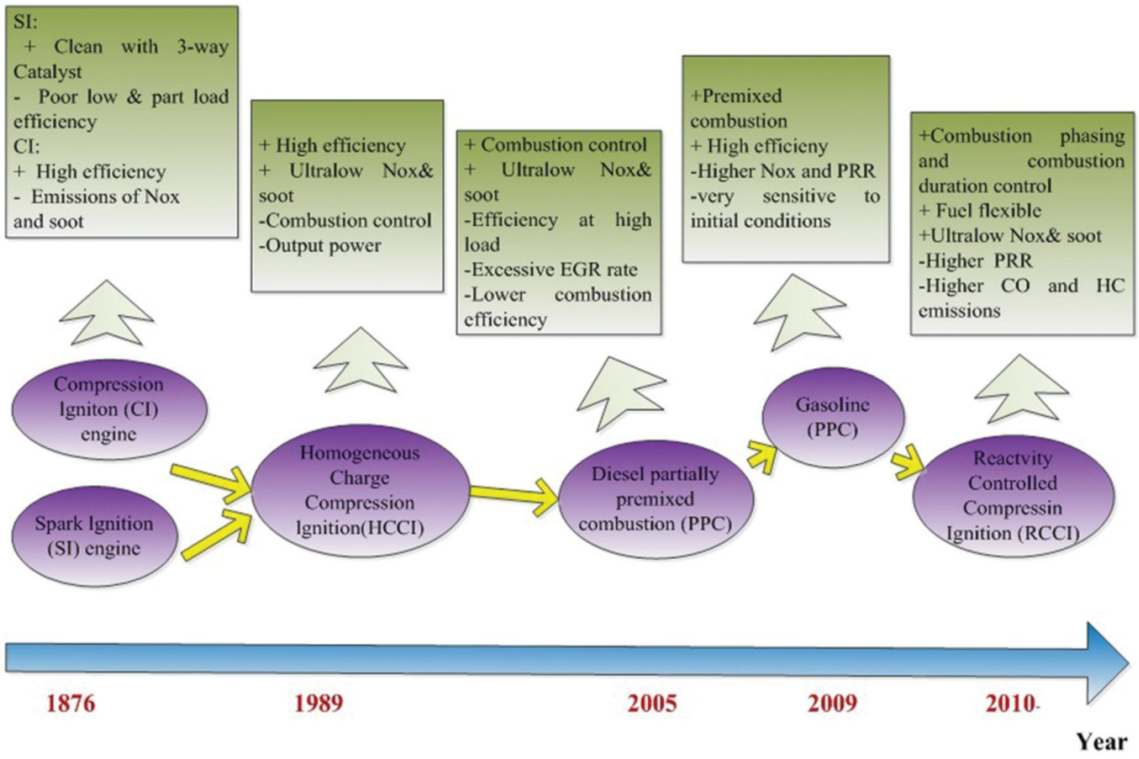

Figure 1.2: Timeline showing different LTC strategies and their advantages and limitations. [12]

RCCI is a dual fuel PCCI combustion which uses the concept of injecting low reactive

fuel(e.g.gasoline or iso-octane) through PFI coupled with single or multiple direct injections of high reactive fuel(e.g.diesel or n-heptane) to control the fuel reactivity and optimize the combustion phasing and duration. RCCI combustion has proved that it can provide better control over the combustion compared to other LTC strategies, HCCI and PCCI. It is also shown recently that RCCI has the capability of achieving 60% higher thermal efficiency [1].

RCCI has got the advantages both ϕ and reactivity stratification. It has been shown before [28, 29] that higher load operation and more advanced phasing in HCCI can be achieved with ϕ stratification of the mixture. But, later Kokjohn and Reitz [30] has observed the effect of introducing reactivity stratification alongwith ϕ stratification. It is seen that with introduction of fuel reactivity gradient there is a distribution of reactive zones in the mixture. The combustion starts earlier with auto-ignition of higher reactive zones. The energy release occurs in stages while the ignition propagates from high to low reactive zone thus extending the combustion duration. This also reduced the peak rise rates due to extended combustion duration. This effect is not seen when only ϕ stratification is considered, since shorter combustion durations has led to rapid PRR in HCCI combustion.

1.3 Research Studies in RCCI

There were many research studies undertaken to overcome the challenges in RCCI and make it possible to come into production. Since 2010, the research with focus towards RCCI has been continuously growing due to its potential advantages. Currently, University of Wisconsin-Madison Engine Research Centre (ERC), has been the main center of attraction for RCCI research among all the research groups in the world. All the current research studies in RCCI can be classified as shown below in Fig. 1.3

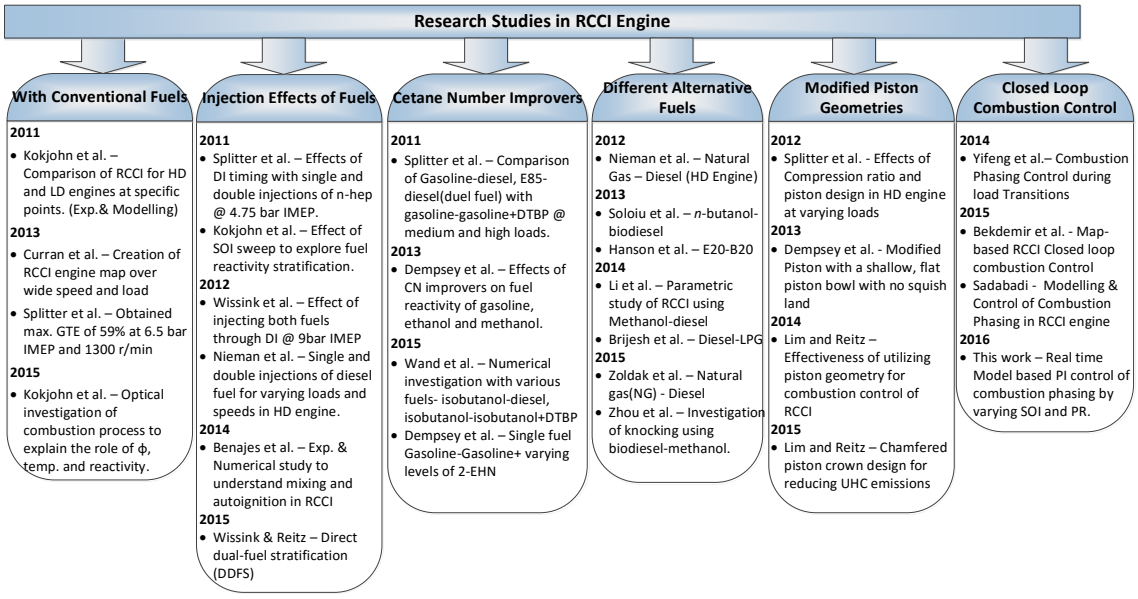

Figure 1.3: Current Research studies in RCCI Engine [1, 10, 12, 31, 32, 33, 34, 35, 36, 37, 38, 39, 40]

As shown in Fig. 1.3, there are very few studies available in the area of closed-loop combustion control of RCCI engines. In order to optimize the performance of RCCI

engines, the control over various engine inputs is required to maintain the engine in the desired operating region. Till now, all the electronic control unit's (ECUs) are embedded with calibration maps which are optimized for a fixed set of operating conditions to operate in open-loop control. These are becoming complex and expensive with increase in number of actuators, sensors for modern ICE's. Closed-loop combustion control has gained more preference over the open-loop for increasing the efficiency from the past few years. These systems use the information from available sensors as feedback to control the desired signals through actuators. Closed-loop combustion control has been used for controlling fuel blending ratio, combustion phasing, exhaust temperatures and load(IMEP) for HCCI combustion to extend the operating region for higher loads.

Model-based controllers have proved to be efficient in terms of computation and cost for controlling desired parameters. So, research has been focused on developing efficient control models to replace map based controllers with these model-based ones in production engines. From the literature study, recently a real time control-oriented model has been developed for controlling combustion phasing, IMEP and blend ratio by varying injection timing , diesel and gas quantities [41] in a Natural gas-Diesel RCCI combustion. They developed a mutli-zone CFD model to predict the combustion parameters and also validated with the experimental data. But, since CFD models are complex and difficult to implement in real time, they initially used map-based control model by generating a desired map using steady state operating

conditions. Apart from this, Yifeng and Reitz [40] investigated the effect of varying premixed ratio(PR) during transients to maintain constant combustion phasing while load-up and load-down transitions. They proposed that in order to maintain constant combustion phasing, PR should be decreased while increasing the load and increase the PR during load-down transition.

Now, this work focuses on controlling inputs premixed ratio of diesel and gasoline and injection timing of the direct injected fuel. In order to achieve higher efficiency, combustion phasing should be controlled to the optimum value by varying these two input parameters.

1.4 Research scope and Thesis Organization

The main objective of this work is to develop a mean value model which can predict RCCI combustion phasing parameters i.e. start of combustion (SOC) and crank angle of 50% fuel burnt (CA50), during both steady-state and transient operating conditions. Then the mean-value model is extended to a dynamic plant model for cycle-by-cycle control of RCCI combustion. After validating the plant model, in order to control the combustion phasing in real time, the physics-based dynamic model is used to design a PI controller to adjust PR and SOI timing to control CA50. The controller is then tested on real engine and compared the trends of both the model

and the engine . For implementing the controller in real time, Field-Programmable Gate Array(FPGA) is used along with dSPACE MicroAutoBox. The RCCI dynamic model from this thesis will be of utility to design advanced multi-input multi-output (MIMO) model-based controllers for RCCI engines. The whole structure of the thesis is shown in Fig. 1.4.

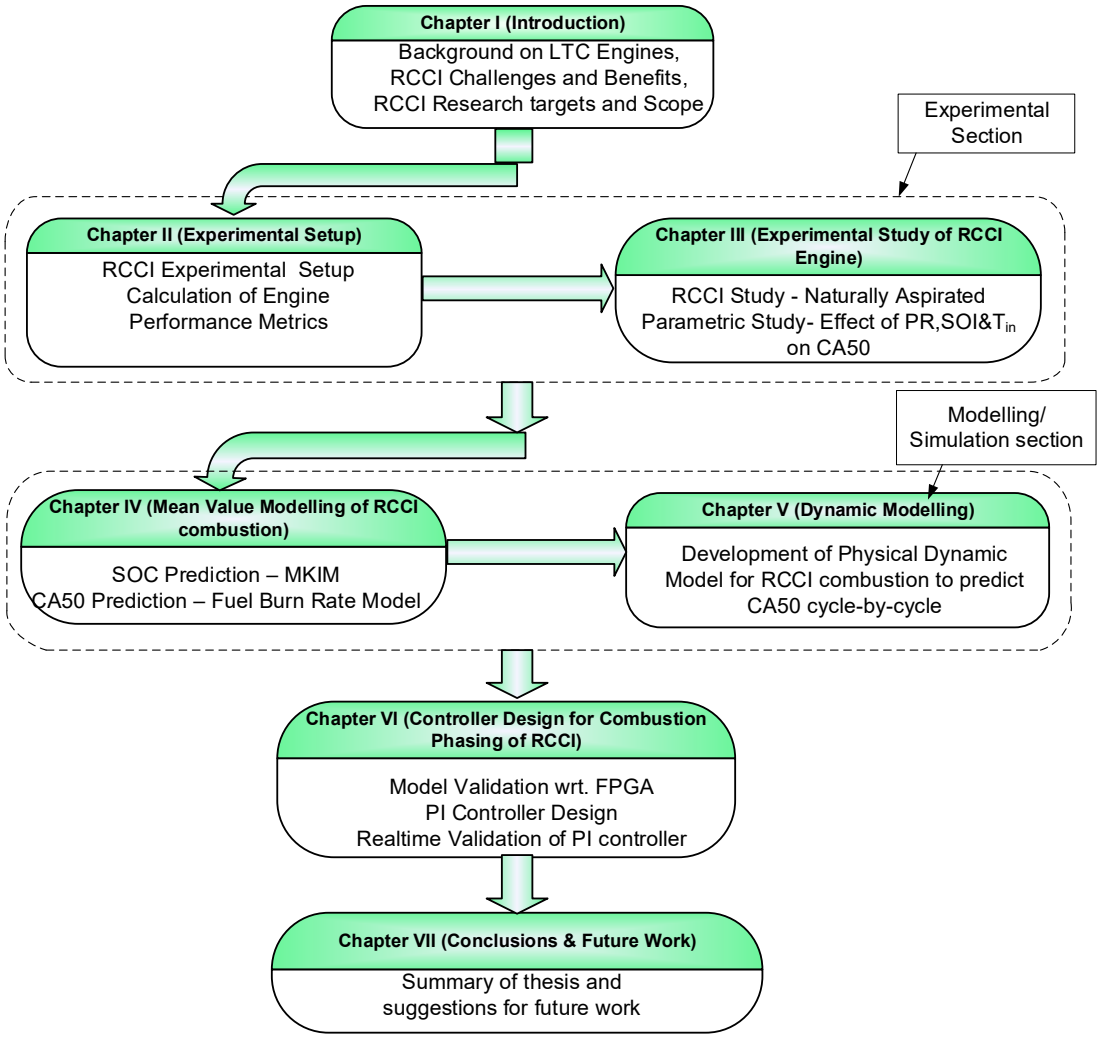

Figure 1.4: Schematic showing Thesis Organization

Chapter 2

Experimental Setup

The Energy Mechatronics Lab (EML) team at Advanced Power Systems and Research Center (APSRC) has been doing significant research on Low Temperature Combustion (LTC) engines in the past four years. Previous research studies [42, 43, 44, 45] were done mostly on Homogeneous Charge Compression Ignition (HCCI) and Premixed Charge Compression Ignition (PCCI). This thesis focuses on developing Reactivity Controlled Compression Ignition (RCCI) combustion strategy and it's performance over different engine speed and load. This chapter provides an overview to the engine setup, instrumentation and calculation of various performance metrics for RCCI combustion.

2.1 Engine Description

The base stock engine is a GM 2.0L Ecotec Turbocharged Gasoline Direct Injection(GDI) LHU Gen 1 engine which was taken from 2011 Buick Regal(vehicle). It was first modified and instrumented in order to run in HCCI mode. Later it was developed to operate in different modes of LTC such as PPCI and RCCI. Basic engine instrumentation, control setup and other contributions for the base engine can be found in previous theses [42, 43, 44, 45]. The schematic setup of the engine is shown in Figure 2.1

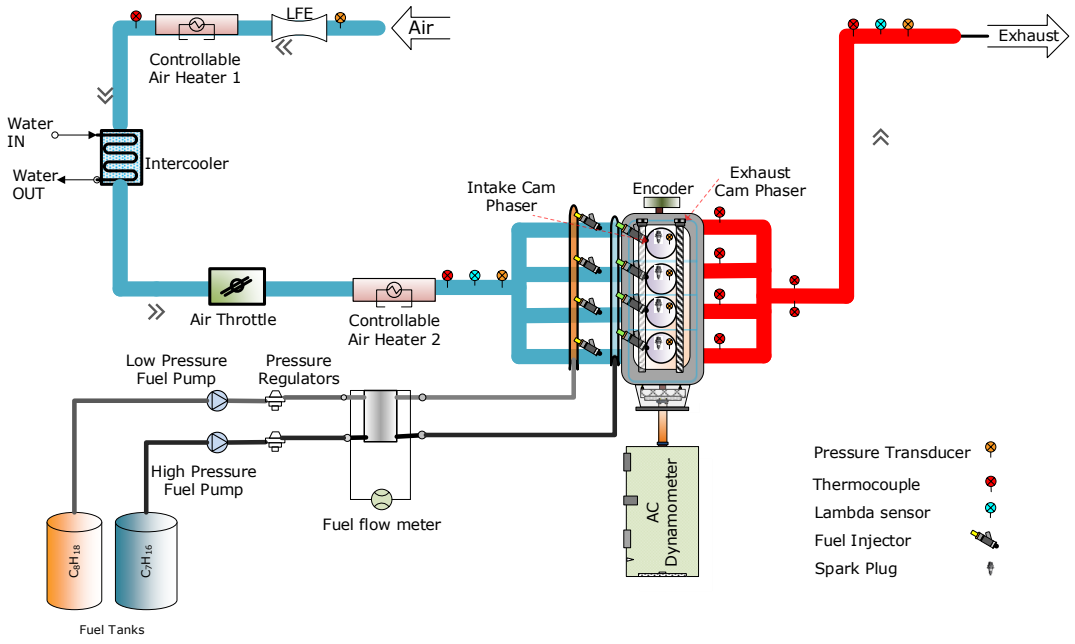

Figure 2.1: Schematic of the RCCI engine experimental setup

The specifications of the engine are mentioned in Table 2.1

Table 2.1
GM 2.0L Ecotec Engine specifications [42, 44]

Parameter [Unit]	**Value**
Bore [mm]	86
Stroke [mm]	86
Connecting rod length [mm]	145.5
Compression ratio [-]	9.2:1
Clearance volume [cc]	61
Displacement volume [cc]	1998
Max engine power [kW@rpm]	164 @ 5300
Max engine torque [Nm@rpm]	353 @ 2400
Firing order [-]	1-3-4-2
IVO [CAD bTDC]	25.5/-24.5
IVC [CAD bBDC]	2/-48
EVO [CAD bBDC]	36/-14
EVC [CAD bTDC]	22/-28
Valve Lift [mm]	10.3

2.2 Experimental Setup

As mentioned in Chapter 1, RCCI being a dual-fuel combustion strategy, it requires injection of two fuels. The two fuels selected for running RCCI experiments were iso-octane and n-heptane. These were chosen due to their extreme octane numbers(ON).i.e. iso-octane having ON-100 and n-heptane having ON-0. In this way, the reactivity of the combined fuel mixture can be controlled by varying the ratio of their injected quantities. The properties of both fuels are given below in Table 2.2.

Table 2.2
Chemical properties of iso-octane and n-heptane[46]

Parameter [Unit]	**iso-octane**	**n-heptane**
Octane number	100	0
Chemical formula	$C_{18}H_{18}$	C_7H_{16}
Molar mass [g/mol]	114.23	100.21
Density [kg/m^3]	692	695
Lower heating value [kJ/kg]	44310	44566

Iso-octane being less reactive is chosen to be injected from port fuel injection (PFI) rail in order to achieve more homogenized mixture. On the other hand, n-heptane being higher reactive is chosen to be injected from direct injection (DI) rail, so that the injection timing and also the reactivity of the mixture can be controlled easily. Previously, in order to achieve HCCI combustion the engine was equipped with two PFI rails. So for RCCI combustion, one of the rails was used for injecting iso-octane while n-heptane was injected using built-in DI rail. PFI rail pressure was kept constant at 3 bar while DI rail pressure can be varied using high pressure fuel pump. The individual fuel quantity to be injected from each rail is controlled using premixed ratio (PR). This ratio is defined as the amount of iso-octane energy present in the mixture containing both iso-octane and n-heptane. It is given by equation shown below.

$$PR = \frac{m_{iso}.LHV_{iso}}{m_{iso}.LHV_{iso} + m_{nhep}.LHV_{nhep}} \tag{2.1}$$

where LHV_{iso} and LHV_{nhep} are lower heating values of iso-octane and n-heptane respectively. m_{iso} and m_{nhep} denote the quantity of fuel injected for iso-octane and n-heptane respectively.

All the tests were carried out without exhaust gas recirculation (EGR). Also, the turbocharger was disabled since all the experiments were carried out at naturally aspirated conditions. The intake air was heated using controllable air heater which was controlled through LabVIEW interface to achieve desired intake temperatures. The engine was warmed up by running in S.I. mode using gasoline fuel and throttle position was controlled using dSPACE. The engine setup in the test cell is shown in Figure 2.2.

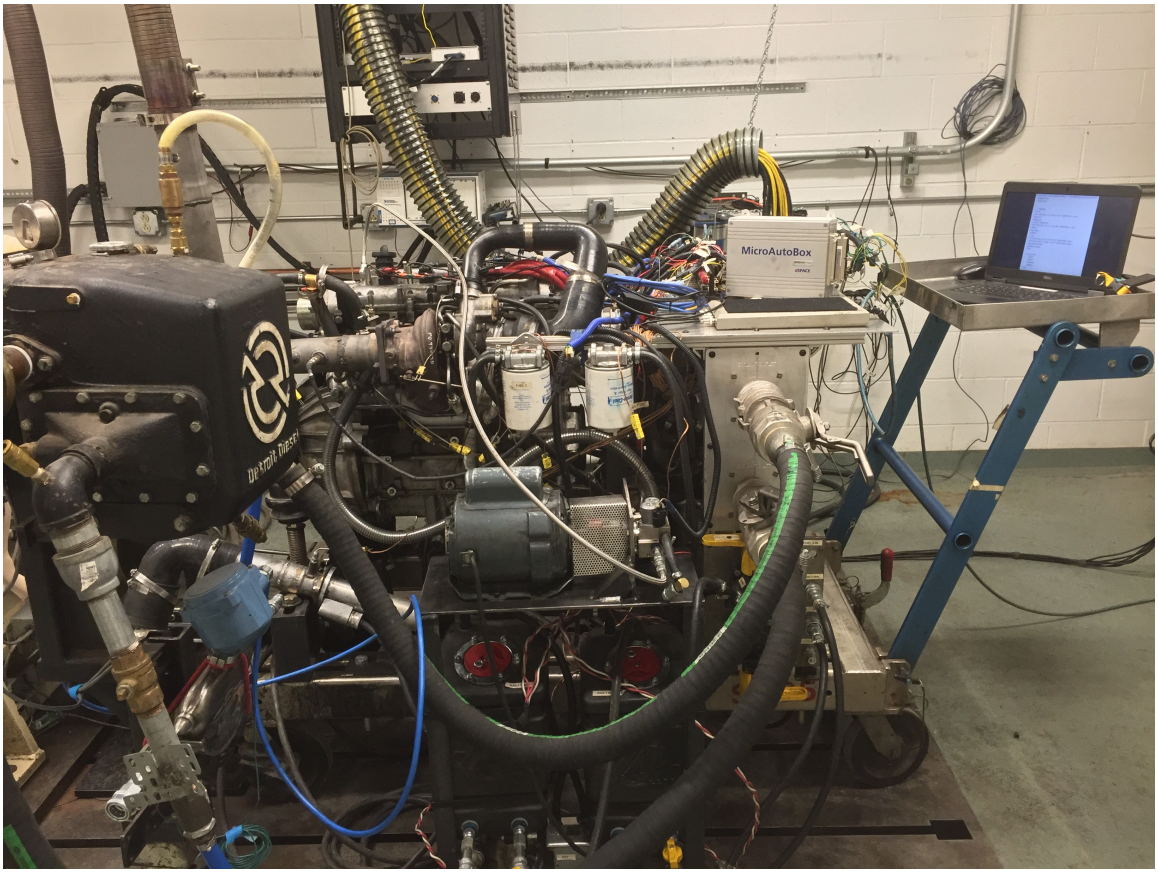

Figure 2.2: Experimental setup of RCCI engine

The three main data acquisition systems used for monitoring the engine were National Instruments (NI) LabVIEW, ACAP and dSPACE. NI LabVIEW was used for controlling dynamometer and intake air temperature. It also measures temperatures of all the thermocouples at different locations on the engine. This helps in monitoring coolant, engine oil, exhaust temperatures. In-cylinder pressure along with crank angle was monitored through ACAP combustion analyser. dSPACE was mainly used for controlling various engine input parameters such as fuel quantity, injection timing, throttle control, spark timing, cam phasing through different actuators. It also gets feedback from different sensors such as lambda sensor, manifold absolute pressure (MAP), fuel rail pressure sensor, throttle position sensor, etc.

2.3 Uncertainty Analysis of Measured and Derived Parameters

Uncertainty, as defined by ISO Guide to the Expression of Uncertainity in Measurment (GUM) [47] is , *" parameter, associated with the result of a measurement, that characterizes the dispersion of the values that could reasonable be attributed to the measurand."* This section highlights the uncertainty propagation from measured variables to the derived parameters. The post processing of the experimental data is mainly based on in-cylinder pressure trace, crank angle, intake temperature, engine

geometry and flow rate parameters of air and fuel. All the measured parameters are classified into one of the above categories. Derived parameters such as IMEP, HRR, CA50, $\eta_{thermal,indicated}$,$\eta_{combustion}$ etc. use the above experimental parameters for calculations. Any uncertainty in measured parameters also propagates to these derived ones. This uncertainty analysis will provide a good estimation on maximum and minimum values of a selected variable and helps to identify the uncertainty propagation from each measured parameter. Table 2.3 provides a list of measured inputs with their range and their uncertanities.

Table 2.3
Measured input parameters and their uncertainities [45]

Parameter [Units]	**Value**	**Uncertainty(±)**
Bore[m]	0.086	0.001
Stroke[m]	0.086	0.001
Length[m]	0.145	0.001
Cylinder Pressure[kPa]	95-4000	1%
Crank Angle[CAD]	0-720	1
λ[-]	1.0-3.0	0.05
T_{in}[°C]	40-100	2%
N[rpm]	800-2200	10
m_{air}[g/s]	12.1 - 31.0	0.72%
m_{fuel}[mg/cycle]	11.0-40.0	0.1%
P_{map}[kPa]	95-105	0.5%
$T_{exhaust}$[°C]	350-700	2%

Next, the effect of uncertainty propagation from measured parameters to derived variables is calculated. If a derived variable is assumed of the form $Y = f(X_1, X_2, ...)$,

where X_1, X_2.. are the measured variables then the uncertainty propagation is calculated using the below Eq. [48].

$$U_y = \sqrt{\sum_i \left(\frac{\partial Y}{\partial X_i}\right)^2 U_{X_i}^2} \tag{2.2}$$

where U_y and U_X are the uncertainties in derived and measured variables respectively. It is assumed that measured variables are uncorrelated and random [48]. Table 2.4 shows the uncertainty analysis for one of the operating points. The percentage weightage of uncertainty for each derived parameter with respect to individual measured parameter is shown in the Table 2.4.

Table 2.4
Uncertainties of derived parameters from measured variables

		% of Uncertainty from respective measured parameter			
Derived parameter [Units]	**Value± Uncertainty**	In-cylinder pressure	Engine speed	m_{fuel}	Crank angle
BD [CAD]	6±1	0	0	0	100
CA50[CAD aTDC]	-1±1	0	0	0	100
ISFC [g/kWh]	202.3±2.2	98	0	2	0
IMEP [kPa]	540.7±28.1	97	0	0	3
$\eta_{indicated,therm}$ [%]	40.0±0.4	0	12.6	87.4	0
$\eta_{combustion}$ [%]	83.0±0.5	0	0	100	0

2.4 Engine Performance Metrics

In this section, all the calculations for performance and combustion metrics were discussed which will be used for analysis, modeling and control in further chapters.

2.4.1 In-cylinder Pressure

In-cylinder pressure is primary measurement from any engine in order to analyze the combustion and study the performance through different metrics. It is measured using PCB piezoelectric pressure transducer in the experimental setup in this study. It is mounted through the cylinder head. It has range of 0-3500 PSI with sensitivity of 1.42 pC/PSI. A charge amplifier is used to amplify this low electric charge into proportional voltage signal. This voltage signal is connected to ACAP combustion analyzer and is monitored through a graphical interface. Pressure referencing(pegging) should be provided to in cylinder pressure signal since the pressure transducer measures relative pressure. Manifold absolute pressure (MAP) provides the best reference, so the pressure signal is pegged with respect to MAP signal where the measured value from the pressure transducer is subtracted from the MAP value to provide absolute pressure. Also, crank angle resolution at which the pressure is measured also determines the accuracy of crank angle based combustion parameters. The higher the

resolution of the encoder, the better the accuracy of the parameters. This engine has crank angle resolution of 1 CAD.

Effective signal conditioning of in-cylinder pressure is very important in order to analyze the heat release rate. Filtering and averaging of the pressure trace over number of cycles will reduce the noise in the signal. Various sources of signal noise can be due to transducer measurement, analog to digital conversion, transmission of signal(bad connections and harnessing) and combustion chamber resonance [49].

2.4.1.1 Filtering Pressure Trace

So as it is said above in order to analyse heat release rate, effective filtering of pressure trace is necessary. Various filters such as Moving average filter, Butterworth low pass filter, Chebyshev filter etc. were analysed during post processing of data. The effect of filtering pressure trace can be observed in heat release rate curve. After analysing above filters, Butterworth low pass filter provides best filtering in terms of roll-off and passband frequencies. Every filter should be designed in terms of an order and a cut-off frequency. It was observed that with higher order the roll-off is very steep. This makes the heat release curve to go for negative values after releasing peak energy in the cycle. This can be seen from the Fig. 2.3 where the filters with different orders are compared.

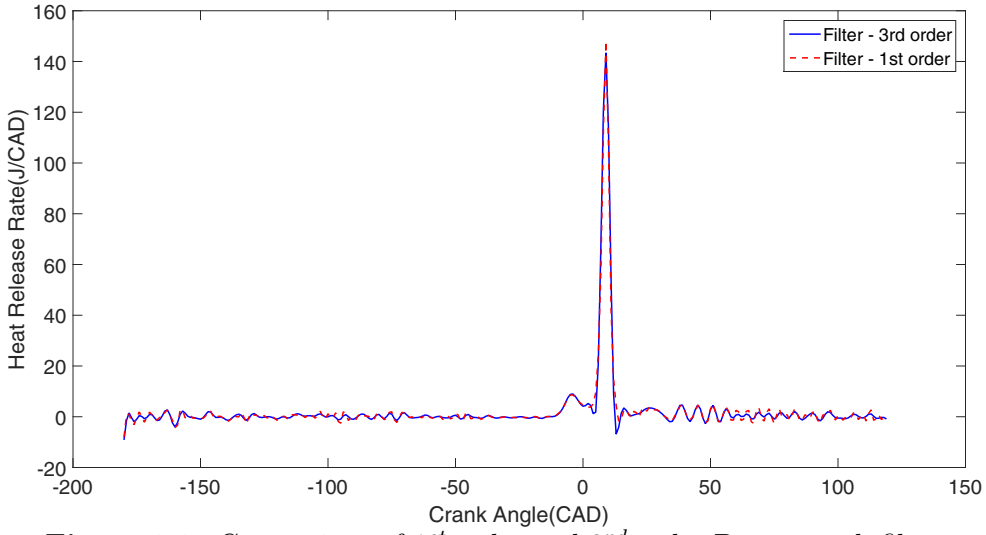

Figure 2.3: Comparison of 1^{st} order and 3^{rd} order Butterworth filters

The cutoff frequency of the filter was decided by observing the frequency spectrum of the pressure trace. It was chosen in such a way that noise from the pressure trace can be filtered from the original pressure trace. Fig. 2.4 shows the frequency spectrum of original and filtered pressure trace with normalized cutoff frequency of 0.5.

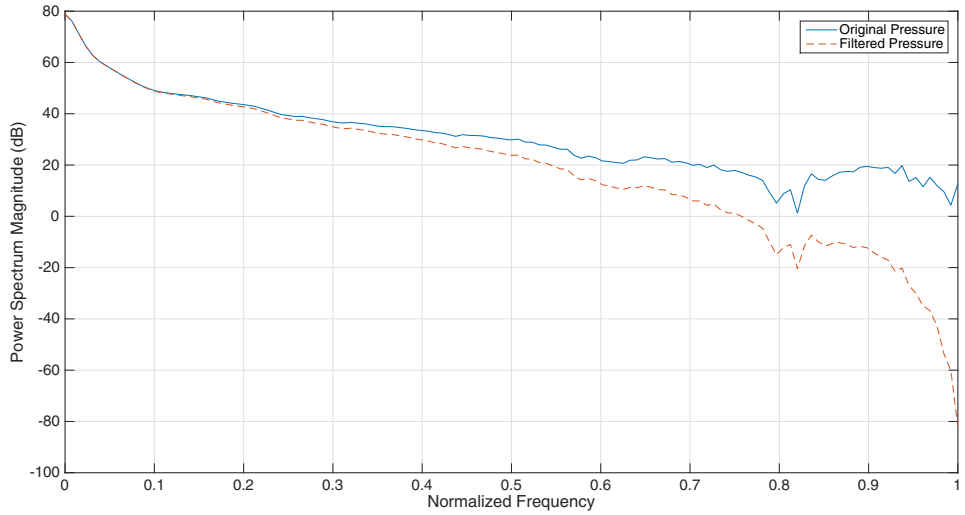

Figure 2.4: Frequency spectrum of Original and Filtered pressure

LogP-LogV plot is a better representation to visualize the effect of filtered pressure trace. Fig. 2.5 shows the filtered mean pressure trace by using Butterworth low pass filter with cutoff frequency 0.5 and order 1 and also original unfiltered pressure trace for 100 cycles.

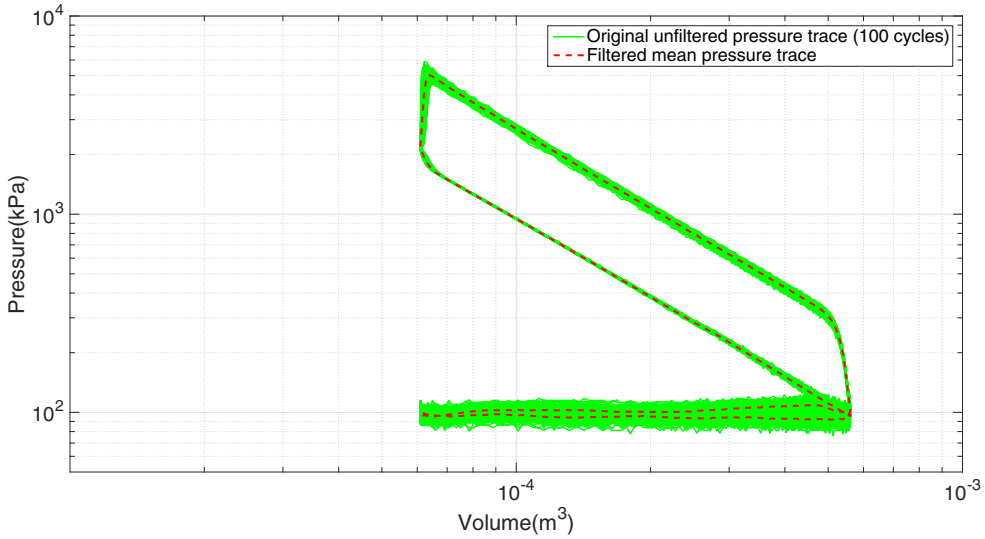

Figure 2.5: Comparison of original and filtered pressure trace using Butterworth filter

2.4.2 Net Heat Release Analysis

Heat Release is an important parameter to be calculated in order to analyse combustion metrics like start of combustion, crank angle at 50% heat released (CA50) and Burn Duration (BD). CA50 is a robust indicator of combustion phasing [50]. Since the slope of heat release with crank angle degree is highest at CA50, it is less sensitive when compared to other locations (CA10 or CA90).Also CA50 calculation is more important for this work for control, it is calculated with more accuracy. First law of thermodynamics is used to model heat release rate (HRR). To be more accurate, heat transfer from in-cylinder to surrounding walls is also included in the calculation. Heat release rate is given by Eq. (2.3).

$$\frac{dQ}{d\theta} = \frac{\gamma}{\gamma - 1}.P\frac{dV}{d\theta} + \frac{1}{\gamma - 1}V\frac{dP}{d\theta} + \frac{dQ_w}{d\theta} \tag{2.3}$$

where γ is a poytropic compression coefficient calculated through slope of the compression region, V is instantaneous volume given by Eq. (2.4),P is in-cylinder pressure.

$$V(\theta) = V_c + \frac{\pi B^2}{4}\Big(l + a - acos\theta - \sqrt{l^2 - (asin\theta)^2}\Big) \tag{2.4}$$

where B is bore diameter, l is length of connecting rod, V_c is clearance volume, a is crank radius.

Q_w is heat transfer from in-cylinder to surrounding walls and is calculated using Modified Woschni heat transfer correlation shown in Eq. (2.5) which is adopted for LTC engines [51].

$$\frac{dQ_w}{d\theta} = \frac{h_c.A_c.(T_g - T_w)}{6.N} \tag{2.5}$$

where N is engine speed, A_c is in-cylinder surface area, T_g and T_w are gas temperature and surrounding wall temperature and h_c is heat transfer coefficient given by:

$$h_c(t) = 3.4.H(t)^{-0.2}P(t)^{0.8}T(t)^{-0.73}\omega(t)^{0.8} \tag{2.6}$$

$$\omega(t) = C_1 S_p + \frac{C_2}{6}\frac{V_d T_r}{P_r V_r}(P - P_{mot}) \tag{2.7}$$

where $H(t)$ is instantaneous cylinder height, $P(t)$ and $T(t)$ are in-cylinder pressure and temperature in time-domain, ω is gas velocity , S_p is the average piston speed, T_r, P_r and V_r are temperature, pressure and volume at IVC, V_d is displacement volume, P and P_{mot} are instantaneous pressure and corresponding motoring pressure. C_1 and C_2 are constant values accounted for expansion and commpression stages.

Net heat release (Q) is obtained by integrating HRR over a window of crank angle degrees (CAD) around TDC, since combustion occurs only near TDC. CA50 is then the crank angle position θ_{CA50} where 50% of net heat release occurs and is given by:

$$Q_{50\%} = \frac{1}{2}(Q_{max} - Q_{min}) \tag{2.8}$$

where Q_{max} and Q_{min} are the maximum and minimum net heat release values.

2.4.3 Start of Combustion(SOC) calculation

It is seen in HCCI combustion [52] that there would be a 2-stage heat release for a mixture of n-heptane and iso-octane. As n-heptane is injected far before from TDC, the mixture more homogeneous resulting in Low Temperature Heat Release (LTHR) at early stage and a High Temperature Heat Release (HTHR) nearer to TDC. While for RCCI combustion, since injection timing of n-heptane is one of the controllable parameters, it depends on this injection timing whether the heat release will occur in two stages or single stage. Fig. 2.6 shows two different HRR curves for different SOI timings. In this work CA50 is calculated for main stage heat release only. For this, SOC should be identified for the main stage instead of whole stage. An algorithm is developed to identify whether the combustion will happen in two-stage or single-stage and CA50 is calculated accordingly.

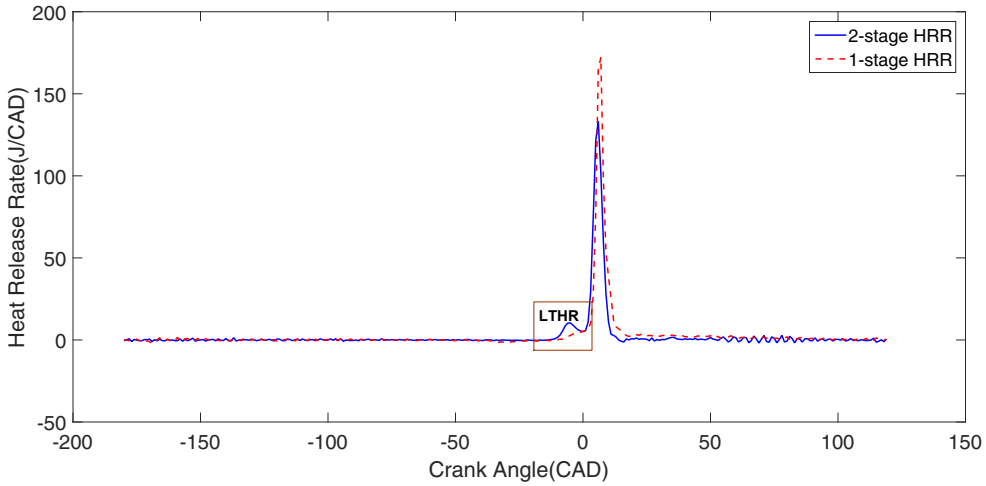

Figure 2.6: 2-stage and 1-stage Heat Release Rate for different SOI

Fig. 2.7 shows all the combustion timings explained on HRR curve. Wholestage is taken as the region between CA90 and CA10 of the complete combustion cycle. While mainstage heat release is defined as the region between 10% and 90% fuel burnt of the HTHR. Start of combustion(SOC) is defined as the 10% fuel burnt of the mainstage heat release.

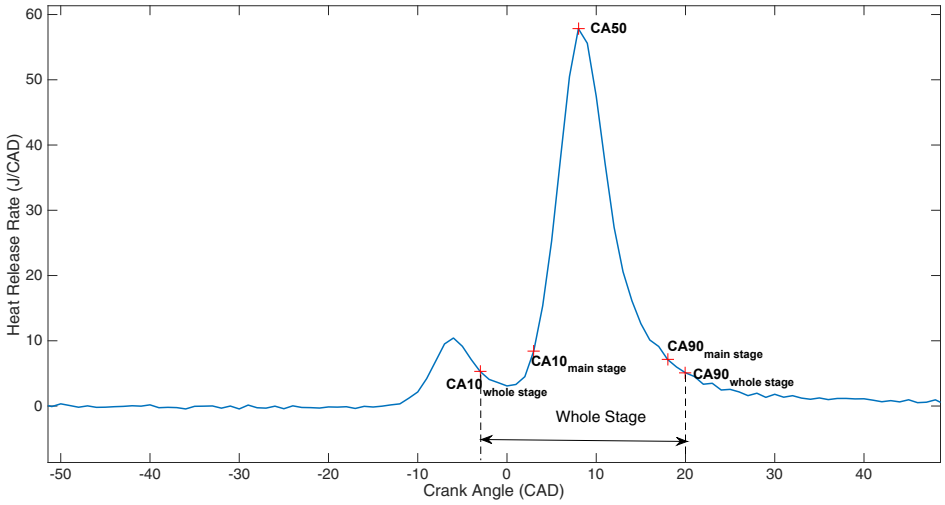

Figure 2.7: HRR curve explaining different combustion metrics

2.4.4 Mass Fraction Burn (MFB)

Mass fraction burn is calculated using Rassweiler and Withrow model [53]. The window for mass fraction burn is decided by burnt duration of the cycle. Burn duration is taken as the time between SOC and CA90 of the mainstage heat release. Eq. (2.9) shows the calculation of MFB [54] with in-cylinder pressure and volume at start and end of combustion.

$$x_b = \frac{P^{1/n}V - P_0^{1/n}V_0}{P_f^{1/n}V_f - P_0^{1/n}V_0} \tag{2.9}$$

where x_b is the mass fraction burn at a given CAD, P_o and V_o are pressure and volume at SOC respectively, while P_f and V_f are pressure and volume at CA90.

2.4.5 Indicated Mean Effective Pressure(IMEP)

IMEP is a key parameter in estimating the amount of work that can be delivered to the piston per cycle for a given displacement volume of the engine. It is useful for comparing relative engine performance of different displacement volumes. Indicated work per cycle $W_{c,i}$ can be calculated using the in-cylinder pressure and corresponding volume at every crank angle. Indicated work can be classified into Gross indicated work per cycle ($W_{c,ig}$) and Net indicated work per cycle ($W_{c,in}$) depending on whether pumping work is accounted in the total work or not [55]. $W_{c,ig}$ includes the work delivered to the piston over compression and expansion strokes while $W_{c,in}$ includes the pumping work as well in addition to $W_{c,in}$ over the complete cycle [55]. In this work, IMEP is calculated based on Gross Indicated work per cycle($W_{c,ig}$) only and is given by:

$$IMEP = \frac{W_{c,ig}}{V_d} \tag{2.10}$$

where V_d is the displacement volume of the engine.

Coefficient of variation of IMEP (COV_{IMEP}) is one of the significant parameter to identify cycle-to-cycle variability for in-cylinder combustion. The higher the COV, the more is the cyclic variability. It is given by Eq. (2.11). As per the studies on LTC combustion it is seen that COV limit is taken between 3%-5% [9, 21]. COV_{IMEP} of 5% limit is used in this study to identify unstable experimental engine data and only

focus on stable engine operating conditions [56].

$$COV_{IMEP} = \frac{\sigma_{IMEP}}{IMEP} \times 100 \tag{2.11}$$

where σ_{IMEP} is the standard deviation of IMEP.

2.4.6 Friction Mean Effective Pressure (FMEP)

In order to find Brake Mean Effective Pressure (BMEP), one should calculate FMEP which accounts for friction of the bearings, pistons and other mechanical components of the engine. Flynn-Chen correlation [57] shown in Eq. (2.12) is used for calculating FMEP based on mean piston speed (S_p) and peak pressure (P_{max}). The constants of the equation were obtained by parameterizing the model for different operating conditions.

$$FMEP = A + B.P_{max} + C.P_{max}^2 + D.P_{max}^3 + E.S_p + F.S_p^2 \tag{2.12}$$

The validation of FMEP from experimental results and Flynn-Chen model is shown in Fig. 2.8. The constants of the equation are also mentioned in the plot.

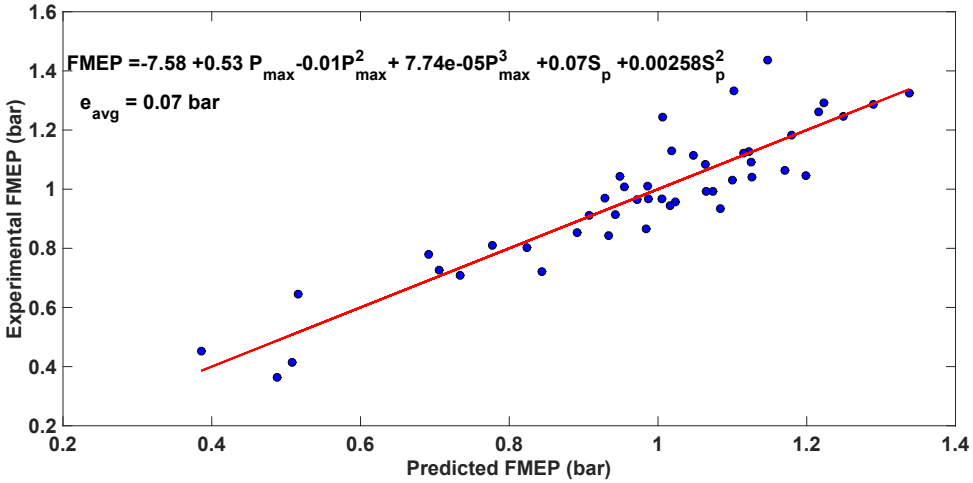

Figure 2.8: Validation of Flynn-Chenn model with experimental data

Break Mean Effective Pressure (BMEP) can be calculated by using the relation

$$BMEP = IMEP_{net} - FMEP. \tag{2.13}$$

2.4.7 Thermal Efficiency- Indicated and Brake

Thermal efficiencies are very important parameters to estimate the amount of work output for a given amount of input fuel energy. They are calculated using the indicated/brake power and energy of the fuel supplied.

Indicated power is calculated by using the following equation:

$$IP = \frac{IMEP \times N \times V_d}{120} \tag{2.14}$$

where N is engine speed in RPM, V_d is displacement volume. Indicated Thermal Efficiency(ITE) is given by:

$$\eta_{therm.,ind.} = \frac{IP}{m_{fuel} \times LHV} \tag{2.15}$$

where LHV is the lower heating value of the fuel and m_{fuel} is the total mass of fuel injected. Similarly Brake Thermal Efficiency (BTE) is calculated using the brake power.

2.4.8 Combustion Efficiency

Combustion efficiency is calculated using net heat release energy and the amount of fuel energy supplied. The equation is given by:

$$\eta_{comb.} = \frac{\sum \frac{dQ}{d\theta}}{m_{fuel}.LHV} \times 100 \tag{2.16}$$

This parameter helps to determine quality of combustion. The lesser the combustion efficiency, the more the incomplete combustion and higher the emissions.

2.5 Selection of Thermocouple

K-type thermocouples are generally used in the test cells due to their higher sensitivity towards change in temperature and also has wide operating range (-200°C - 1250°C) that can measure temperatures from intake to exhaust [58]. These thermocouples were installed at different locations such as intake port of every cylinder, exhaust port, oil sump, crankcase, intercooler, coolant lines, etc.

A fast response K-type thermocouple is installed on the exhaust port for measuring the exhaust gas temperature (EGT). This thermocouple response will be used for transient control of EGT. The specifications of this thermocouple are mentioned in Table 2.5.

Table 2.5
Thermocouple Specifications

Part Name	TJC36-CAIN-032E-6-SMP-M
Model	TJC36 - Compact Transition Joint Probe, 36” cable
Type	K-Type(CA)
Sheath Material	Inconel 600.(IN)
Sheath Diameter	0.032 in
Junction Type	E-Exposed
Probe length	6 inches

2.5.1 Thermocouple Lag

The response time of the thermocouple limits how fast it can respond to an instantaneous step change in temperature [59]. In general, the exhaust gas temperatures increase with higher equivalence ratios. When the engine is operated at higher equivalence ratios, the amount of unburnt fuel increases and releases in the form of soot in the tailpipe. These gases absorb the in-cylinder temperatures resulting in higher exhaust temperatures. During transient conditions, due to slower response of the thermocouple there exists a lag associated with it to reach the desired temperature which can be seen from Fig. 2.9. In order to use the exhaust temperature as feedback parameter for control purpose one needs to take care of this lag time. This can be done by developing a first order transfer function and identifying gain and time constant using measured exhaust temperature. The model can be of the form :

$$G(s) = \frac{k_p}{\tau \mathtt{s} + 1} \tag{2.17}$$

where k_p , τ are gain and time constant of the thermocouple model respectively.

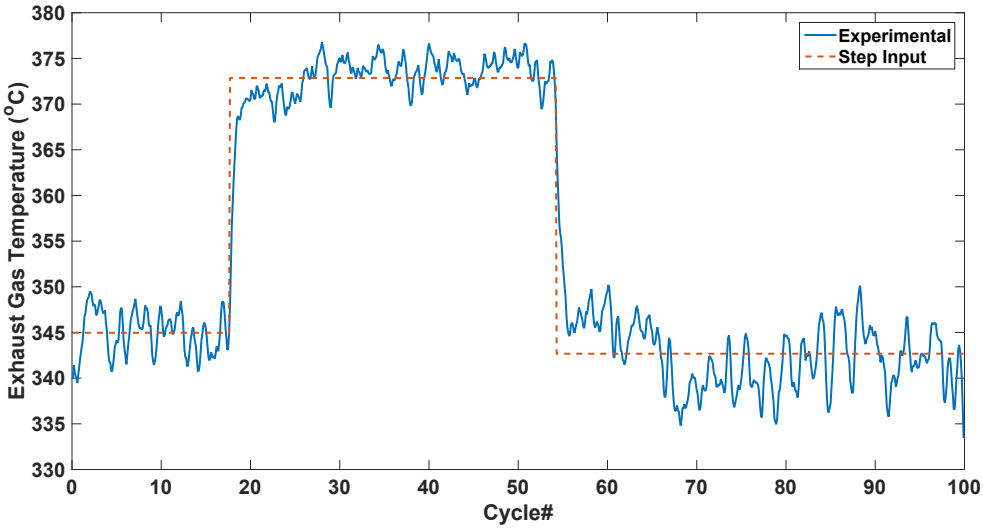

Figure 2.9: Comparison of step input and measured exhaust gas temperature

In order to find the lag time for the first order model a step temperature is provided as an input to the engine and the output is compared to the measured exhaust temperature from the thermocouple. Fig. 2.9 shows both step input and measured thermocouple temperatures before the model is introduced. The outputs from the model and thermocouple were analyzed using System Identification Toolbox in MATLAB. The model was tuned accordingly and the time constant τ and gain k_p of thermocouple model were found to be 0.6 s and 1, respectively. Fig. 2.10 shows both the simulated and measured exhaust temperatures after the model was introduced with the lag τ.

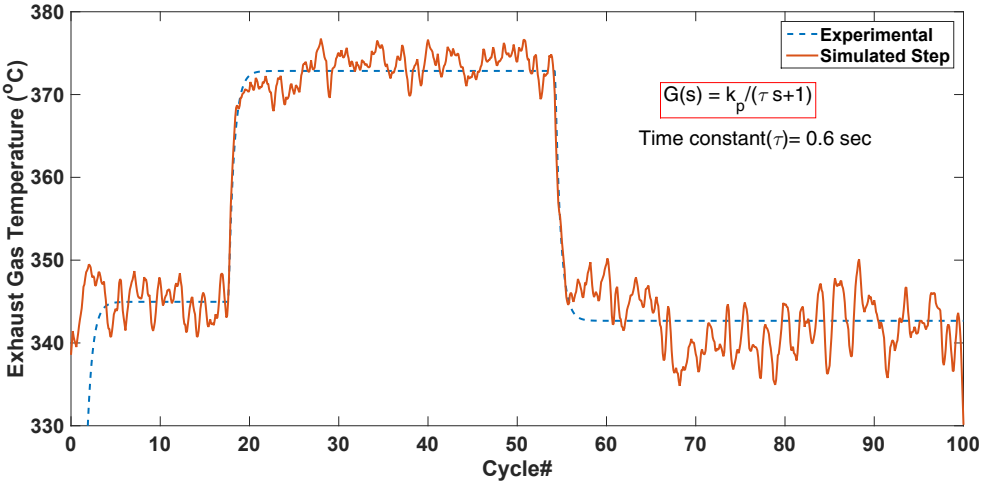

Figure 2.10: Comparison of simulated and measured exhaust temperature after introducing first order lag model

Chapter 3

Experimental Study of RCCI Engine under Naturally Aspirated Conditions

In this Chapter, experimental study and results are discussed for the engine operating in RCCI mode. Firstly, the experimental procedure was explained and the operating conditions were mentioned. Later, the operating regions of RCCI at different conditions and their performance results were explained. Finally, the parametric studies were performed to study the effect of each individual parameter (SOI, PR and T_{in}) on both the performance and combustion metrics.

3.1 Experimental Procedure

As it was discussed in previous chapters, in order to operate the engine in RCCI mode dual fuels should be supplied i.e. one from the port injection and the other from direct injection. In this study, iso-octane was used for port fuel injection whereas n-heptane was used for direct injection. n-Heptane and iso-octane are common surrogate fuels which represent diesel and gasoline fuel respectively. PR refers to Premixed Ratio which quantifies the amount of premixed fuel, i.e. iso-octane here, energy percentage in a mixture consisting of both iso-octane (PR-100) and n-heptane (PR-0). SOI refers to the Start of Injection of n-heptane fuel during the compression stroke. All the experiments were performed without EGR. Also, tests were run at naturally aspirated conditions without applying any boost pressure.

Engine operating maps were created over different speed and load range by varying speed, fuel quantity, intake temperature and PR. SOI was adjusted accordingly in order to maintain a constant combustion phasing (CA50) of around $6 - 10$ CAD aTDC [60]. At every engine speed for a given PR, fuel quantity was varied between knock (MPRR ≤ 10 bar/CAD) and misfire limits ($COV_{IMEP} \leq 5.0\%$). This procedure was followed for different intake temperatures. All the operating conditions were mentioned in Table 3.1. For each operating point 100 cycles of data was logged from the data acquisition systems. All the data was post processed using developed script

in MATLAB. All the maps were created with operating points having COV_{IMEP} less than or equal to 5.0% [56].

Table 3.1
RCCI operating conditions in this study

Parameter(Units)	**Operating value**
PR (-)	20,30,40,60
SOI (CAD bTDC)	15-70
Manifold pressure (kPa)	95
T_{in}(°C)	40:20:100
Speed (RPM)	800:200:2000
λ (-)	1.0-3.8

3.2 Operating Regions and Performance Maps

This section discusses both the operating regions and peformance maps of RCCI engine under naturally aspirated conditions shown in Table 3.1

3.2.1 Operating Regions

Fig. 3.1 shows the operating regions of the engine with respect to IMEP and engine speed at different PR and intake temperatures of 40°C, 60°C and 80°C.

It can be seen from Fig. 3.1a that operating region decreases with increase in PR at a given engine speed. At lower speeds, the mixture gets more time for premixing so the local equivalence ratio decreases making it leaner [9]. In order to achieve

lower loads, PR should be maintained at lower values, i.e. should increase higher reactivity fuel percentage, so that reactivity of the mixture increases which aids the combustion. At the same time to go for higher loads, PR should be increased so that charge gets diluted by iso-octane thereby pushing the knock limit. It can also be seen that the lean limit at lower PRs is more compared to higher PR values. This is due to availability of more reactive fuel at lower PRs which extends the lean limit when compared to higher PR values.

The operating region is very limited at higher speeds for PR-60. At higher speeds there is less availability of time for premixing and at the same time operating at higher PR reduces auto-ignition points which makes it difficult for combustion to happen. This limits the operating region to lower engine speeds. Also, due to less compression ratio of this engine, PRs more than PR-60 couldn't be achieved due to knock limit. The operating region could have been expanded to higher loads if the compression ratio is higher.

This trend changes with increase in intake temperature. It can be seen from Fig. 3.1b and Fig. 3.1c that the operating region expands over different speeds for every PR with increase in intake temperature. This is because with higher intake temperature, chemical reactions gets more accelerated between oxygen and hydrocarbon molecules [61] which favors autoignition to happen and also reduces the ignition delay. This helps in combustion to happen at higher speeds which is not possible at

lower intake temperatures. It can also be further observed that with increase in intake temperature to 60°C, the leaner limit for a given PR zone is extended when compared to the corresponding same PR zone at 40°C. This is due to decrease in the charge density with increase in intake temperature which allows more air intake.

(a) T_{in}-40°C

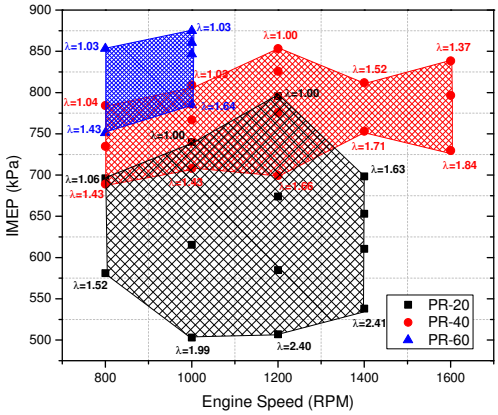

(b) T_{in}-60°C

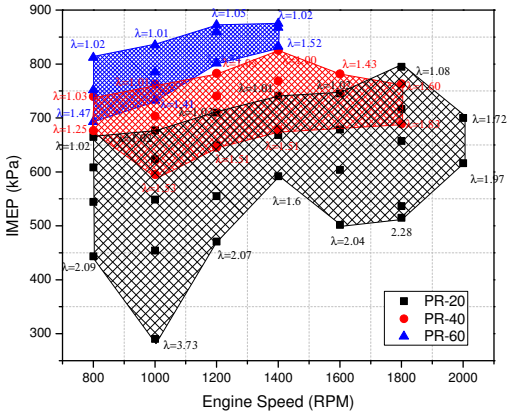

(c) T_{in}-80°C

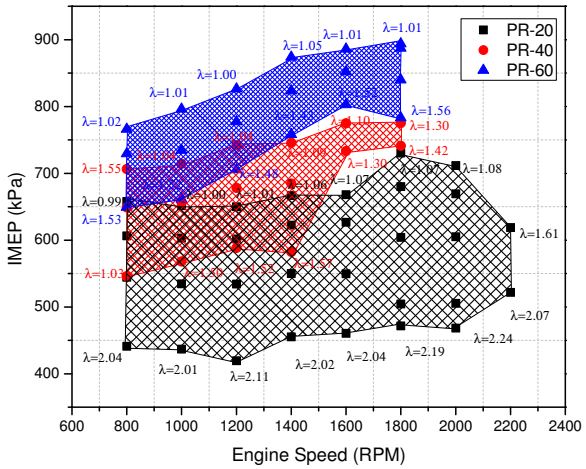

Figure 3.1: RCCI engine operating maps for different intake temperatures

3.2.2 Performance Maps

Fig. 3.2 shows the maps for indicated specific fuel consumption (ISFC) for PR-20, PR-40 and PR-60 at intake temperature of 60°C. ISFC maps provide a good information on minimum required fuel for generating 1 kWh of indicated power. It was seen in Section 3.2.1 that the operating range decreases with increase in PR at higher speeds and loads. It can be seen from Fig. 3.2a and Fig. 3.2b that the best ISFC region was shifted towards higher loads with increase in PR. At 1800 RPM the minimum ISFC at PR-20 was observed to be 174.8 g/kW.h at 515 kPa IMEP whereas at PR-40 the best ISFC was seen as 177.8 g/kW.h but at higher IMEP of 690 kPa. As we saw earlier that as the gasoline percentage increases in the mixture, the mixture becomes less reactive and can go to higher loads of operation. It can also be observed that for a given load of around 680 kPa IMEP and 800 RPM, ISFC was minimum for PR-60 than compared to PR-40 and PR-20 fuels. From the above observations, it can be inferred that in order to operate at higher loads and at lower RPMs, PR-60 provides less fuel consumption. Whereas to operate at low to medium loads at all engine speeds PR-20 can be seen as the best choice. Medium to higher loads at higher engine speeds are achieved with PR-40.

(a) PR-20 **(b)** PR-40

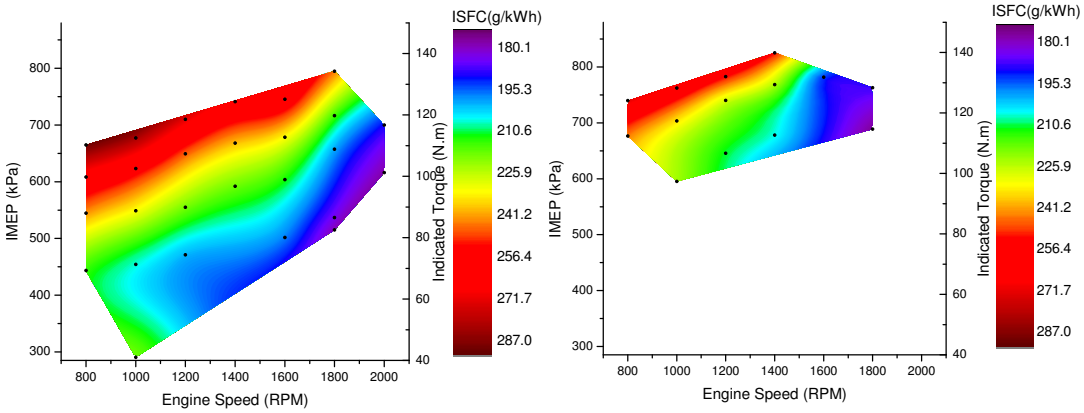

(c) PR-60

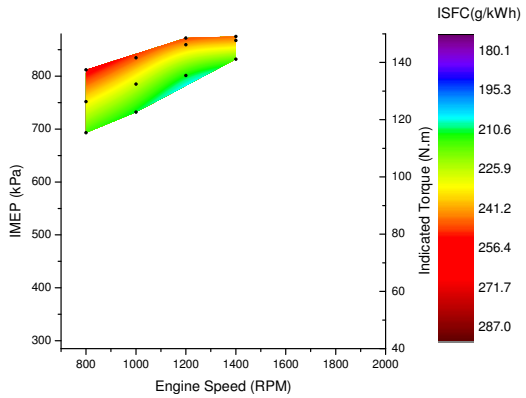

Figure 3.2: ISFC maps for different PRs at intake temperature of 60°C

(a) PR-20 **(b)** PR-40

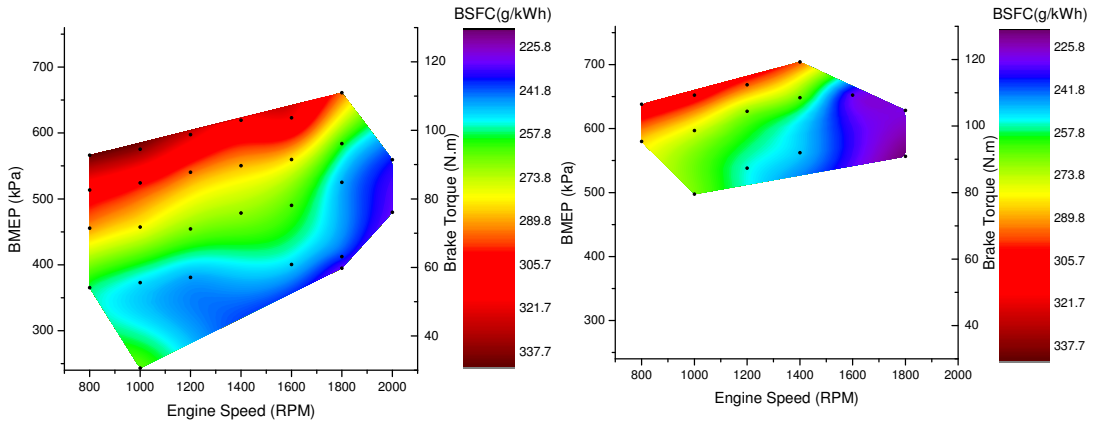

(c) PR-60

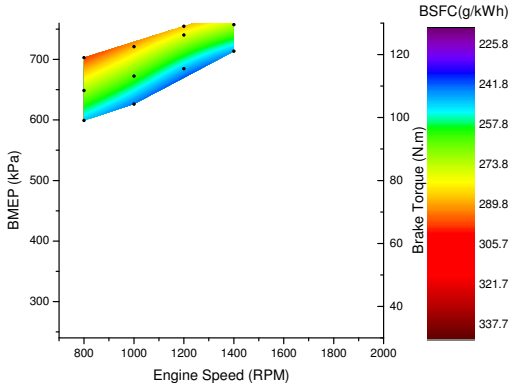

Figure 3.3: BSFC maps for different PRs at intake temperature of 60°C

Fig. 3.3 shows the maps for brake specific fuel consumption (BSFC) for PR-20, PR-40 and PR-60 at intake temperature of 60°C. This follows the same trend as ISFC maps above but at increased magnitudes. Due to friction losses the BSFC increases as compared to ISFC. This loss will be more at higher speeds and loads which increases BSFC further due to more fuel being consumed to overcome the friction.

(a) PR-20 **(b)** PR-40

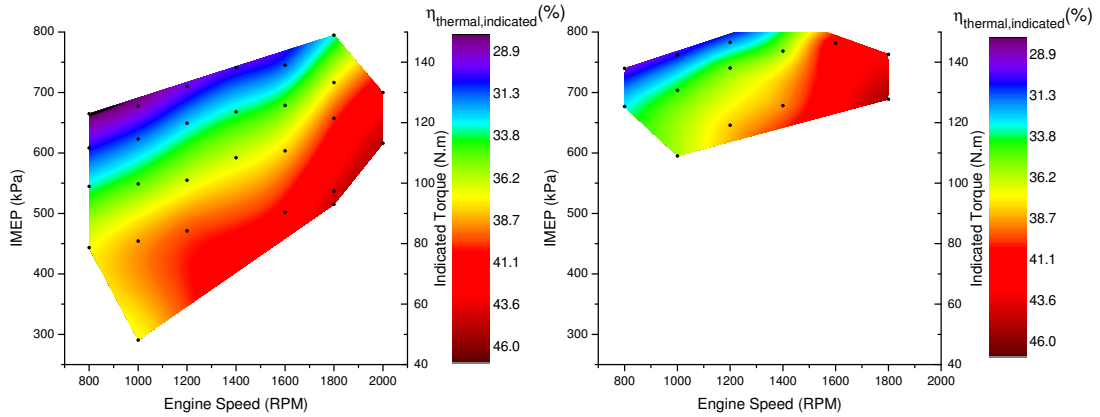

(c) PR-60

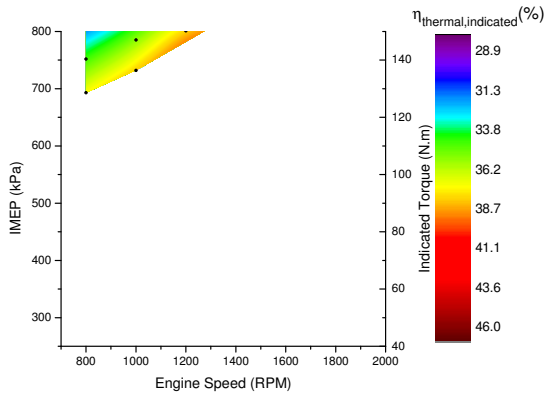

Figure 3.4: ITE maps for different PRs at intake temperature of 60°C

Fig. 3.4 shows the maps for Indicated Thermal Efficiency (ITE) for PR-20, PR-40 and PR-60 at intake temperatures of 60°C. Indicated thermal efficiency signifies the amount of indicated power that can be extracted from the available fuel energy. Since ISFC and ITE, from their definitions, are inversely related to each other, ITE maps should follow opposite trend to that of the ISFC maps. This can be seen by comparing Fig. 3.2 and Fig. 3.4. For instance, if we compare both Fig. 3.4b and Fig. 3.4c at 1000 RPM and and at constant IMEP around 760 kPa, it can be seen that ITE increases from around 30% to 37%. This is because as we saw in Fig. 3.1b at PR-60 (more premixed) the amount of fuel energy required to achieve the same IMEP is less compared to PR-40.

(a) PR-20 **(b)** PR-40

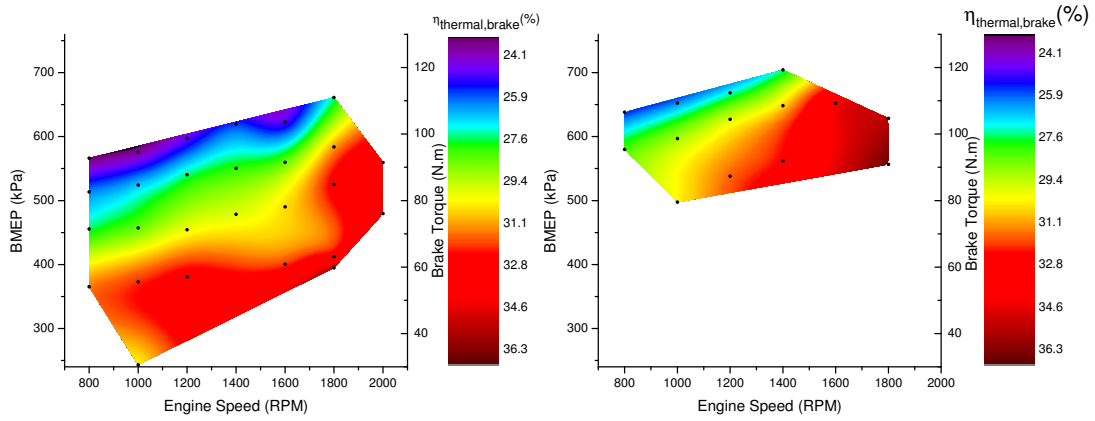

(c) PR-60

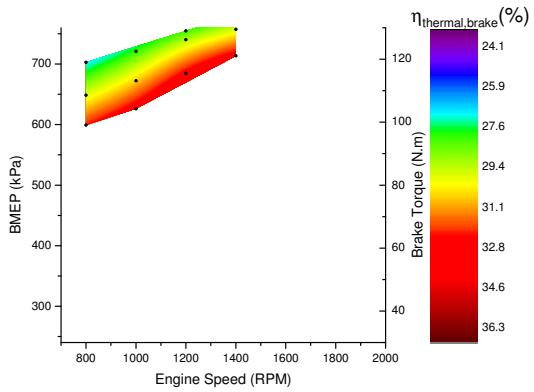

Figure 3.5: BTE maps for different PRs at intake temperature of 60°C

Figure 3.5 shows the maps for Brake Thermal Efficiency (BTE) for PR-20, PR-40 and PR-60 at intake temperature of 60°C. BTE maps also follow the same trend as ITE maps. But, as discussed before, due to frictional losses the brake power decreases which also reduces the BTE. Also, at higher RPM due to more frictional losses the efficiency decreases further which can seen from Fig. 3.5a around 1600- 1800 RPM.

Fig. 3.6 shows the maps for exhaust gas temperature for PR-20, PR-40 and PR-60 at intake temperature of 60°C. With increase in PR and at higher loads, the combustion efficiency decreases due to decrease in amount of more reactive fuel (here n-heptane) [31, 62]. As we can see from Fig. 3.6a, exhaust temperatures are very less at lower loads and speeds. This poses a problem for oxidation catalysts to work effectively in this region since the temperatures are less than catalyst light off temperature. This will increase CO and HC emissions in the tailpipe.

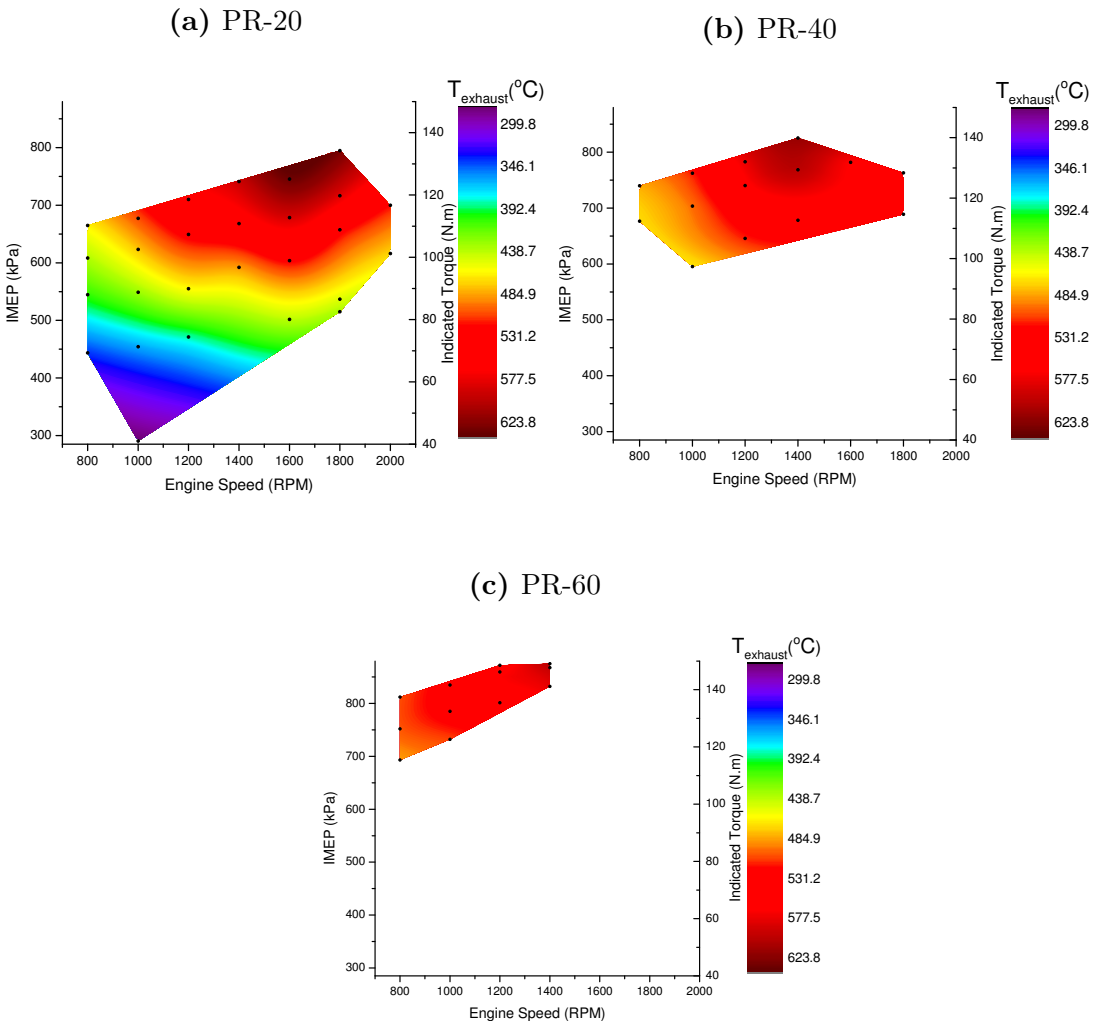

Figure 3.6: Exhaust gas temperature maps for different PRs at intake temperature of 60°C

3.2.3 Optimized RCCI Maps

All the optimized maps were created from the best optimum points chosen from the data set shown in Appendix A. Optimum points were selected by choosing highest

ITE and least ISFC points for a given load (IMEP) and engine speed. All the operating points for these maps have COV_{IMEP} less than or equal to 5.0% [56] and MPRR less than or equal to 10 bar/CAD. CA50 is maintained around 5-10 CAD aTDC by adjusting SOI timing. These maps will provide good information on the operating regions of the engine to achieve the best efficiency. Specific fuel consumption (SFC) and thermal efficiency maps will help in identifying engine's best fuel conversion efficiency and maximum power output for every combination of engine torque (N.m) and engine speed (RPM). In order to achieve higher fuel economy the operating conditions with the lowest SFC and highest thermal efficiency point should be selected, provided emissions and noise constraints are met.

3.2.3.1 Optimized Indicated Maps

(a) Optimized ISFC map. **(b)** Optimized $\eta_{therm.,ind.}$ map.

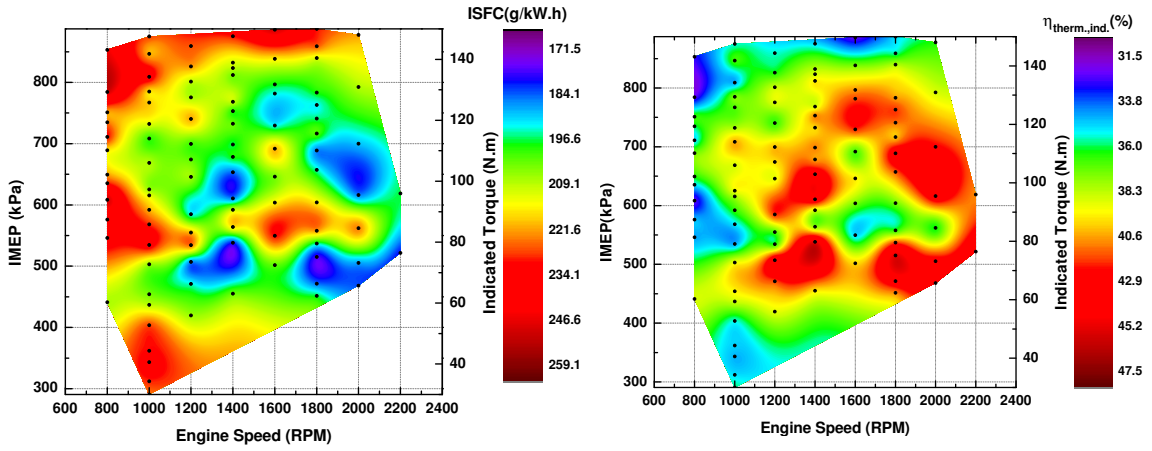

Figure 3.7: Optimized indicated maps.

Fig. 3.7a shows the optimized ISFC map for the engine operating at naturally aspirated conditions. It can be seen that the best operating regions in terms of less ISFC (shown as blue colored regions) were possible at medium - high loads and between 1400-2200 RPM. The least ISFC was observed to be 167.4 g/kWh and was achieved at 1400 RPM and IMEP of 539 kPa with PR, SOI and T_{in} as 20, 60 CAD bTDC and 40°C. The combustion efficiency at this point was 95% and CA50 was 9 CAD aTDC. Beside Fig. 3.7b shows the map for optimized ITE for the same operating points. It can be seen from this Fig. 3.7b that the best efficiency (dark red region) was observed to be 48.3% for the same operating point. At higher speeds and loads

the best efficiency points were observed to be at PR 40. This is because, as it was said in previous sections, at higher loads the mixture should be more stratified and premixed with iso-octane which helps in increasing the knock limit. It also helps in achieving better and complete combustion for a given fuel quantity. So, a given load can be achieved with less amount of fuel at PR-40 than compared to PR-20. It is also observed from the optimized points that the combustion efficiency is more than 93% at the red regions observed in Fig. 3.7b. This also supports the observation that efficient operating region can be achieved at these points. ISFC was observed to be high (red regions) at lower speeds (800-1000 RPM) and also at higher loads(800-850 kPa IMEP). It was seen that at these regions the operating points are either at higher intake temperatures (60°-100 °C) or at lower PRs. The combustion efficiencies were very low at these points which might be responsible for lower thermal efficiencies. The effect of intake temperature and PR on engine performance will be discussed in the upcoming sections.

3.2.3.2 Optimized Brake Maps

(a) Optimized BSFC map

(b) Optimized $\eta_{therm.,brake}$ map.

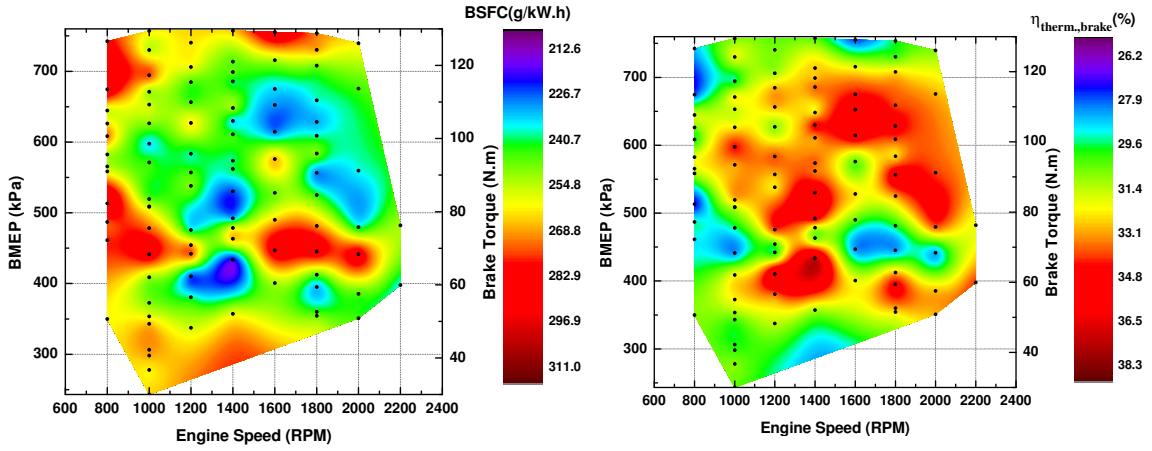

Figure 3.8: Optimized brake maps.

Fig. 3.8 shows optimized BSFC and BTE maps which were created using the same optimized points used for the indicated maps in Fig. 3.7a. Since BSFC and ISFC were differentiated by frictional losses, BSFC is always higher than ISFC for a given operating point. Also, at higher speed and load the frictional losses will increase which results in reducing brake power. This ultimately leads to increase in BSFC as well as decrease in BTE. This can be observed in Fig. 3.8, as BSFC follows the same trend (but at increased magnitudes) as ISFC at lower speeds but at higher speeds (1800-2200 RPM) BSFC was even more higher. It can also be seen that the best operating point remains the same from both the maps.

Thus, it can be concluded that for low to medium loads the best efficiency can be obtained by operating at lower PR (PR-20) and at intake temperature of 40-60°C. While at medium to higher loads and at engine speeds more than 1200 RPM the best efficiency was achieved using PR-40 and intake temperatures of 40-60°C. Studies [1] have shown that RCCI engines have the capability of achieving 60% gross indicated thermal efficiency. It can be seen from the indicated maps that the current indicated thermal efficiencies were achieved to maximum extent of 48% under naturally aspirated conditions at different loads. This can be further improved with increase in boost pressure and compression ratio of the engine. The compression ratio of the current engine is 9.2 which is significantly low to operate an engine in RCCI mode. Since RCCI falls under the category of compression ignition engines, which in general have higher compression ratios of around 13-17.

3.2.3.3 Optimized Exhaust Gas Temperature Map

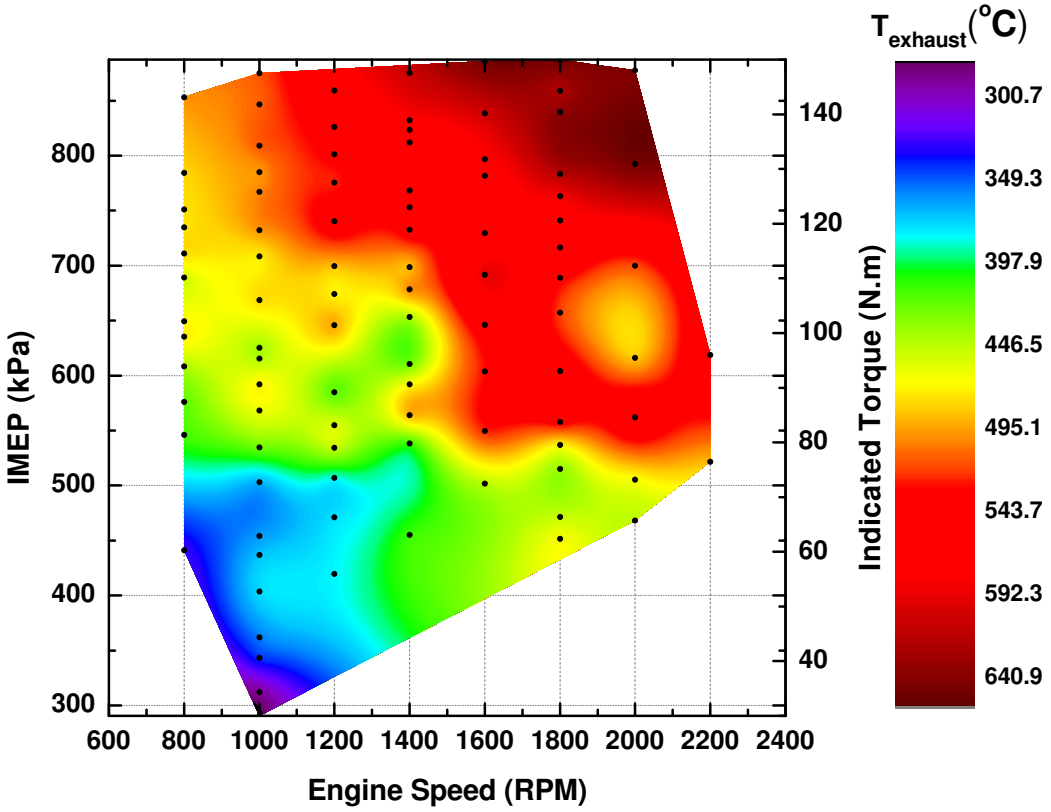

Figure 3.9: Exhaust gas temp. map for the data points shown in Fig.3.7a

Fig. 3.9 shows the map for exhaust gas temperature for the same operating points used for previous optimized maps. It can be seen that exhaust temperatures increase with speed and load since the time available for heat transfer to the walls decreases at higher speeds which reduces the heat loss [21]. Also, the in-cylinder temperature increases with load which also results in higher exhaust temperatures. The lower exhaust temperatures at low speed and load will pose a challenge for after-treatment systems like diesel oxidation catalysts to oxidize CO and HC emissions.

3.3 Parametric Studies - Effect of SOI, PR and Intake Temperature

3.3.1 Effect of SOI

This section explains the effect of injection timing of DI fuel, i.e. n-heptane, on performance and combustion metrics. Fig. 3.10 shows the effect of SOI on in-cylinder pressures and heat release rates at PR-20, intake temperature of 40°C and 1000 RPM. As seen in Table 3.2 all other operating conditions were kept constant and SOI is varied from 80 CAD (bTDC) to 20 CAD (bTDC). It can be observed that at earlier injections of n-heptane, heat release occurs in two stages while for the injection timing approaching near to TDC it is gradually changing to single stage heat release. With earlier injection timings of n-heptane, the mixture gets more homogenized which reduces both local ϕ and the fuel reactivity gradients [56]. The combustion becomes more like HCCI type, where both significant LTHR and HTHR can be seen, with earlier injections due to more premixing of the charge. Also, it can be seen from Fig 3.11(c), CA50 starts retarding with late injection timings nearer to TDC. Burn duration also follows the same trend. At injections closer to TDC, there is less time for mixing of both fuels, making higher reactive fuel to confine at particular location while surrounded by most of the iso-octane [63]. So, the ignition delay increases due

to combustion of surrounded iso-octane which results in prolonged burn duration and retarded combustion phasing [64].

Table 3.2
Operating conditions for SOI parametric study

Parameter(Units)	Operating value
SOI(CAD bTDC)	20-40-50-60-80
PR(-)	20
T_{in}(°C)	40
P_{in}(kPa)	95-Naturally Aspirated
IVO(CAD bTDC)	25.5
EVC(CAD bTDC)	22
Speed(RPM)	1000
Fuel mass(mg/cyc)	15
λ(-)	1.92

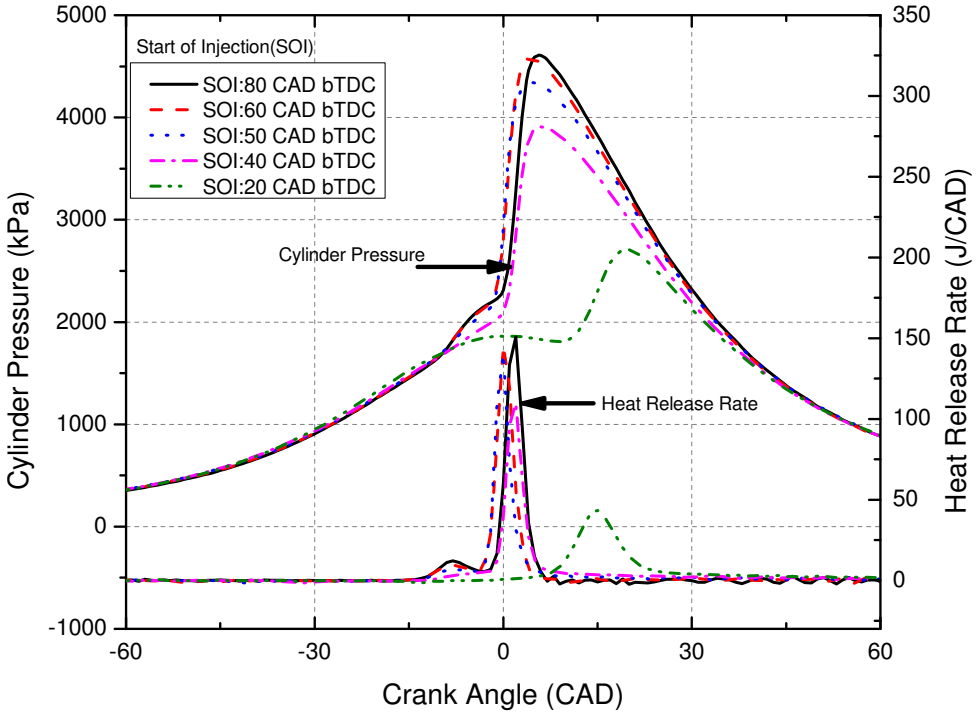

Figure 3.10: Pressure and heat release rates at different SOI of n-heptane for PR-20, $T_{in} = 40^{o}$C, 1000 rpm

It can be seen from Fig. 3.11(c) and Fig. 3.11(d) that with advancing injection timing before TDC, CA10 and CA50 advance until SOI of around 60 CAD bTDC and then starts slightly retarding with further advancing SOI. This is because the mixture becomes too premixed and the reactivity gradient decreases with further advancing of SOI [56]. The mixture starts getting weaker due to lack of sufficient ignition source and may also result in unstable combustion [65]. With injection timings nearer to TDC, the emissions (HC and CO) also get increased due to less available time for diesel to mix with gasoline-air mixture which leads to local rich equivalence ratios [65].

Fig. 3.12(d) shows that with advance in injection timing IMEP also increases. It can be seen from Fig. 3.10, the peak pressures and the area under pressure-volume curves increase with advancing SOI. The area under P-V curve is proportional to IMEP. Therefore, IMEP also increases with earlier injections. But IMEP reduces with further advancing injections, since the mixture gets too premixed and the combustion becomes difficult. Similar trend is also seen for indicated thermal efficiency in Fig 3.12(c). Combustion efficiency also increases due to better mixing until certain SOI but later it drops as well. Peak pressure rise rate also shows the same trend in Fig. 3.12(a).

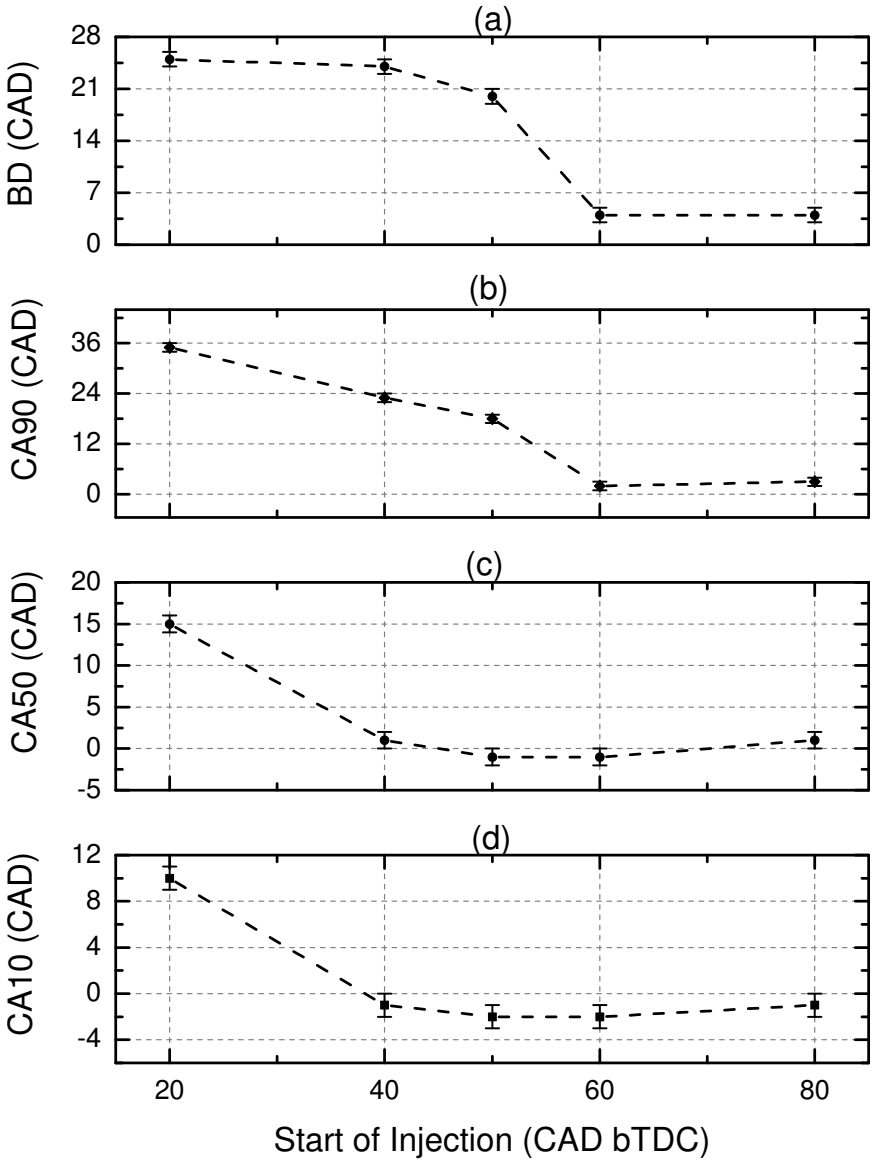

Figure 3.11: Effect of SOI on RCCI combustion timings

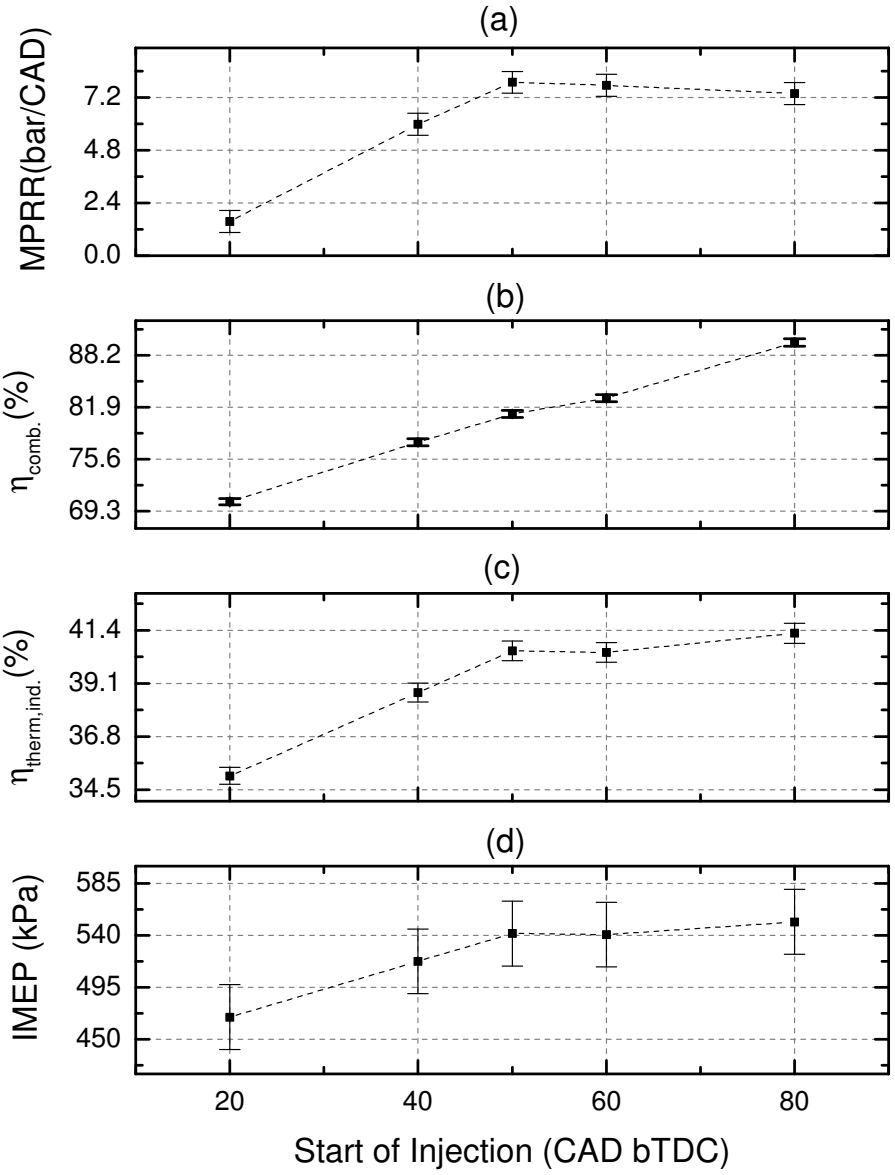

Figure 3.12: Effect of SOI on performance metrics

3.3.2 Effect of PR

Premixed Ratio (PR) is already defined in Chapter 2 but is given here again for reference.

$$PR = \frac{m_{iso}.LHV_{iso}}{m_{iso}.LHV_{iso} + m_{nhep}.LHV_{nhep}} \tag{3.1}$$

where LHV_{iso} and LHV_{nhep} are lower heating values of iso-octane and n-heptane respectively. m_{iso} and m_{nhep} denote the quantity of fuel injected for the respective fuel. This parameter signifies the amount of premixed fuel energy present in a given mixture. The higher the PR value, the more the amount of premixed fuel, i.e.iso-octane, is present in a given mixture. Iso-octane being less reactive fuel compared to n-heptane, the reactivity of the mixture decreases with increase in PR. For the current engine, due to low compression ratio of 9.2, tests were performed at even lower PR values. The lesser the compression ratio, the higher the amount of n-heptane is required for autoignition to occur at lower loads [9]. In general, studies on RCCI engine were performed on higher compression ratios which allowed them to operate at higher PR. However, this section focuses on using the PR for control of combustion phasing (CA50).

Fig. 3.13 shows the effect of varying PR on pressure and heat release rates for RCCI combustion. Operating conditions were shown in Table 3.3. It can be seen that with increase in PR the peak pressure and heat release rates decrease. At lower PRs,

i.e. around PR-20, the mixture is dominated by n-heptane so the combustion can be assumed to be similar to diesel combustion. As PR is increased, the amount of iso-octane injected from PFI increases. Since the total fuel quantity is kept constant, with increase in iso-octane the amount of more reactive fuel, i.e. n-heptane, decreases. n-heptane being more reactive serves as the source of auto-ignition point which causes combustion to happen [31]. With increase in PR, the number of auto-ignition points decreases which makes the ignition difficult [66] and leads to increase in ignition delay [9, 67]. This causes peak pressure and heat release rates to decrease.

Table 3.3
Operating conditions for PR parametric study

Parameter(Units)	**Operating value**
PR(-)	20-40-60
SOI(CAD bTDC)	30
T_{in}(°C)	80
P_{in}(kPa)	95
IVO(CAD bTDC)	25.5
EVC(CAD bTDC)	22
Speed(RPM)	1000
Fuel mass(mg/cyc)	19.5
λ(-)	1.01

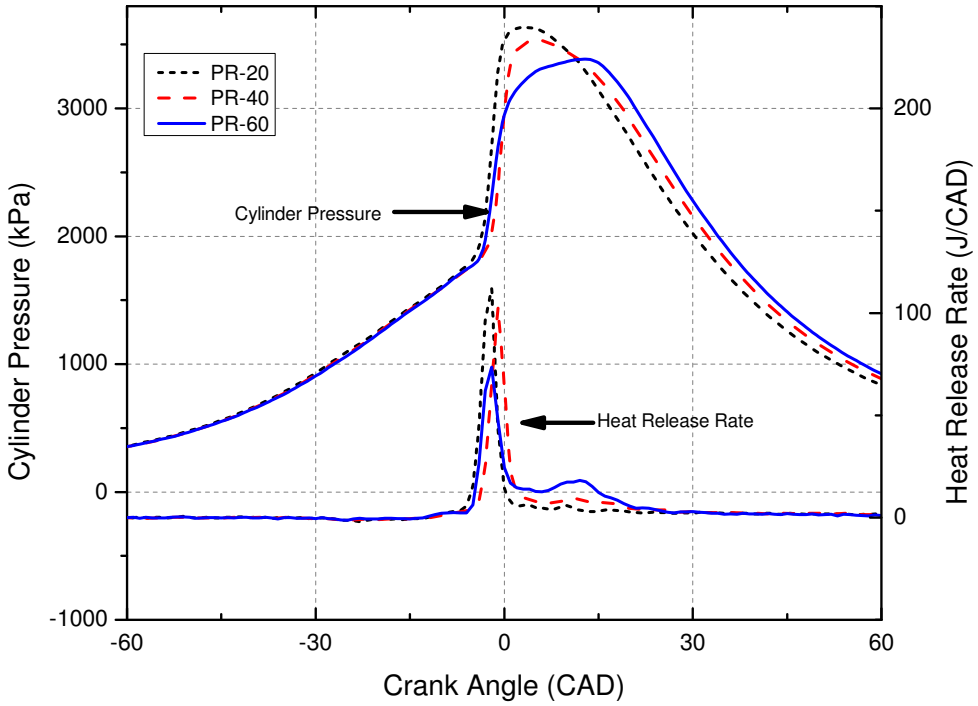

Figure 3.13: Pressure and heat release rate plots for PR-20, PR-40 and PR-60 at 1000 RPM

With increase in ignition delay CA50 gets retarded as well. This can be seen from Fig. 3.14(c). As PR increases from 20 to 60, CA50 gets retarded from -3 CAD to 3 CAD. This ease of control over combustion phasing with variation in PR makes the RCCI more advantageous compared to other LTC modes. The amount of direct injected fuel can be varied and also the injection timing can be controlled which is the major advantage over HCCI and PCCI. These trends were also observed in CFD modelling of RCCI combustion previously done by Nazemi [65].

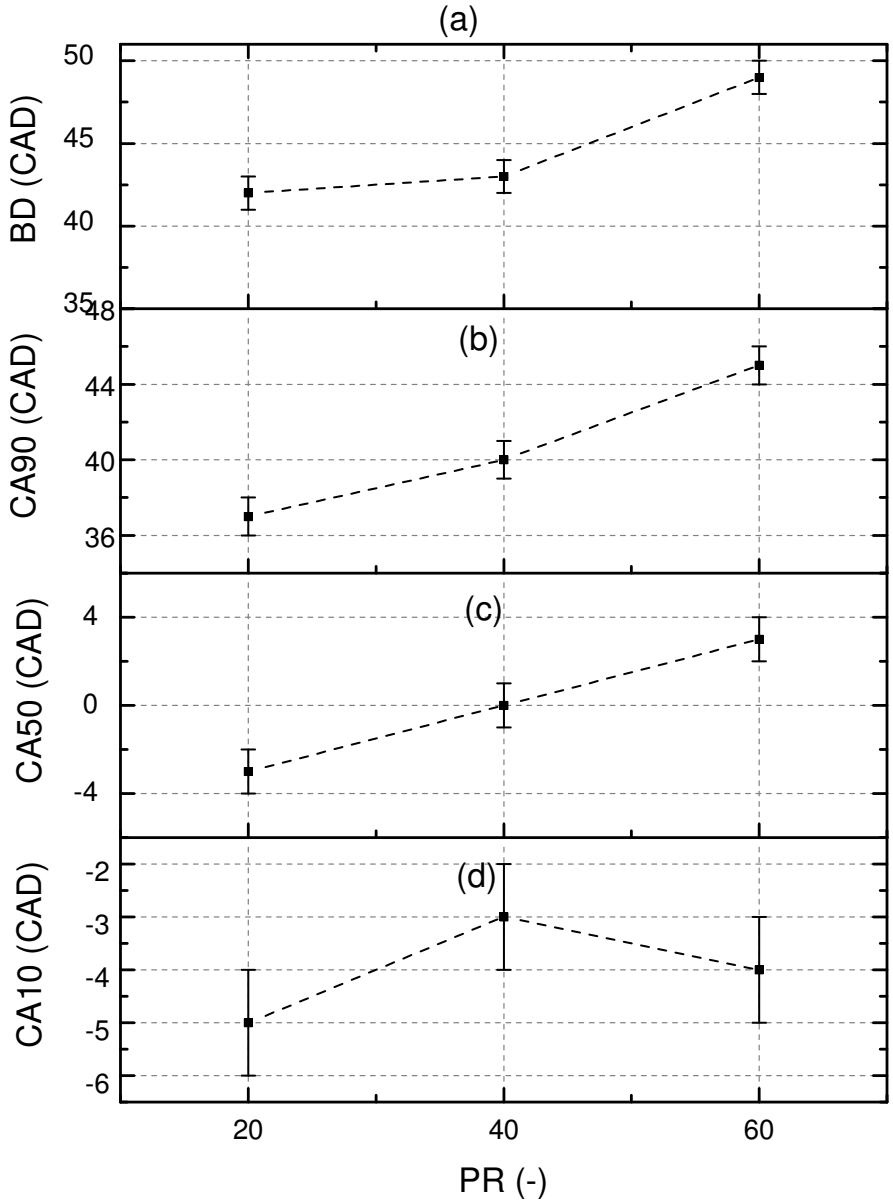

Figure 3.14: Effect of PR on RCCI combustion timings

It can also be observed from Fig. 3.13 that with increase in PR, a small heat release region starts developing after the main stage heat release. This can be due to late

combustion of extra gasoline present at higher PR values. This effect is seen at higher intake temperatures (80°C in this case) which improves the auto-ignition characteristics resulting in late combustion of iso-octane. The burn duration also gets delayed due to prolonged combustion which can be seen from Fig. 3.14(a)

As seen from Fig. 3.15(d) with increase in PR, IMEP increases as well. IMEP can be directly related to the area under pressure-volume diagram. Since the area increases with PR, it is expected the same trend with IMEP as well. With further increase in PR, it may lead to misfire/partial burn due to insufficient amount of higher reactive fuel. The combustion efficiency generally drops with higher amount of iso-octane because the amount of HC and CO emissions increase as they cannot be converted fully into their respective products [65]. But here due to higher intake temperatures these are getting oxidized and combustion efficiency increases with increase in PR.

Maximum pressure rise rate (MPRR) which is related to the tendency of knocking also decreases with increase in PR. As seen in Fig. 3.13 the pressure drops with increase in PR which also reduces high peak rise rate. This trend can be seen in Fig. 3.15(a)

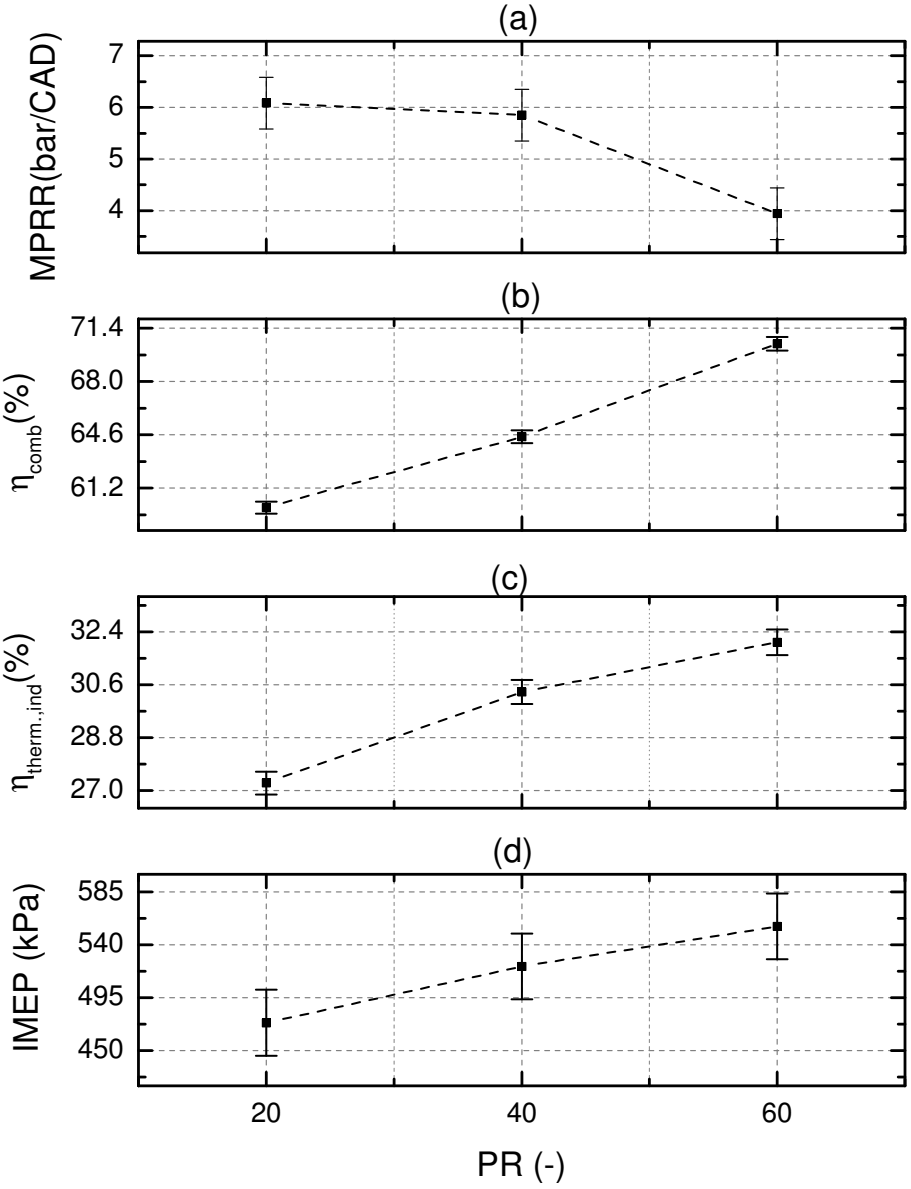

Figure 3.15: Effect of PR on RCCI performance metrics

3.3.3 Effect of Intake Temperature

In order to investigate the effect of intake temperature on combustion phasing, temperature sweep was done at three different intake temperatures. Fig. 3.16 shows pressure and heat release rate traces for varying intake temperatures of 40°, 60°and 80°C. The other operating parameters PR, SOI and RPM were kept constant and are shown in Table 3.4.

Table 3.4
Operating conditions for intake temperature parametric study

Parameter(Units)	**Operating conditions**
T_{in}(°C)	40-60-80
PR(-)	40
SOI(CAD bTDC)	40
P_{in}(kPa)	95-Naturally aspirated
Speed(RPM)	1000
IVO(CAD bTDC)	25.5
EVC(CAD bTDC)	22
Fuel mass(mg/cyc)	28
λ	1.01

RCCI combustion is sensitive to the properties at IVC since the combustion is predominantly controlled by the auto-ignition. Increase in intake temperature mainly affects the intake charge properties at IVC which accelerates the RCCI thermo-reactions [61]. Since the combustion happens at faster rate with increase in intake temperatures, the ignition delay reduces and the auto ignition will happen early. This advances the combustion and CA50 as well. Peak pressure and heat release rates also increase due

to rapid chemical reactions occurring at nearly constant volume inside the cylinder.

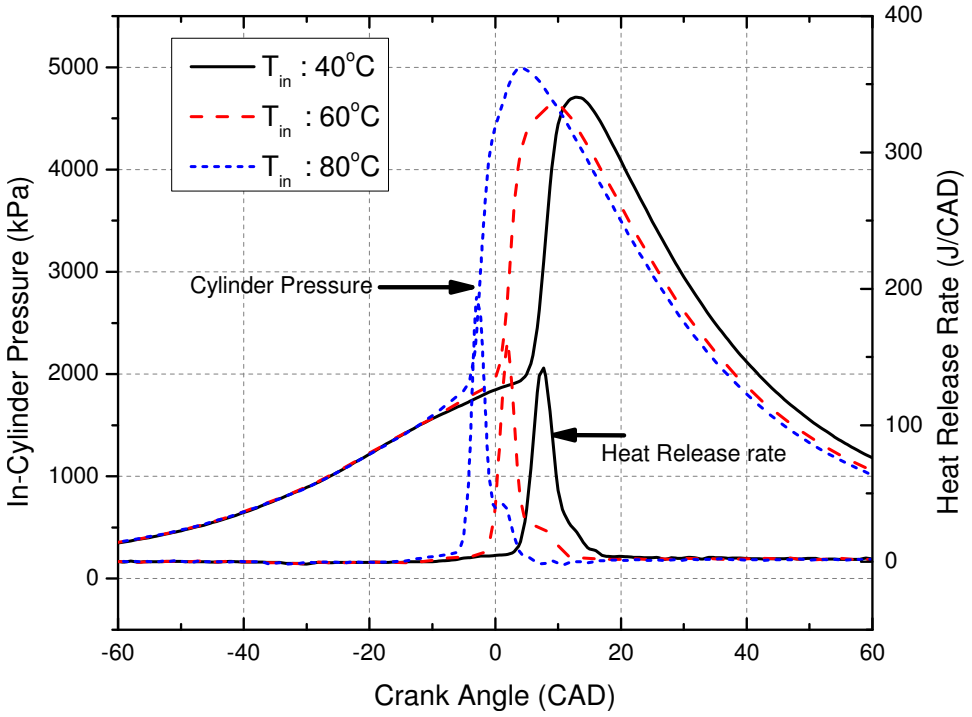

Figure 3.16: Pressure and heat release rates for three different intake temperatures at 1000 RPM

With higher intake temperatures, the vaporization of the higher reactive fuel, which is injected from DI injectors also increases. This leads to better mixing which reduces reactivity gradient and local equivalence ratios. Ignition delay increases with decrease in local ϕ [64]. This should retard the combustion phasing. But the effect of rapid chemical kinetic reactions predominate this effect leading to advancing combustion phasing [61, 62]. This can be seen from Fig. 3.17.

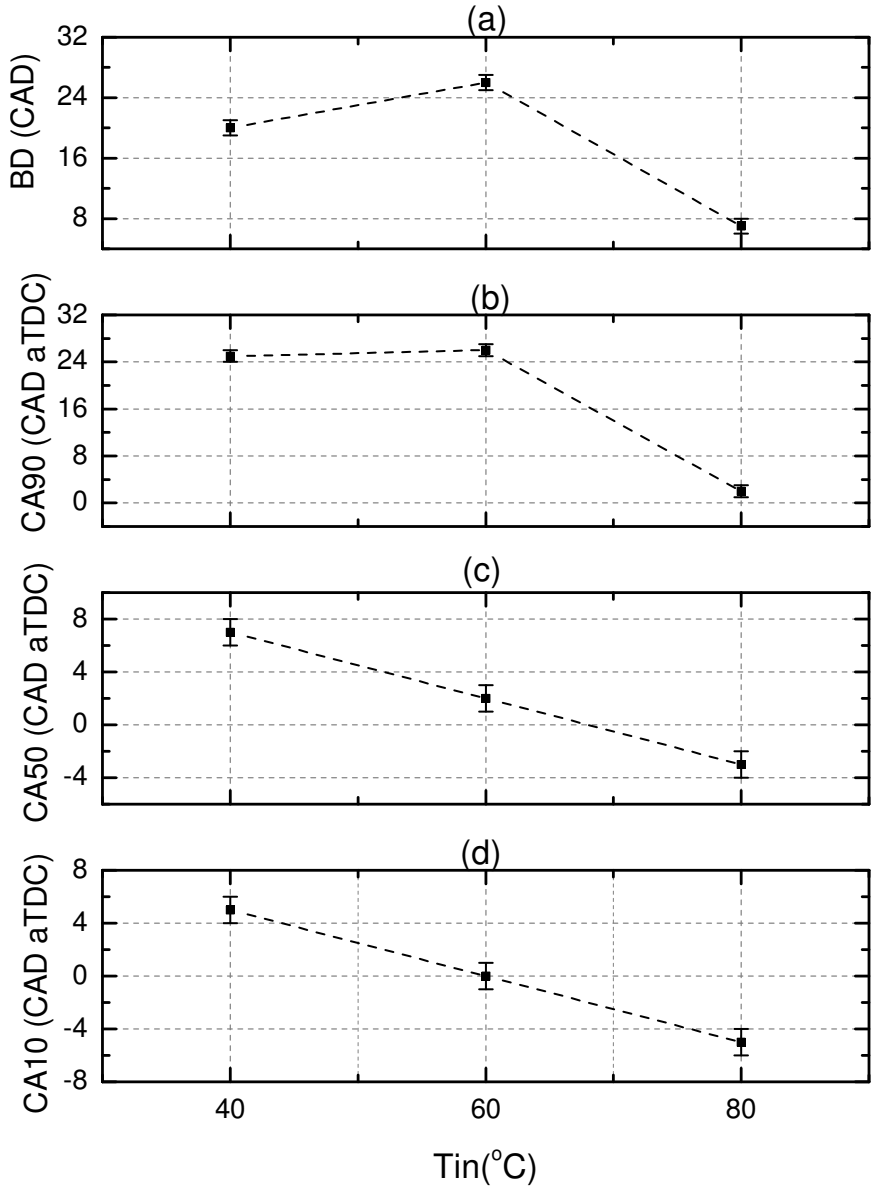

Figure 3.17: Effect of intake temperature on RCCI combustion timings

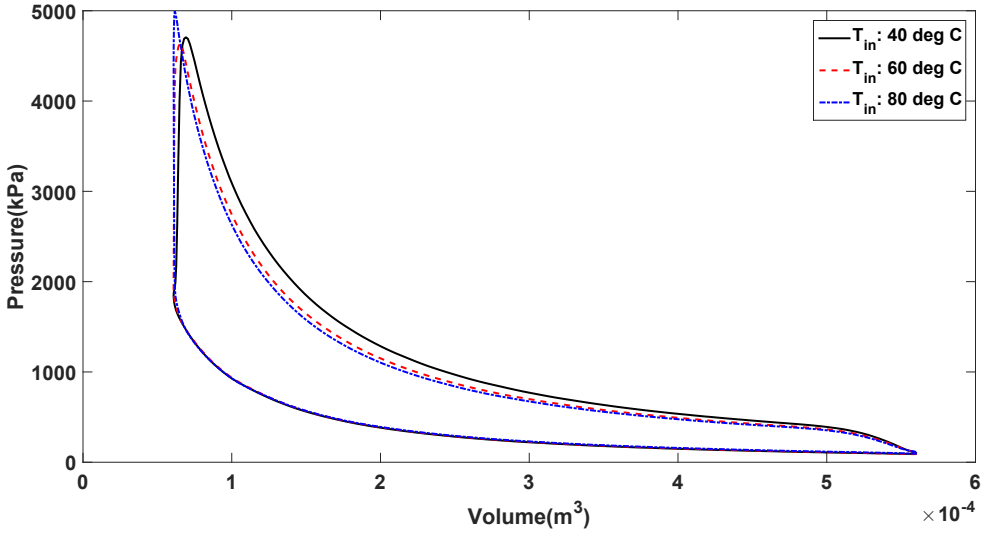

Figure 3.18: Pressure vs Volume curves for different intake temperatures.

As seen from Fig. 3.18 that even though the peak pressures increase with increase in temperature the PdV work, i.e. the area under the pressure-volume diagram, decreases. Also, the ratio of specific heats decrease with increase in intake temperature [68] leading to lesser work during expansion stroke. This explains why IMEP in Fig. 3.19(d) decreases. ITE also follows the same trend which can be seen in Fig. 3.19(b). Increase in MPRR in Fig. 3.19(a) can be attributed to increase in peak pressures in Fig. 3.16.

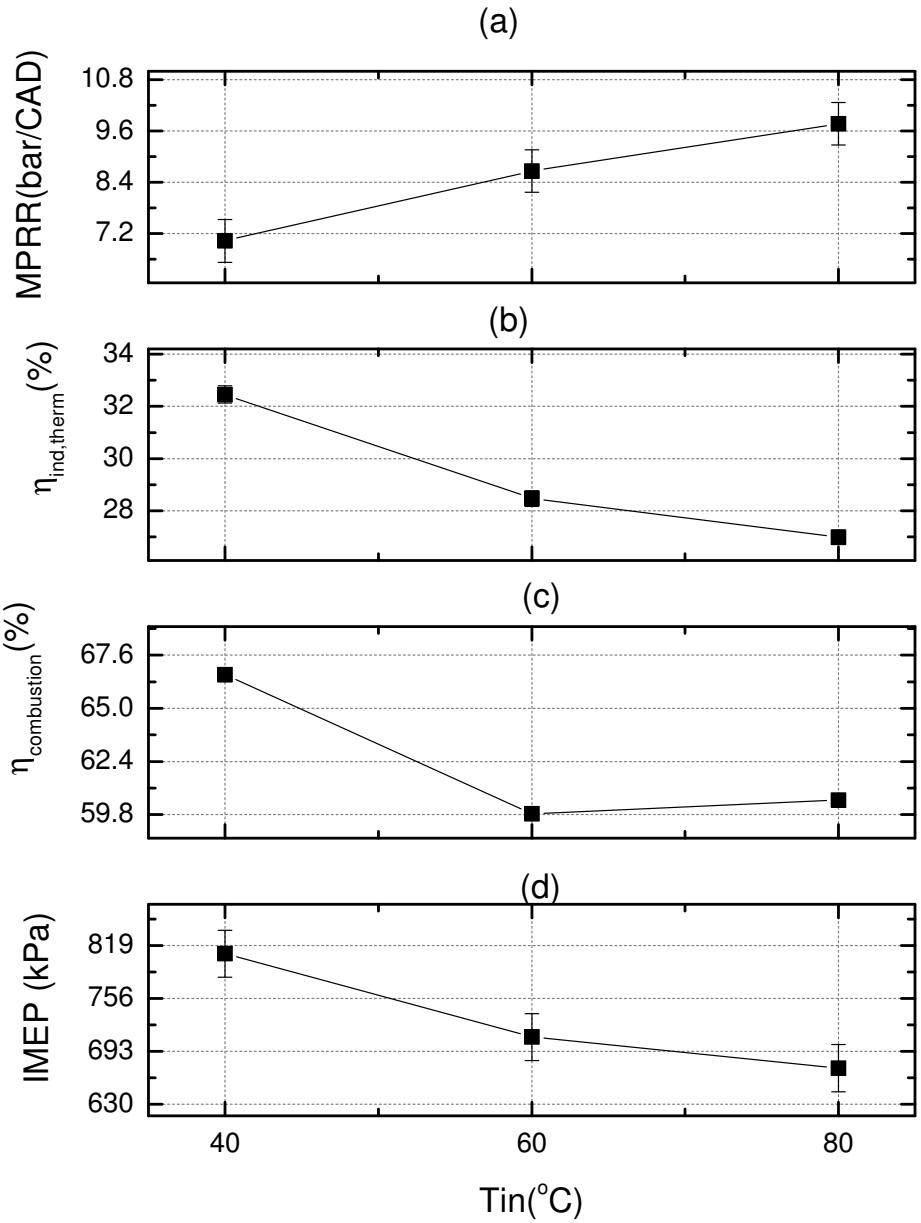

Figure 3.19: Effect of intake temperature on RCCI performance metrics

3.3.4 Characterization Map for Two-Stage Heat Release

RCCI combustion is a stratified combustion of both high and low reactive fuels. RCCI provides control over both ϕ and reactivity stratification of charge inside the cylinder by controlling both PR and SOI which are not available in single-fuel HCCI. Start of combustion primarily depends on SOI of n-heptane from direct injection, PR of the mixture, intake temperature and pressure of the air charge. Heat release can happen either in two stages or single stage depending upon the combination of these control parameters. This section focuses on the probability of getting two-stage heat release and it's associated operating conditions.

Two stage heat release consists of Low Temperature Heat Release (LTHR) region along with the main stage heat release, also called High Temperature Heat Release (HTHR). This was already observed in previous Fig. 3.10 with variation of SOI timing. Also, Fig. 3.20 explain the growth of LTHR with variation of SOI and PR. Wholestage refers to complete HRR and 10% heat release of complete HRR is defined as CA10. It is seen that with advancing SOI and reducing PR we can expect a significant two-stage heat release. As per Kokjohn [9] LTHR is mainly due to decomposition of n-heptane. The earlier the SOI, the more premixing of fuel will occur and the more the possibility of decomposition of n-heptane. As seen in Fig. 3.10 the difference between CA10 (wholestage) and SOC (mainstage) increases with advancing SOI and

lower PR. Increase in $|CA10 - SOC|$ implies that there is development of two-stage heat release with LTHR [67].

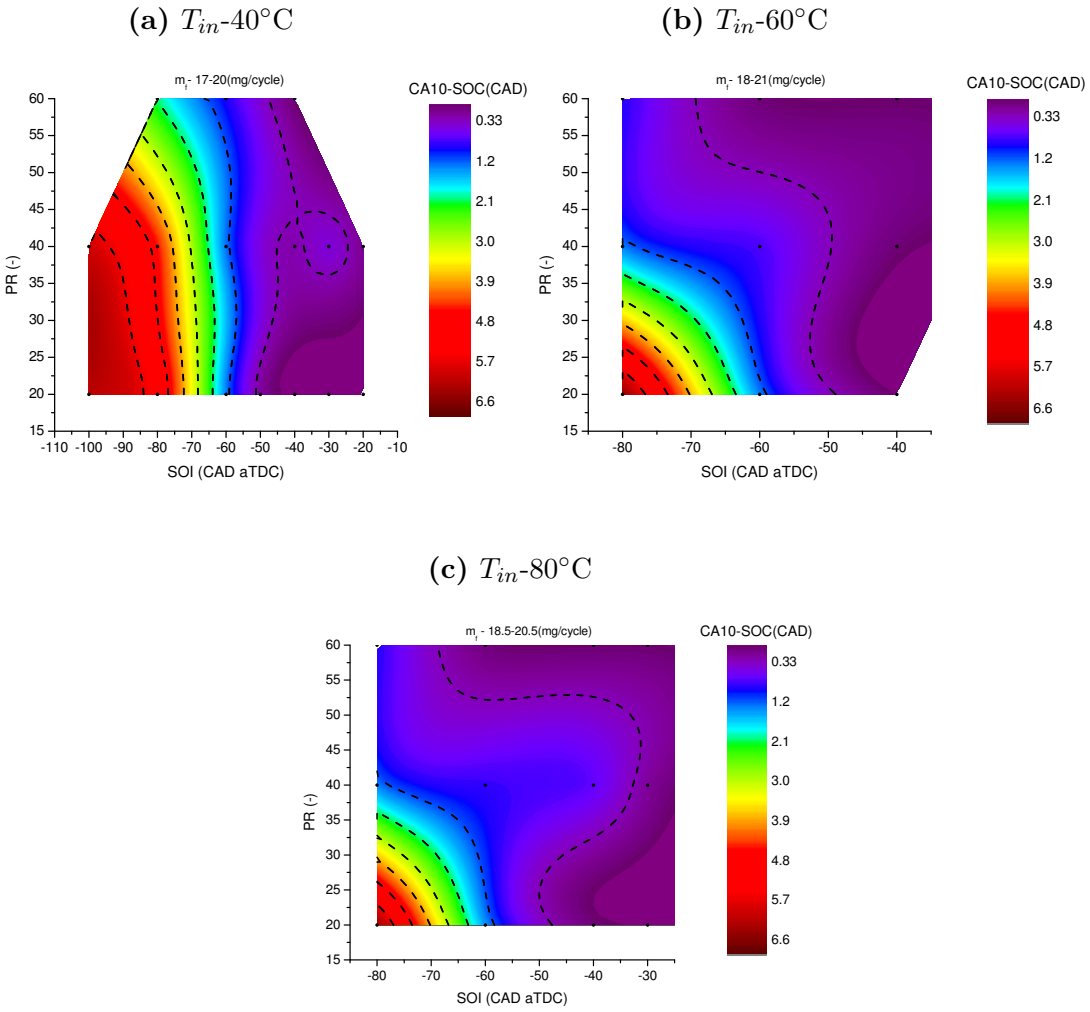

Figure 3.20: Difference between mainstage and whole stage characterized by the difference between CA10(wholestage) and SOC(mainstage).

3.3.5 Combined Effect of SOI, PR and Intake Temp. on Combustion Phasing

Control of combustion phasing is the primary objective of this work. For that, we need to know the operating region where the engine should be operated in order to maintain desired combustion phasing. CA50 is a robust indicator of combustion phasing [69] Fig. 3.21 shows the variation of mainstage CA50 with respect to PR, SOI and T_{in}. This will be helpful in designing a real time combustion controller which provides information about the input parameters in order to maintain desired CA50. As it is seen in Fig. 3.11 by advancing SOI, CA50 initially advances but with further advancing SOI, CA50 will slowly start retarding. This can be seen from Fig. 3.21a. It is also seen in Fig. 3.14 that increasing PR will retard CA50. It is the same trend with T_{in} as well. Fig. 3.21 also provides a summary of the parametric studies (Section 3.3)for CA50 with respect to individual control parameters.

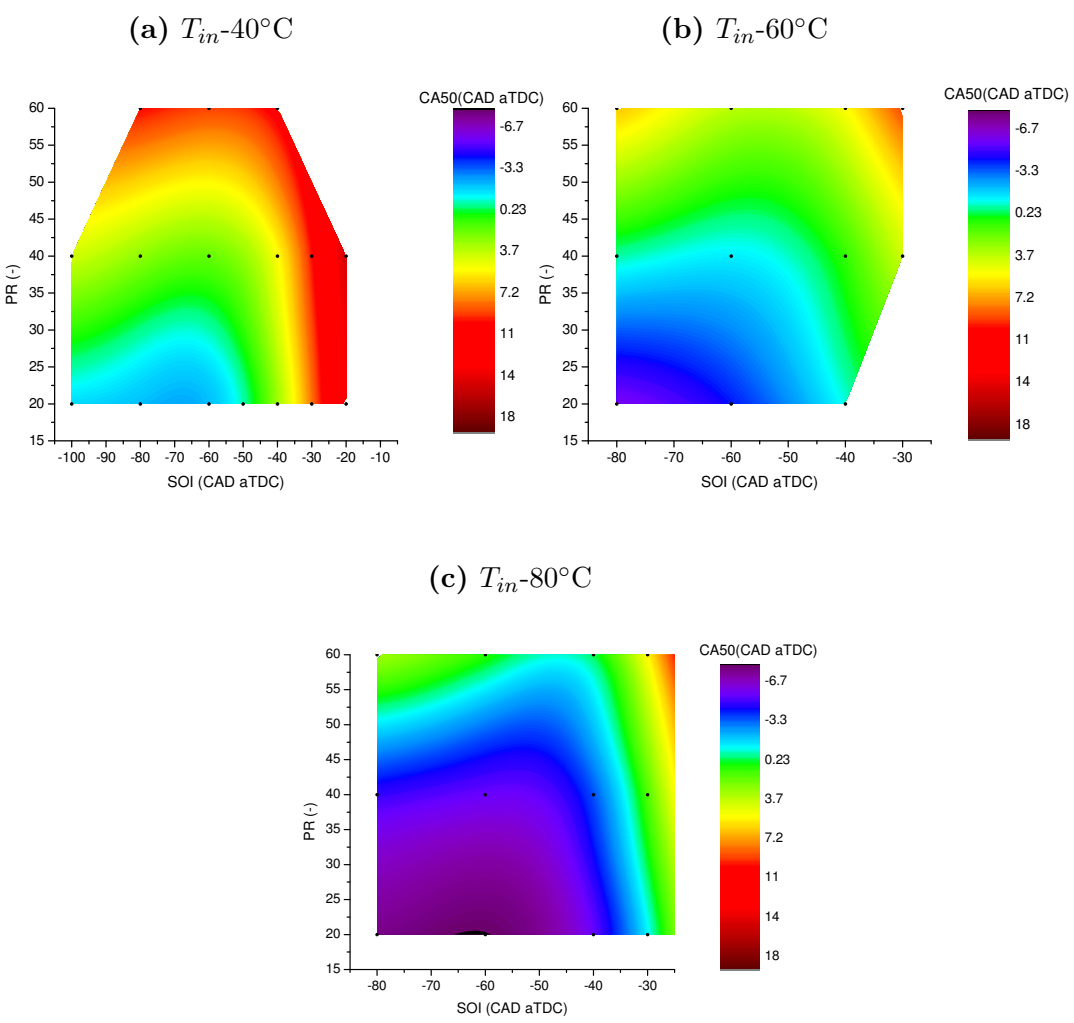

Figure 3.21: CA50 operating map as a function of SOI and PR at different intake temperatures

Chapter 4

Mean Value Modelling of RCCI Combustion Phasing

4.1 Modelling Introduction

Various models ranging from complex CFD models [9, 63, 70] and multi-zone models [41, 71] to simpler control-oriented models (COMs) [39, 41] have been proposed for modelling combustion phenomenon in RCCI engines. Since this work focuses on implementing real-time model-based controller, the model chosen should be accurate enough to predict combustion phasing with low computational effort. There should be a compromise between accuracy and computational time of the model. Complex

CFD models provide more accurate prediction than the other models, but they require high computational effort which renders them impractical for real time control. Research studies on HCCI [14, 16, 21] and RCCI [39] proved that COMs can predict combustion phasing with reasonable accuracy and also with low computational time which makes them suitable for implementing in real-time controllers as well. Also, most of the studies on COMs in LTC strategies were done on HCCI combustion for controlling combustion phasing. There are very few COMs available for predicting combustion phasing in RCCI engines. A control model for RCCI was developed by Sadabadi [39] to predict combustion phasing and burn duration. The previous COM [39] was based on numerical simulations using KIVA CHEMKIN rather than experimental investigation. In addition, the COM in [39] was parametrized only for the variation in PR. The current study is based on experimental study and a new COM is developed to capture the effects of both SOI and PR.

COMs can be classified into two categories based on the operating mode [21]. The first category predicts combustion phasing for steady-state operation. The models in the first category provide mean-value combustion phasing using measurable input parameters. For simpler approach, static-look up tables were used to predict combustion parameters [41] by mapping the engine over various operating ranges. This requires tedious experimental work and may not work outside the mapping region. Next, various autoignition models were developed for compression ignition combustion to predict start of combustion. These models are summarized in Fig. 4.1 which

shows separately for HCCI, conventional CI and RCCI engines. This work builds upon the Modified Knock Integral Model (MKIM) developed in [39]. The second category deals with transient operation which includes various dynamics involved from cycle to cycle. These models will help in cycle-to-cycle control of RCCI combustion while switching between different operating regions and also help in transition between RCCI to SI or CI operation [21]. The dynamic model will be discussed more in the Chapter 5.

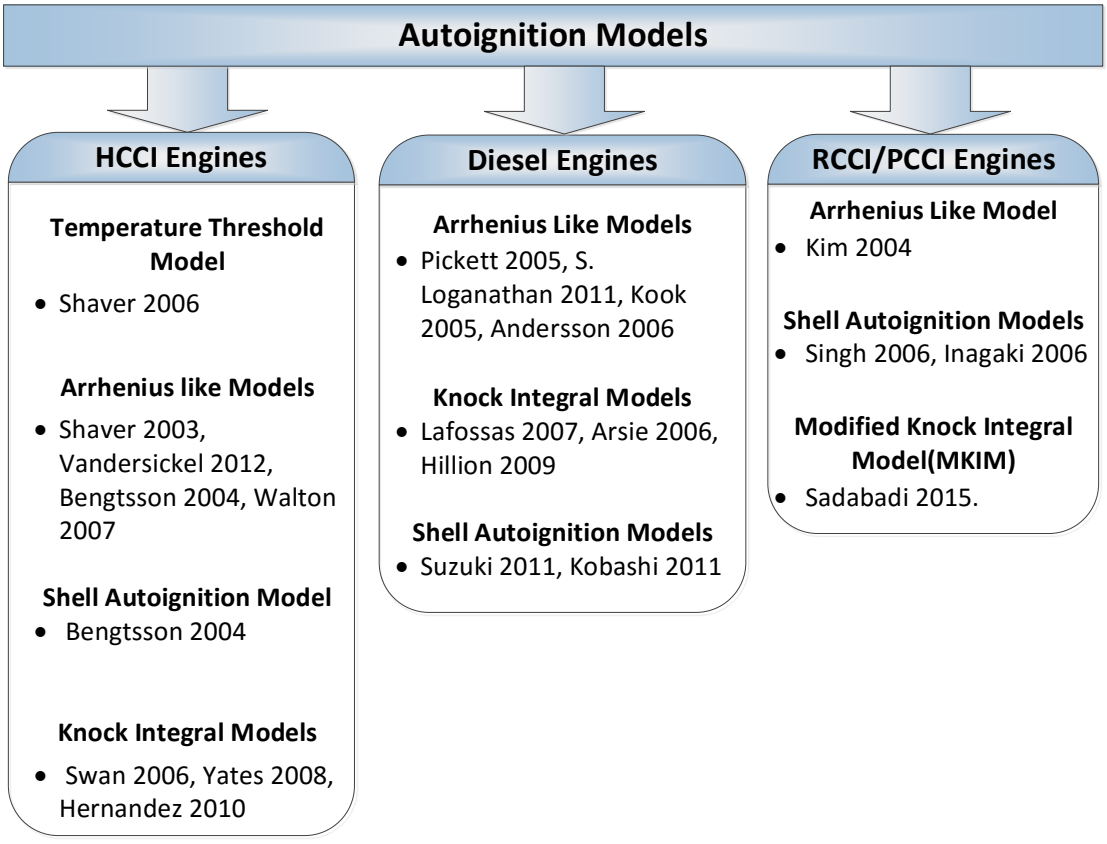

Figure 4.1: Mean value control-oriented Autoignition models for compression ignition engines

This chapter explains about the mean-value models (MVMs) developed for predicting

start of combustion (SOC) and combustion phasing (CA50) for the RCCI engine in this thesis. Fig. 4.2 shows an overview of submodels used for predicting combustion phasing for a given operating condition. The MKIM model requires measurable input parameters and also properties at IVC. Since the properties at IVC are difficult to measure directly, they are estimated using measurable parameters at intake manifold by using a correlation. MKIM then predicts SOC using the available input parameters. Finally, CA50 is predicted using a fuel burn rate model [21] with the help of predicted SOC. The following sections explain further about these models.

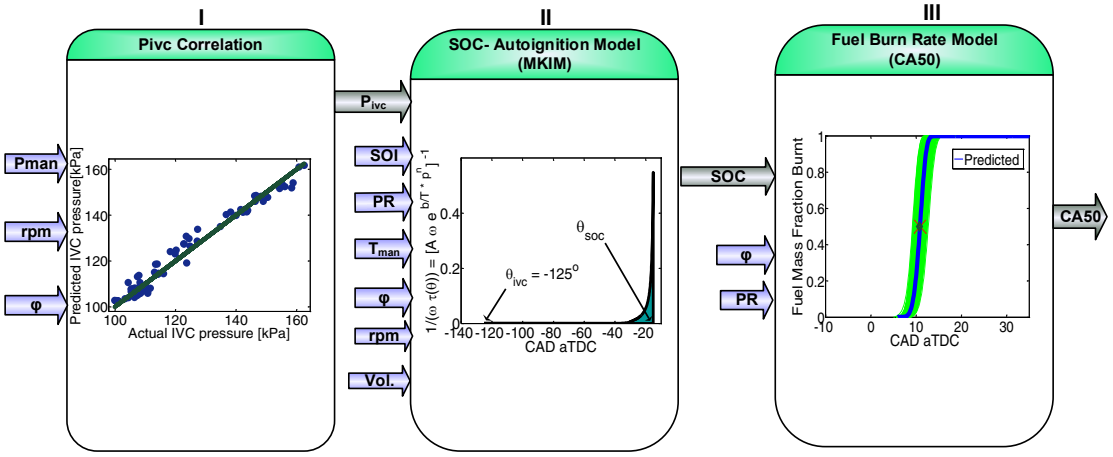

Figure 4.2: Schematic showing mean-value models used for predicting SOC and CA50

4.2 Start of Combustion - SOC

4.2.1 Modified Knock Integral Model - MKIM

MKIM is developed from original Knock Integral Model (KIM) developed by Livengood and Wu for predicting knock in SI engines and later modified for HCCI combustion in [21]. Later it was extended for RCCI combustion by Sadabadi [39]. MKIM predicts SOC for the current cycle by using the available input conditions. The input parameters required for MKIM are PR, SOI, RPM, ϕ, P_{ivc}, T_{ivc} and n_c. The model is divided into two stages for RCCI combustion. The first stage is from IVC to SOI of high reactive n-heptane fuel. The first stage primarily includes the compression of premixed iso-octane fuel. The second stage is from SOI to SOC. SOC occurs due to auto-ignition of the stratified mixture consisting of both n-heptane and iso-octane [9]. This stage is more important as this decides the SOC and further propagation of combustion. SOC mainly depends on amount of reactivity of the mixture which is decided by PR, charge properties at IVC, fuel concentration (ϕ) and also the point at which n-heptane is injected during the compression stroke. The equation to predict SOC is given by [39]:

$$\int_{SOI}^{SOC} \frac{d\theta}{A_2 N\left(\phi_{DI}^{B_{2DI}} + \phi_{PFI}^{B_{2PFI}}\right) exp\left(\frac{\frac{C_2}{CN_{mix}+b}(P_{ivc}v_c^{n_c})^{D_2}}{T_{ivc}v_c^{n_c-1}}\right)} + \int_{IVC}^{SOI} \frac{d\theta}{A_1 N \phi_{PFI}^{B} exp\left(\frac{C_1(P_{ivc}v_c^{n_c})^{D_1}}{T_{ivc}v_c^{n_c-1}}\right)} = 1 \tag{4.1}$$

where A_1, A_2,B_{2DI},B_{2PFI},B,C_1,C_2,D_1,D_2,b are the constants which need to be estimated for the prediction of SOC. Since the sum of the both integrals unite to one, SOC being unknown variable is marked at CAD where the integral reaches to unity.

PR is given by Eq. (4.1). n_c is polytropic compression coefficient which is calculated by taking the slope of compression region for every steady state operating point. The average value is found to be 1.33 from the experimental data used for parametrization. P_{ivc} and T_{ivc} are pressure and temperature at IVC respectively which are estimated using intake manifold conditions. Since for this engine, IVC is 2 CAD before BDC, T_{ivc} is assumed to be the same as the manifold temperature. v_c in the Eq. (4.1) is the ratio of volume at IVC to the instantaneous volume at each given crank angle.

$$v_c = \frac{V_{IVC}}{V(\theta)} \tag{4.2}$$

and ϕ is the global equivalence ratio of combined fuels. Depending on the PR, the total fuel will be distributed into iso-octane and n-heptane. CN_{mix} refers to cetane number of the fuel blend and signifies the reactivity gradient of the mixture after the

injection of DI (n-heptane) fuel. That's why this term is introduced only in the first part of the integral. CN_{mix} is calculated by:

$$CN_{mix} = \frac{\left(FAR_{st,nhep}\phi_{DI}CN_{nhep} + FAR_{st,iso}\phi_{PFI}CN_{iso}\right)}{FAR_{st,nhep}\phi_{DI} + FAR_{st,iso}\phi_{PFI}} \tag{4.3}$$

where $FAR_{st,nhep}$ and $FAR_{st,iso}$; CN_{iso} and CN_{nhep} are stoichiometric fuel-air ratios and cetane numbers of n-heptane and iso-octane, respectively. The equivalence ratios are given by:

$$\phi_{DI} = (1 - PR).\phi \tag{4.4a}$$

$$\phi_{PFI} = PR.\phi \tag{4.4b}$$

Also, since all the experiments were performed at naturally aspirated conditions P_{ivc} doesn't vary much when compared to atmospheric pressure. But for extending the model in future for different speeds and valve timings a correlation is used from Shahbakhti [21] for estimating pressure at IVC which is given by Eq. (4.5).

$$P_{ivc} = \frac{N^{-0.00121}\phi^{0.00223}}{T_{in}^{-0.0019}}.P_{in} \tag{4.5}$$

where N is the engine speed in RPM, T_{in} and P_{in} are temperature (°C) and pressure (kPa) at the intake manifold.

The P_{ivc} equation is parametrized and validated with steady state experimental data. The equation predicts the pressure at IVC with an average error of 0.5 kPa. The parametrization and validation results are shown below in Fig. 4.3 and Fig. 4.4

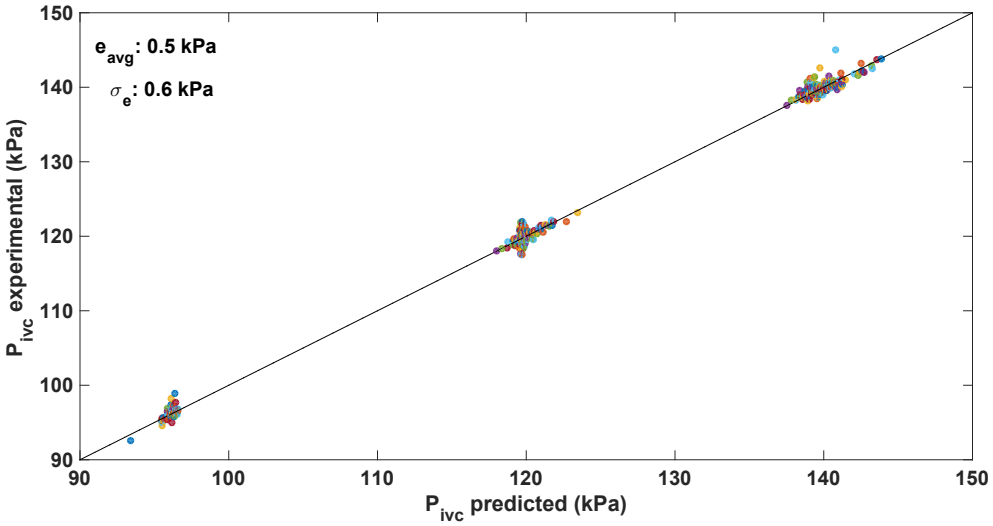

Figure 4.3: Estimation of P_{ivc} correlation using steady state data

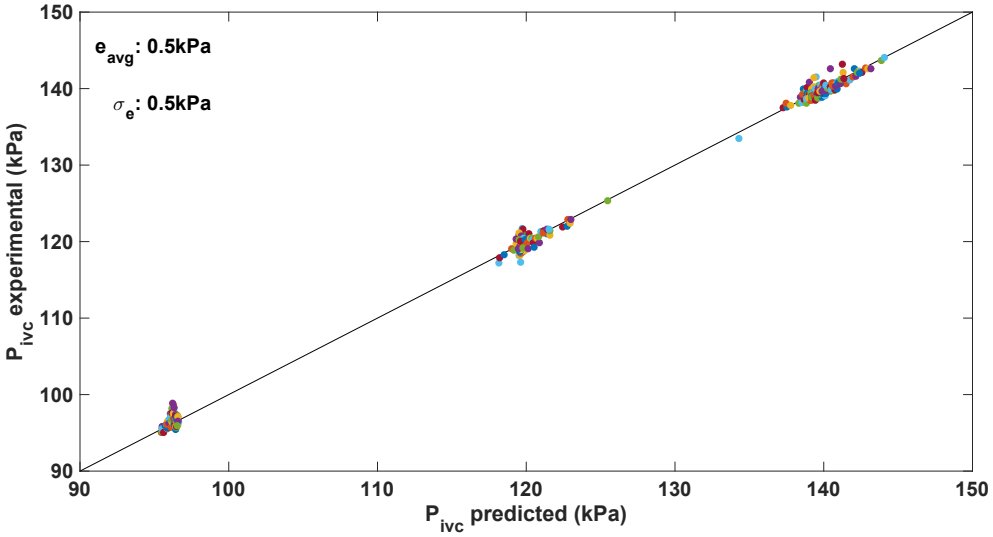

Figure 4.4: Validation of P_{ivc} correlation using steady state data

4.2.2 Parameterization of MKIM

Eq. (4.1) contains constant parameters which need to be estimated for predicting SOC. These parameters are calculated by optimizing the model to reduce the error between experimental and predicted SOC. Since the model should be able to predict SOC at different operating conditions, the experiments were run to obtain sweep of SOI, PR, ϕ and T_{in}. All the experimental data used for parametrization is specified in Appendix Table A.2. The operating conditions used for parameterizing MKIM are given below in Table 4.1. An optimization algorithm called *fminsearch* which is based on Nelder-Mead simplex minimization method [72] is used in MATLAB for parameterizing the model. This algorithm finds optimum parameters for a given model through minimizing the error between experimental and predicted values. For estimation of parameters about half of the steady state experimental data was used covering all the operating regions. The remaining half was used for validation of the model. A step size of 0.1 CAD is used for integrating the model until the integrand value reaches 1.0. The optimized parameters are given in Table 4.2 which are then used for predicting SOC through MKIM.

Table 4.1
Operating conditions for estimation and validation of MKIM model

Parameter [Units]	**Operating value**
PR [-]	20-30-40-60
SOI [CAD bTDC]	20-30-40-50-60
T_{in} [deg C]	40-60-80
λ [-]	2.5-1.0
P_{in} [kPa]	95
IVO [CAD bTDC]	25.5
EVC [CAD bTDC]	22
Speed [RPM]	1000

Table 4.2
Optimized parameters for MKIM model

A_1	B	C_1	D_1	A_2
0.5454	-0.00714	5.0313	-2.8994e-04	0.002526
B_{2DI}	B_{2PFI}	C_2	b	D_2
0.001646	7.41810e-05	1.5642e+06	1.70895e+02	-0.2300

4.2.3 Steady state estimation and validation of MKIM

A total of 54 steady state operating points covering different regions, as shown in Table 4.1, were used for estimating the parameters of MKIM. The model was also validated against 51 operating points which are different from those used for parametrization of the model. The estimation and validation results are shown in Fig. 4.5 and Fig. 4.6, respectively. It can be seen that model is predicting SOC within 2.0 CAD as compared to experimental data. The diamond symbol in Fig. 4.5 refers to the

experimental average value of SOC for 100 cycles while the blue cross indicates the model predicted SOC.

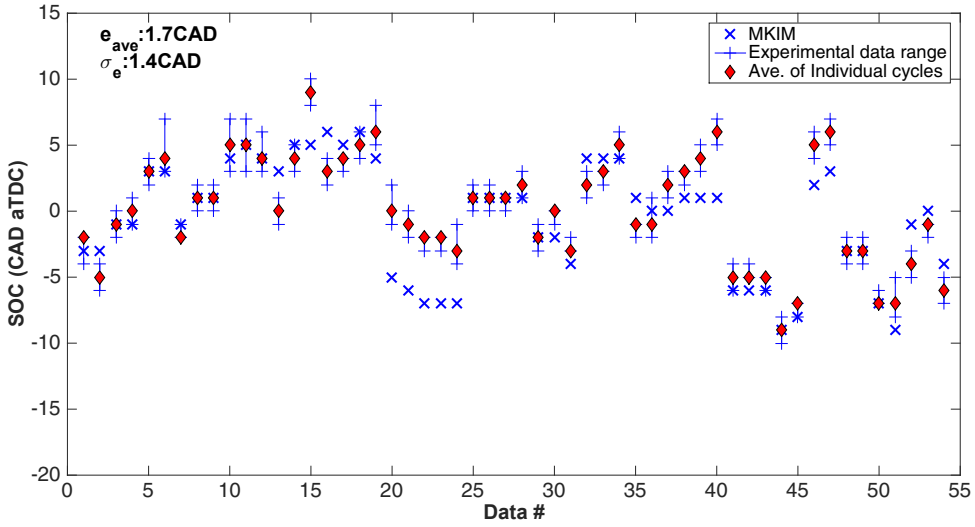

Figure 4.5: Estimation of MKIM using 54 steady state operating points

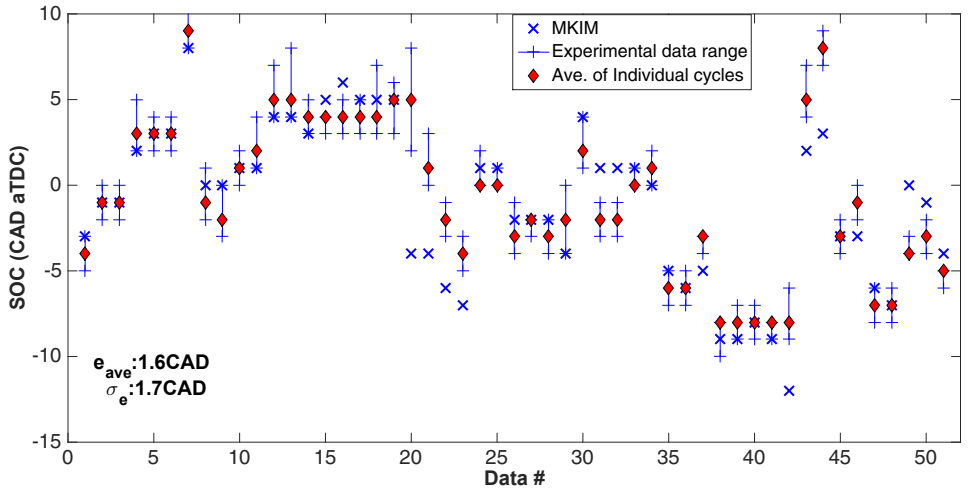

Figure 4.6: Validation of MKIM for 51 steady state operating points that were not used to parametrize the model

4.3 Combustion Phasing (CA50) Model

4.3.1 CA50 model description

The main objective of developing a control-oriented model in this thesis is to control combustion phasing, i.e. CA50 (crank angle by which 50% fuel is burnt), for this engine. Since different combustion durations can happen with the same SOC, prediction of SOC is not sufficient for model-based control of RCCI combustion [21, 39]. CA50 acts as a robust feedback indicator for HCCI combustion [69]. Since, RCCI also follows similar combustion phenomenon with an added control knob of SOI timing, CA50 is selected as the main parameter for analyzing combustion performance of the engine in this thesis.

Shahbakhti [21] developed a model for predicting combustion phasing for HCCI combustion. It is a modified Weibe function which is used for finding fuel burn fraction (x_b) and predicting CA50. In this work, it is modified for RCCI combustion by including fuel stratification from both PFI and DI fuels. This modified model is used for predicting CA50.

$$x_b(\theta) = 1 - exp\bigg(- A\bigg[\frac{\theta - \theta_{soc}}{\theta_d}\bigg]^B\bigg) \tag{4.6}$$

where, θ_{soc} is SOC predicted from the MKIM. θ_d is given by Eq. (4.7).

$$\theta_d = C(1 + X_d)^D.(\phi_{DI}^E + \phi_{PFI}^F) \tag{4.7}$$

where, X_d is the dilution fraction which accounts for the EGR and residual gases. ϕ_{DI} and ϕ_{PFI} are already specified in Eq. (4.4).

The model outputs the θ_{CA50} value when fuel burn fraction (x_b) reaches 0.5 in Eq. (4.6).

4.3.2 Parametrization of CA50 model

The equations (4.6) and (4.7) need to be parametrized in order to find the constant parameters A, B, C, D, E and F which are necessary for predicting CA50 using this model. About half of the data is used for determining the model parameters. The same algorithm, using the Nelder-Mead Simplex minimization method [72], is used. The same operating conditions and experimental data that are used for parameterizing the MKIM model are used for CA50 model too. The optimized parameters are given in Table 4.3.

Table 4.3
Optimized parameters for CA50 model

A	B	C
0.18760	14.11901	2.0849
D	E	F
0.2551	0.4141	0.18448

4.3.3 Steady state estimation and validation of CA50 model

Fig. 4.7 and Fig. 4.8 show both estimation and validation results of predicting CA50 using the CA50 model. It can be seen that the model predicts CA50 with sufficient accuracy as the average error and standard deviation are 1.5 CAD and 1.2 CAD respectively when compared to experimental CA50. This shows that developed model can predict CA50 for any given operating conditions with a minimal error. This helps in analyzing experimental trends of RCCI engine for varied operating conditions.

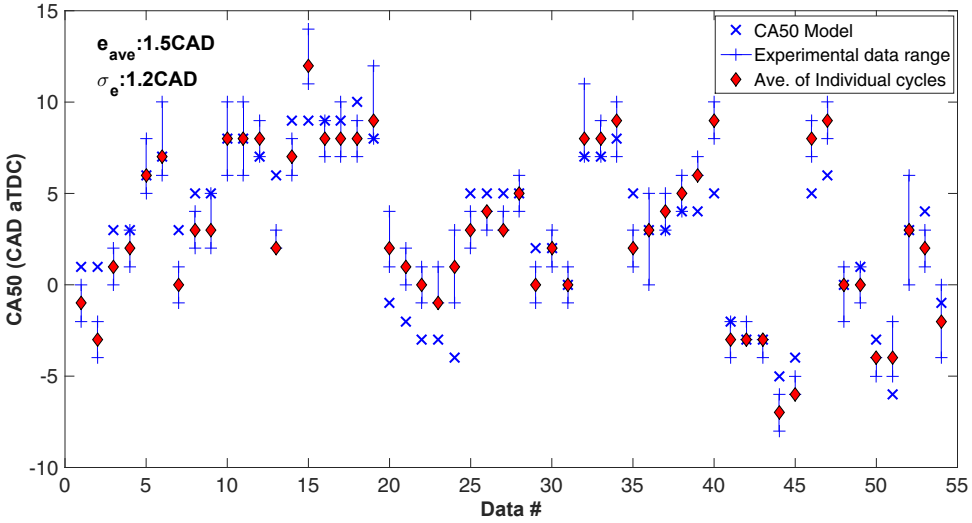

Figure 4.7: Estimation of CA50 model using 54 steady state operating points

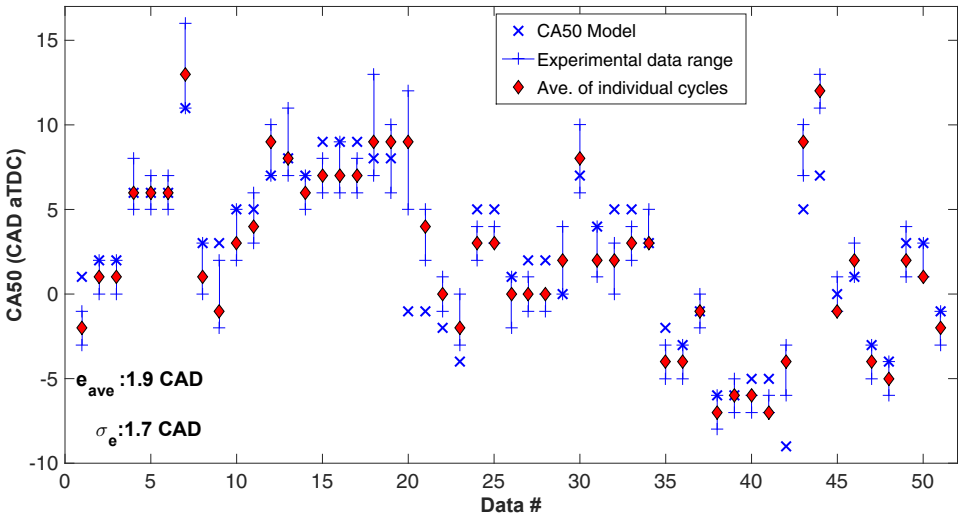

Figure 4.8: Validation of CA50 model for 51 steady state operating points that were not used to parametrize the model

4.4 Effect of Individual Parameters

Test cases are developed using the MKIM and CA50 optimized parameters in order to study the trends and variations in SOC and CA50 with respect to PR, SOI, T_{ivc}, ϕ_{DI}, ϕ_{PFI}, ϕ and compare with the experimental trends for validating the models. All the cases are shown in Table 4.4. The test cases are developed to investigate the effect of each individual parameter by fixing all the other parameters as constant. This will provide an insight of how each individual parameter affects the SOC and CA50. This also gives a proof that whether the model trends are in agreement with the experimental trends observed in Chapter 2 or not. In this way, we can confirm that these models can be used for predicting the real time combustion with the given input parameters. The trends are shown in Fig. 4.9.

Table 4.4
Test cases for validation of MKIM and CA50 models

Cases	Case-1	Case-2	Case-3	Case-4	Case-5	Case-6
Speed[RPM]	1000	1000	1000	1000	1000	1000
P_{ivc}[kPa]	95	95	95	95	95	95
T_{ivc}[K]	310	310	310	310	310	**280-380**
ϕ_{DI}	**0.1-1.5**	0.6	(1-PR)ϕ	(1-PR)ϕ	0.6	0.6
ϕ_{PFI}	0.4	**0.1-1.5**	PR.ϕ	PR.ϕ	0.4	0.4
ϕ	$\frac{\phi_{PFI}}{PR}$ or $\frac{\phi_{DI}}{1-PR}$	$\frac{\phi_{PFI}}{PR}$ or $\frac{\phi_{DI}}{1-PR}$	**0.05-1.5**	$\frac{\phi_{PFI}}{PR}$ or $\frac{\phi_{DI}}{1-PR}$	0.6	$\frac{\phi_{PFI}}{PR}$ or $\frac{\phi_{DI}}{1-PR}$
PR [-]	$\frac{\phi_{PFI}}{\phi_{PFI}+\phi_{DI}}$	$\frac{\phi_{PFI}}{\phi_{PFI}+\phi_{DI}}$	40	**20-80**	$\frac{\phi_{PFI}}{\phi_{PFI}+\phi_{DI}}$	$\frac{\phi_{PFI}}{\phi_{PFI}+\phi_{DI}}$
SOI[CAD bTDC]	40	40	40	40	**20-100**	40

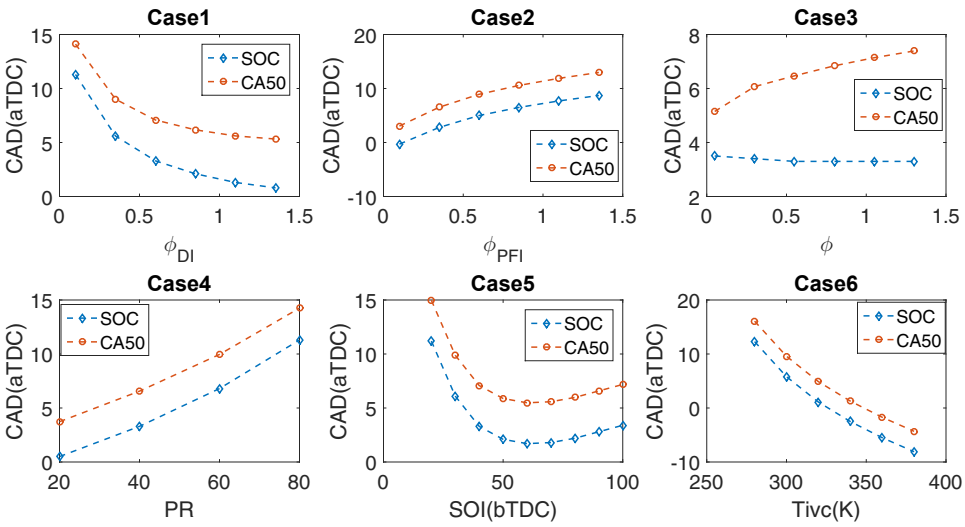

Figure 4.9: Effect of individual parameters on SOC and CA50

As it is seen from Fig. 4.9, for Case-1 with increase in ϕ_{DI}, the SOC and CA50 get advanced, as expected since with increase in high reactive fuel quantity, the mixture gets more reactive and auto-ignition happens earlier. Whereas this trend will be opposite in Case-2 with increase in ϕ_{PFI} . In the current engine setup we have control over total fuel quantity rather than the individual fuels. Depending on the PR ratio, the individual quantity of fuel to be injected will be decided. So it is seen from Case-3 that with constant PR and SOI, increase in equivalence ratio is not affecting much on SOC and a gradual retard in CA50. This may be possible since the PR is kept constant, the reactivity of the mixture also will be constant which doesn't advance or retard the auto-ignition timing.

But as it is seen from Case-4, with increase in PR, SOC and CA50 also get retarded.

This trend is also observed in the experimental results in Section 3.3.2. This is seen because with increase in PR, the ratio of iso-octane injected with respect to n-heptane will increase which decreases the reactivity of the mixture. This increase the ignition delay resulting in retarded SOC and CA50.

As seen in Case-5, with advanced injection of n-heptane, the combustion becomes more premixed and this leads to development of two-stage heat release gradually. SOC which is defined as CA10 of main stage advances initially but after certain point it starts retarding. This is possible since with earlier injection of DI fuel the mixture gets more homogenized and less reactive which leads to increase in ignition delay. This trend is also seen in Section 3.3.1 for the studied experimental results.

Case-6 shows the effect of T_{ivc} on combustion phasing. In this work, as it is said there is no external EGR and internal residuals are kept low. The temperature at IVC can be increased by increasing the intake manifold temperature. As we saw in Section 3.3.3 that with increase in intake temperature, the in-cylinder gas temperature increases and the reactions between oxygen and hydrocarbon molecules gets more accelerated [61] which advances the auto-ignition timing. So the model also confirms the trend we have observed in the experimental results.

With above models confirming the trends observed with respect to experiment results, these models can be used for developing a full plant RCCI model to track the combustion for every engine cycle and at varying operating conditions.

Chapter 5

Dynamic Modelling of RCCI Combustion

As it was discussed in Chapter 4 that in order to develop a COM for transient conditions, all the combustion events from IVO to EVC should be taken into consideration. Also, various engine dynamics such as fuel transport dynamics in the intake port, actuator dynamics, residual gas dynamics should be considered in order to develop a detailed physical dynamic plant model. In this chapter, the mean value models developed in Chapter 4 were combined with other physics-based equations in order to complete the whole engine operating cycle. The cycle-to-cycle thermal coupling was included by incorporating residual gas dynamics. The other dynamics were not considered at this point but need to be included in the future model.

5.1 Dynamic COM for RCCI engine

5.1.1 Intake Stroke ($IVO \rightarrow IVC$)

Properties at Inlet Valve Closing (IVC)

Mixture pressure at IVC, i.e. P_{ivc}, is estimated using Eq. (4.5) [21] which was discussed in the previous chapter. T_{ivc} is assumed to be equal to the intake manifold temperature (T_{in}) since IVC is 2 CAD before BDC. Also, the other input parameters that need to be provided for completing a full engine cycle are engine speed (RPM), total mass of fuel injected (m_{fuel}), premixed ratio (PR), start of injection (SOI) and exhaust pressure (P_{exh}). Since the mean-value model requires equivalence ratio (ϕ) instead of m_{fuel}, a constant air flow rate (m_{air}) is assumed based on the steady state data. This is because, the speed is maintained constant at 1000 rpm with full throttle open with no supercharging and also the cam timing is fixed. A conversion will be done using m_{air}, m_{fuel} and $(A/F)_{st}$ to obtain ϕ. The exhaust pressure is taken as the mean value of the pressure at EVC from the experimental data. The index $i+1$ denotes the current engine cycle and the index i denotes the previous engine cycle.

Mixing Temperature at IVC

Residual gases create a thermal coupling between the previous cycle and the current

cycle. The temperatures of residual gases at the end of exhaust valve closing (EVC) for the previous cycle affect the fresh charge temperature at IVC for the current cycle. Since the temperature at IVC affects the combustion phasing, as seen before in Section 4.4, the mixing temperature at IVC should be estimated for every cycle which is given by Eq. (5.1). This type of cycle-to-cycle dynamics is commonly seen in HCCI combustion modelling [73].

$$T_{mix,i+1} = (1 - X_{rg,i}).T_{ivc,i+1} + X_{rg,i}.T_{rg,i} \tag{5.1}$$

where X_{rg} is the residual gas mass fraction. $T_{rg,i}$ is the temperature of residual gases of the previous cycle. In order to initialize the dynamic COM, an initial guess for T_{rg} is assumed to solve for the equations. For the residual gas fraction, the initial value is obtained using residual gas estimation model developed by Cavina [74] and is given by Eq. (5.2).

$$X_{rg} = \overbrace{\sqrt{\frac{1}{C}}.\frac{\pi.\sqrt{2}}{360}.\frac{r_c - 1}{r_c}.\frac{OF}{N}\sqrt{\frac{R.T_m|P_{exh} - P_m|}{P_{exh}}}.\left(\frac{P_{exh}}{P_m}\right)^{\frac{k+1}{2k}}}^{\alpha} + \overbrace{\frac{1}{C}.\frac{r_c - 1}{r_c}\phi\frac{V_{ivo}}{V_{dis}}.\left(\frac{P_{exh}}{P_m}\right)^{\frac{1}{k}}}^{\beta} \tag{5.2}$$

where r_c is the compression ratio, OF is the overlap factor which is calculated based

on the intake and exhaust valve geometries and timings, T_m is intake manifold temperature, P_{exh} is exhaust pressure, R is gas constant, k is the ratio of specific heats, V_{ivo} is the volume at IVO and V_{disp} is the displacement volume. C is a parameter given by:

$$C = \left[1 + \frac{LHV}{c_v T_m (\frac{m_t}{m_f}).r_c^{k-1}}\right]^{\frac{1}{k}} \tag{5.3}$$

where c_v is specific heat capacity at constant volume at IVC moment and LHV represents the lower heating value of the blended fuel of both n-heptane and iso-octane which is given by:

$$LHV = (1 - PR).LHV_{DI} + PR.LHV_{PFI} \tag{5.4}$$

where LHV_{DI} and LHV_{PFI} are lower heating values of n-heptane and iso-octane respectively whereas PR is expressed as fraction of premixed fuel energy to the total fuel energy.

This value of X_{rg} will be used only for the initialization of the first cycle. An updated X_{rg} is estimated at the end of the cycle by calculating the mass of residuals m_r using the exhaust conditions. X_{rg} is given by

$$X_{rg} = \frac{m_r}{m_t} \tag{5.5}$$

where m_t is total mass of the charge defined as:

$$m_t = m_{air} + m_r \tag{5.6}$$

Since there is no external EGR, its mass is not included in Eq. 5.6. Otherwise mass of EGR should be taken into account for calculating the total mass.

With this updated value of X_{rg} an iterative loop is developed until this value converges to a terminal value determined at end of the cycle. Similarly, T_{rg} is calculated from EVC conditions and is iterated along with X_{rg}. Finally, after converging to a terminal value both the updated values are provided for the next cycle.

5.1.2 Polytropic Compression ($IVC \rightarrow SOC$)

By assuming a polytropic process for compression, the instantaneous values of gas temperature and pressure can be estimated at SOC. In order to calculate pressure and temperature at SOC using polytropic relation, SOC needs to be determined. For this, the mean value model developed for predicting SOC using MKIM in Chapter 4 is used after providing the required input parameters at IVC. After predicting SOC, the temperature and pressure at SOC are given by Eq. 5.7 and Eq. 5.8

$$T_{soc,i+1} = T_{mix,i+1}\left(\frac{V_{ivc}}{V_{soc,i+1}}\right)^{n_c-1} \tag{5.7}$$

$$P_{soc,i+1} = P_{ivc,i+1}\left(\frac{V_{ivc}}{V_{soc,i+1}}\right)^{n_c} \tag{5.8}$$

where n_c is the polytropic compression coefficient determined using steady-state experimental data for this engine. V_{ivc} and V_{soc} are the cylinder volume at the instant of IVC and SOC. Cylinder volume at each crank angle is calculated using slider crank mechanism equation [55] given by Eq. (2.4).

5.1.3 Combustion Period ($SOC \rightarrow EOC$)

CA50 is predicted using the CA50 model developed in Section 4.3. End of combustion (EOC) is predicted using the following Burn Duration (BD) model.

5.1.3.1 BD Model for EOC state estimates

BD model for RCCI combustion is originally developed by Sadabadi [39] and is utilized here for predicting temperature and pressure at EOC.

The introduction of high reactive fuel into the charge creates a reactivity gradient and results in the formation of ignition pockets [9]. The combustion duration depends on

the ignition front speed (S_{ig}). This is correlated to BD by the following equation:

$$BD = K_2(S_{ig})^t \tag{5.9}$$

where K_2 and t are the fitting parameters which are required to be estimated. S_{ig} depends on gradients in ignition delay and stratification of equivalence ratio [75]. The following correlation was proposed by Sadabadi [39] for estimation of ignition front speed in an RCCI engine.

$$S_{ig} = \frac{1}{|\frac{d\tau}{d\phi_{DI}}||\nabla\phi_{DI}|} \tag{5.10}$$

where τ is the ignition delay estimated by denominator of MKIM Eq. (4.1) from SOI to SOC period. The gradient of equivalence ratio is given by:

$$|\nabla\phi_{DI}| = \frac{K_1}{ID^p}.\phi_{DI}^r \tag{5.11}$$

where ID refers to ignition delay and is calculated using:

$$ID = SOI - SOC \tag{5.12}$$

EOC is calculated using predicted BD and SOC which is given by the Eq. (5.13)

$$EOC = SOC + BD \tag{5.13}$$

After calculating EOC, the temperature and pressure at EOC are determined using the following equations:

$$T_{EOC} = T_{SOC} + e_1.\Delta T \tag{5.14}$$

$$P_{EOC} = P_{SOC} + e_2.\Delta T \tag{5.15}$$

where ΔT refers to the rise in temperature during the combustion period. ΔT is calculated by:

$$\triangle T = \frac{LHV_{DI}(F/A)_{st,nhep}.\phi_{DI} + LHV_{PFI}.(F/A)_{st,iso}.\phi_{PFI}}{c_v((F/A)_{st,nhep}.\phi_{DI} + (F/A)_{st,iso}.\phi_{PFI} + 1)} \tag{5.16}$$

e_1 and e_2 in equations (5.14) and (5.15) account for the compression heating or expansion cooling. The e_1 and e_2 parameters depend on SOC. The earlier the combustion, the lower the average temperature and pressure will be and the more the combustion duration [39]. A longer combustion duration will result in increased heat losses and results in drop of e_1 and e_2 parameters. These are estimated to be second order polynomials which are given by:

$$e_1 = a_0 + a_1\theta_{soc} + a_2\theta_{soc}^2 \tag{5.17}$$

$$e_2 = b_0 + b_1\theta_{soc} + b_2\theta_{soc}^2 \tag{5.18}$$

The constant parameters which need to be estimated from the BD model are

$a_0, a_1, a_2, b_0, b_1, b_2, p, r, K_1, K_2$ and t. These parameters are estimated through optimization by minimizing the error between predicted BD and experimental BD. Experimental BD is taken as combustion duration between CA90 and CA10 of the mainstage. The parameters are given in Table 5.1

Table 5.1
Optimized parameters for the BD model

K_1	t	K_2	a_0	a_1	a_2
9.8183	0.07338	53.8840	-0.1439	0.000246	2.981e-07
b_0	b_1	b_2	p	r	
-0.54928	4.436e-04	1.5005e-05	4.0509e-06	0.97675	

5.1.4 Polytropic Expansion ($EOC \rightarrow EVO$)

Expansion of burned gases after EOC is modeled as a polytropic process [76]. The temperature and pressure, when the exhaust valves open (EVO) are given by Eq. (5.19) and (5.20):

$$T_{evo,i+1} = T_{eoc,i+1}\left(\frac{V_{eoc,i+1}}{V_{evo}}\right)^{n_e-1} \tag{5.19}$$

$$P_{evo,i+1} = P_{eoc,i+1}\left(\frac{V_{eoc,i+1}}{V_{evo}}\right)^{n_e} \tag{5.20}$$

where n_e is the polytropic expansion coefficient in the expansion process which is evaluated using the slope of expansion region in log P - log V curve. The average

value is found to be 1.32 using the collected steady-state experimental data. V_{eoc} is the volume at EOC which is calculated using the location of EOC and Eq. (2.4).

5.1.5 Exhaust Stroke ($EVO \rightarrow EVC$)

The exhaust gas temperature (T_{ex}) is estimated using the following model [39]:

$$T_{ex,i+1} = T_{evo,i+1}\left(\frac{P_{ex,i+1}}{P_{evo,i+1}}\right)^{\frac{(k_e-1)}{k_e}} + \Delta T_{ht}. \tag{5.21}$$

The Eq. (5.21) assumes a polytropic relation for the exhaust process. ΔT_{ht} accounts for the heat transfer loss to the surroundings during the exhaust stroke. The ΔT_{ht} is calculated by comparing the experimentally measured exhaust port temperature with the term $T_{evo,i+1}\left(\frac{P_{ex,i+1}}{P_{evo,i+1}}\right)^{\frac{(k_e-1)}{k_e}}$. In the current engine setup the thermocouple measuring exhaust temperature is at the exhaust port close to the exhaust valves. The exhaust gas temperature model is parametrized using the experimental data for the estimation of ΔT_{ht}. The estimation and validation results are shown in Fig. 5.1 and Fig. 5.2, respectively. The same experimental data used for parameterizing MKIM and CA50 models in Chapter 4 is used here as well.

The color bar on the right side of Fig. 5.1 shows the mass of fuel injected. It can be observed that with increase in injected fuel quantity, residual gas temperatures also increase. This is expected, since the higher chemical energy of the fuel results in

increasing exhaust gas temperature.

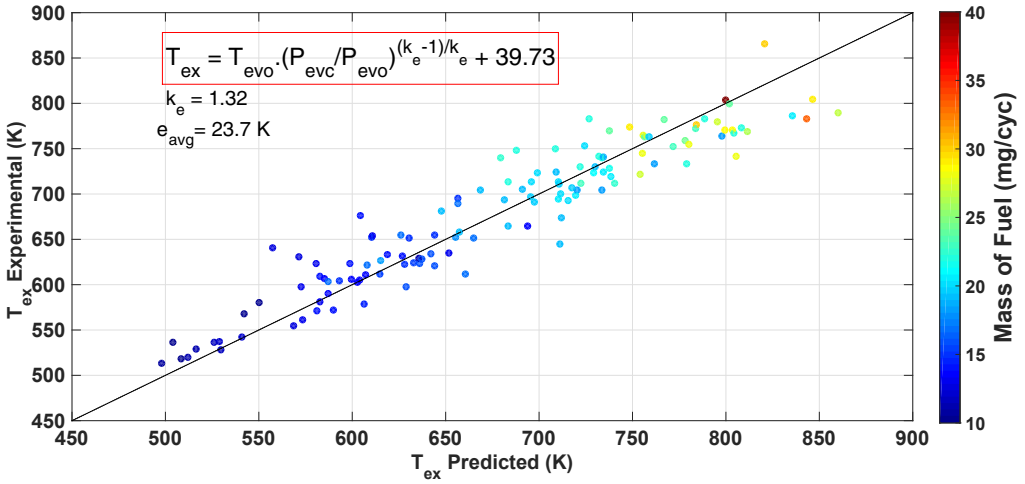

Figure 5.1: Estimation of exhaust gas temperature using steady-state operating points

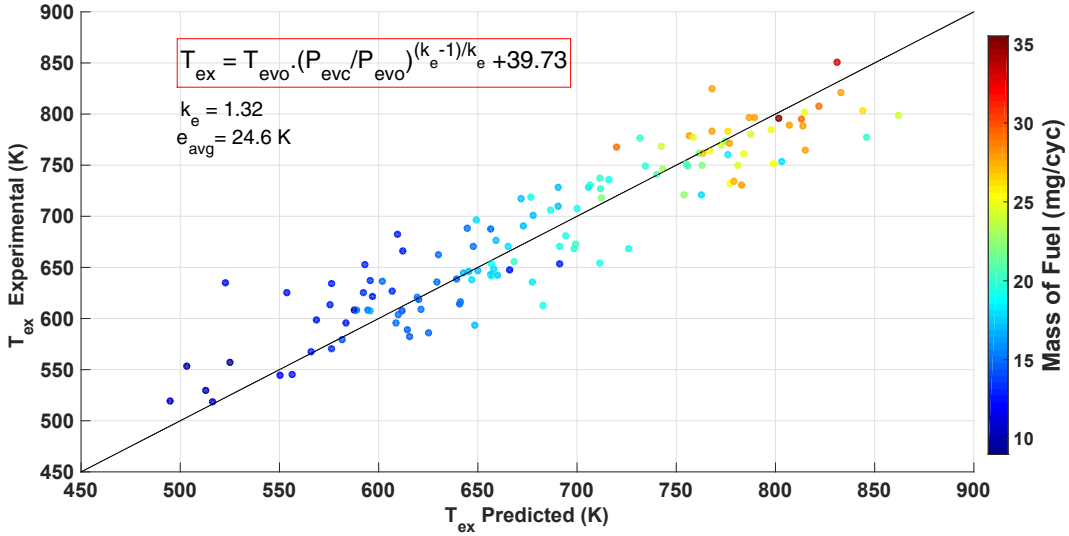

Figure 5.2: Validation of exhaust gas temperature for steady-state operating points

Finally m_{evc} is obtained by applying the ideal gas equation at Exhaust Valve Closing

(EVC):

$$m_{evc,i+1} = \frac{P_{ex,i+1}.V_{evc}}{R_{evc}.T_{rg,i+1}}, \tag{5.22}$$

where P_{ex} is the measured exhaust pressure that is assumed to be equal to pressure at EVC while R_{evc} is gas constant at EVC. The mass at the end of EVC given by Eq. (5.22) and is also assumed to be the mass of trapped residuals at the end of cycle. The residual gas fraction is obtained as a mass fraction of residual gases to the total mass of the charge and hence is calculated by:

$$X_{rg,i+1} = \frac{m_{evc,i+1}}{m_{t,i+1}}. \tag{5.23}$$

The schematic of the full-cycle engine model is shown in Fig. 5.3.

5.2 Experimental Validation of Dynamic Model

A number of simplifying assumptions were made in developing the full-cycle dynamic control-oriented RCCI plant model. Thus, it is critical to experimentally validate the model. To this end, the transient tests were performed to validate the developed COM for predicting cycle-to-cycle CA50. A step change in PR and SOI was performed while maintaining the other control parameters as constant.

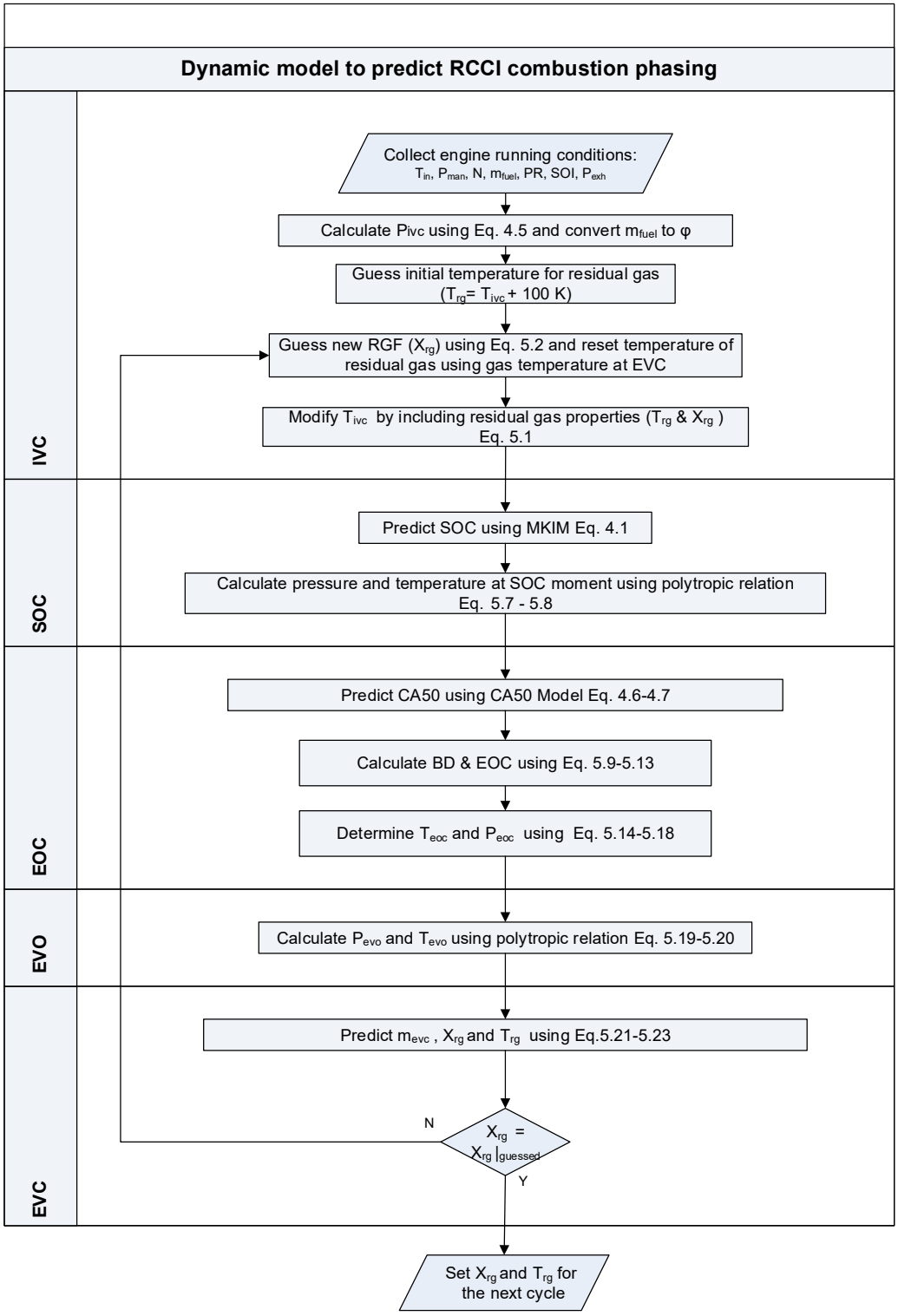

Figure 5.3: Dynamic Model of RCCI Engine

5.2.1 Transient Validation - PR step

The operating condition for PR transient test is given in Table 5.2. As seen from Fig. 5.4, the COM predicts CA50 and SOC with an average error of 1.1 CAD and 1 CAD, respectively. It can be also seen that with increase in PR, CA50 gets retarded due to decrease in reactivity of the mixture. As PR changes from 20 to 60, CA50 gets retarded from -3 CAD to 4 CAD aTDC.

Table 5.2
Operating condition for step change in PR

Parameter [Units]	**Operating value**
PR [-]	**20↔60**
SOI [CAD bTDC]	40
T_{in} [°C]	60
m_{fuel} [mg/cyc]	22
λ [-]	1.3
P_{in} [kPa]	96.5
IVO [CAD bTDC]	25.5
EVC [CAD bTDC]	22
Speed [RPM]	1000

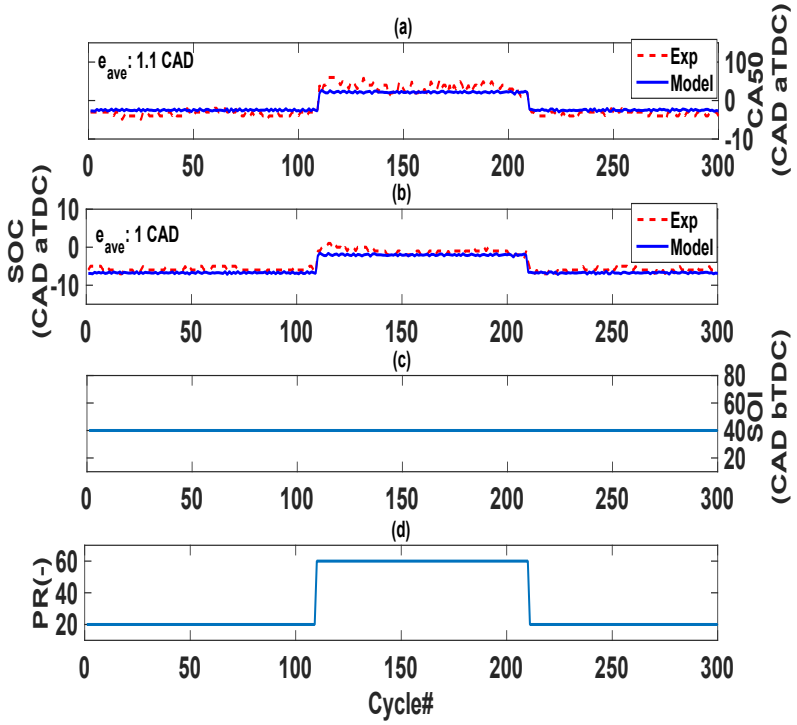

Figure 5.4: Dynamic COM validation for transient RCCI engine operation during step-up and step-down changes in PR

5.2.2 Transient Validation - SOI step

The operating point for the SOI transient test is given in Table 5.3. It can be seen that the COM is able to predict the experimental CA50 and SOC with an average error of 2 CAD and 2.1 CAD, respectively. As expected, advancing SOI before TDC will advance CA50 and SOC as well. This can be seen from the Fig. 5.5. As SOI is advanced from 30 to 50 CAD bTDC, CA50 is also advanced from 10 to 1 CAD aTDC.

Table 5.3
Operating condition for step change in SOI

Parameter [Units]	Operating value
PR [-]	20
SOI [CAD bTDC]	**30↔50**
T_{in} [°C]	40
m_{fuel} [mg/cyc]	21
λ [-]	1.4
P_{in} [kPa]	96.5
IVO [CAD bTDC]	25.5
EVC [CAD bTDC]	22
Speed [RPM]	1000

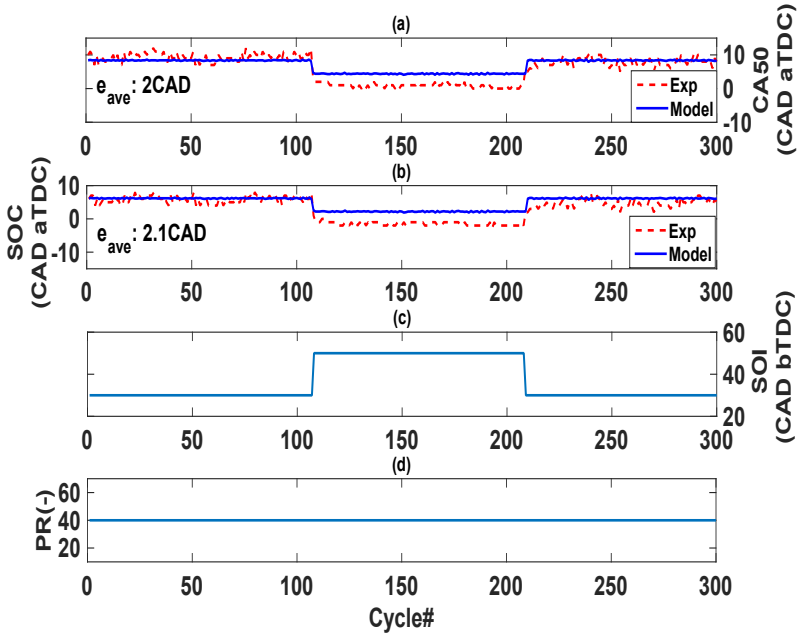

Figure 5.5: Dynamic COM validation for transient RCCI engine operation during step-up and step-down changes in SOI

Chapter 6

Design of RCCI Combustion Phasing Controller

This chapter focuses on design of RCCI combustion controller, using the RCCI dynamic model as a virtual engine plant. Proportional-Integral (PI) controllers are designed to track the desired combustion phasing by varying PR and SOI. Initially, the mean-value model and the dynamic COM developed in Chapter 4 and Chapter 5 are calibrated based on the data from an Field-Programmable Gate Array(FPGA) setup that is used for real time combustion feedback for controls. Then the COM is used to design a PI combustion controller by finding proportional and integral gains to enable tracking the desired combustion phasing. The obtained gains were tested on engine setup by embedding the controller in dSPACE MicroAutobox (MABx). The

results from both the experiment and the model are validated and discussed.

6.1 FPGA Validation

Previously, CA50 was monitored using ACAP combustion analyser in the test cell. But the feedback CA50 from ACAP is difficult to use for closed-loop combustion control, i.e. for cycle-to-cycle control, due to its slow processing time. Therefore, in order to control cycle-to-cycle CA50 and reduce the processing time, a specialized hardware setup based on FPGA was programmed in the dSPACE MABx setup. A model was built in FPGA using Xilinx software to output CA50 for every cycle [77]. To minimize the modelling uncertainty due to the difference between ACAP and FPGA calculated CA50, the author decided to parametrize the COMs using FPGA data. This is essential since the real-time combustion controller will use CA50 from FPGA for real-time combustion feedback.

Intake temperatures will have slower response time when compared to other control parameters such as SOI, PR and ϕ; thus, intake temperature is not an appropriate control knob for transient operation of the RCCI engine. The operating regions are classified based on the intake temperature and the model is parametrized for different intake temperature regions. The controller retrieves its gains depending on the intake temperature region. All the results shown in this chapter are for intake temperature at 40°C.

6.1.1 Steady State Validation

Table 6.1 shows the operating conditions for intake temperature at 40°C. The same method used in Chapter 4 for parameterizing MKIM and CA50 models is used here as well. The optimized parameters are given in Table 6.2 and Table 6.3. The experimental data used for this parametrization is shown in Table A.3.

Table 6.1
Operating condtions for steady state validation of FPGA data

Parameter [Units]	**Operating value**
PR [-]	20-40
SOI [CAD bTDC]	30-40-50
T_{in} [°C]	40
m_{fuel} [mg/cyc]	15-19-21
P_{in} [kPa]	96.5
IVO [CAD bTDC]	25.5
EVC [CAD bTDC]	22
Speed [RPM]	1000

Table 6.2
Optimized parameters for MKIM model calibrated with FPGA steady-state data

A_1	B	C_1	D_1	A_2
0.5322	-0.00725	5.1943	-2.8124e-04	0.002423
B_{2DI}	B_{2PFI}	C_2	b	D_2
0.001655	7.34486e-05	1.4888e+06	1.68196e+02	-0.2414

Table 6.3
Optimized parameters for CA50 model calibrated with FPGA steady-state data

A	B	C
0.1424	11.4984	6.1718
D	E	F
0.1175	0.11242	0.13217

Fig. 6.1 and Fig. 6.2 show the steady state validation for the operating conditions mentioned in Table 6.1. It can be seen that both models are able to predict SOC and CA50 with an average error of 1 CAD. This shows that the developed models are robust and accurate in predicting RCCI combustion phasing for the studied operating range.

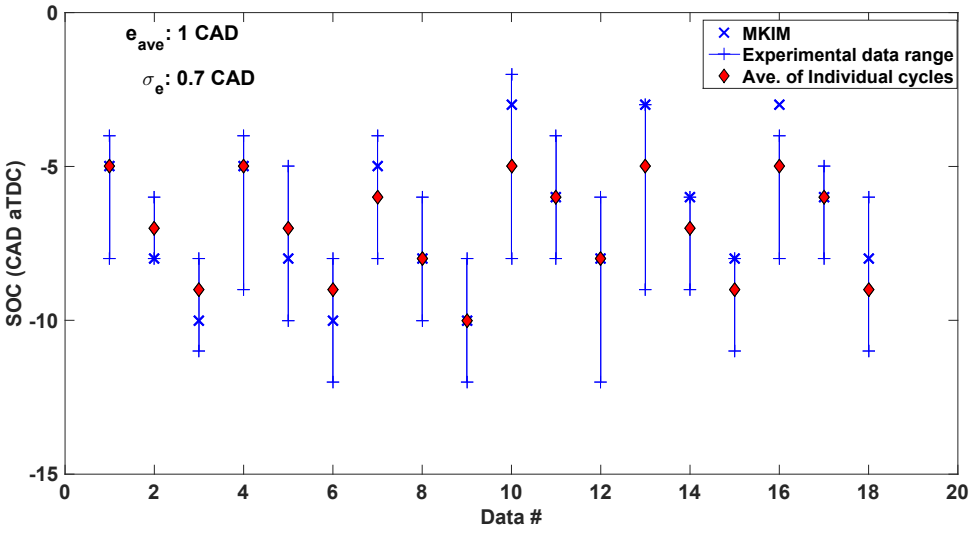

Figure 6.1: Validation of MKIM model using FPGA steady-state data with conditions listed in Table 6.1

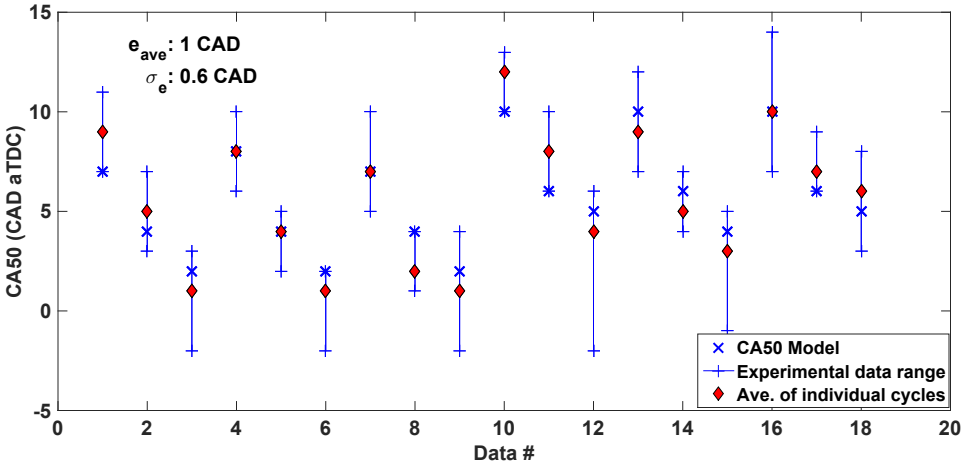

Figure 6.2: Validation of CA50 model using FPGA steady-state data with operating conditions listed in Table 6.1

6.1.2 Transient Validation

The dynamic COM is also validated for transient tests with data collected using FPGA. Fig. 6.3 and Fig. 6.4 show the validation results for the transient step change in PR and SOI, respectively. Operating condition for PR step transient is given in Table 6.4, while for SOI step transient it is given in Table 6.5. It can be seen that the model's accuracy is very good within the range of 2 CAD to predict cycle-to-cycle CA50 and SOC. This validation results prove that the developed COM can be used for controller design as it is able to predict the experimental trends with minimal error.

Table 6.4
Operating condition for FPGA PR transient test

Parameter[Units]	Operating value
PR[-]	**20↔40**
SOI[CAD bTDC]	40
T_{in}[°C]	40
m_{fuel}[mg/cyc]	21
P_{in}[kPa]	96.5
IVO[CAD bTDC]	25.5
EVC[CAD bTDC]	22
Speed[RPM]	1000

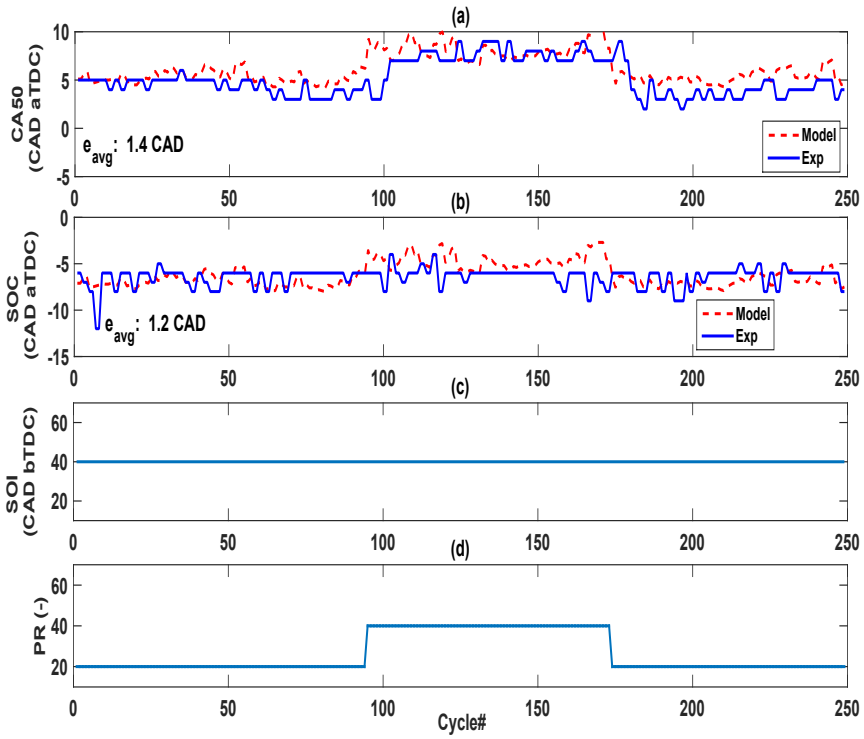

Figure 6.3: FPGA transient validation for step change in PR at a constant SOI

Table 6.5
Operating condition for FPGA SOI transient test

Parameter(Units)	Operating value
PR[-]	20
SOI[CAD bTDC]	**30↔50**
T_{in}[deg C]	40
m_{fuel}[mg/cyc]	15
Throttle opening[%]	100
P_{in}[kPa]	96.5
IVO[CAD bTDC]	25.5
EVC[CAD bTDC]	22
Speed[RPM]	1000

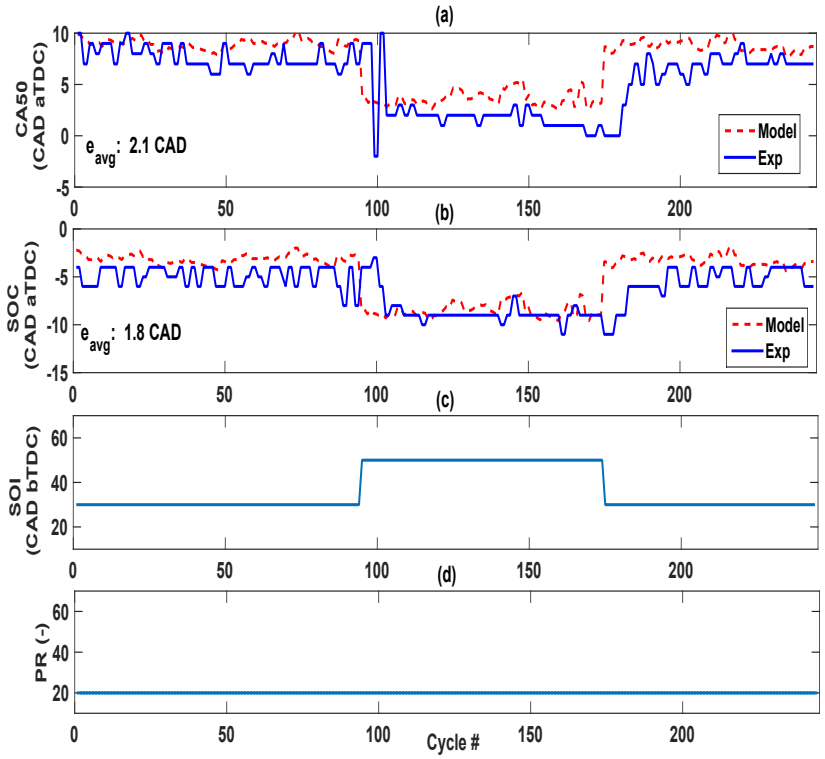

Figure 6.4: FPGA transient validation for step change in SOI at a constant PR

6.2 Model-Based PI Controller Design

After successfully validating the dynamic COM plant model, it can be used as a virtual engine for designing a combustion controller. In this way, the calibration effort can be significantly reduced for developing a real-time controller on the engine test bed. The main objective is to design a controller which can track the desired combustion phasing (CA50) by varying SOI and PR. For this, a basic PI controller was chosen since it is easier to design and simple to control single-input single-output (SISO) systems in the real-time as well. A similar PI controller is also developed in dSPACE MABx for controlling cycle-to-cycle CA50 in real-time. After getting PI gains from the off-line plant model, the same gains will be tested on the real-time controller as well. The operating conditions are maintained same for both off-line and real-time testing. Also, to improve the tracking performance and disturbance rejection, a feed-forward controller (look-up table) is also used along with a PI controller. A static look-up table is designed using steady state data so that an optimal control output can be obtained from the table for a desired combustion phasing. Feedback PI controller will help in tracking the set point and reduce the steady state error.

Fig. 6.5 shows the schematic of control structure developed for controlling CA50 through PR or SOI. The detailed physical dynamic COM from Chapter 5 is used as a virtual RCCI engine to design the PI combustion controller. Based on the given

input conditions, the model predicts CA50 and is provided as a feedback for PI controller. The PI controller then minimizes the error between desired and feedback CA50 and outputs a corresponding control output in terms of either PR or SOI. If the control output is PR, SOI is kept constant and vice-versa. The constant value will be provided by the look-up table. For the real-time control, the physical plant model will be replaced by the engine and the feedback CA50 will be obtained from FPGA.

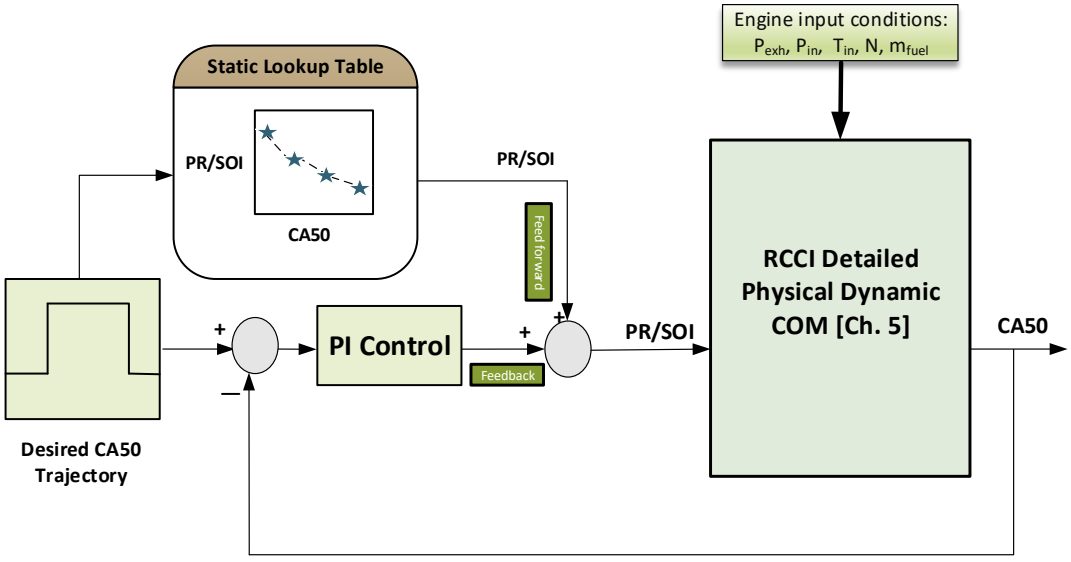

Figure 6.5: Schematic of RCCI combustion phasing PI controller

6.2.1 CA50 control by SOI

This section provides both the model and the experimental results for controlling CA50 by adjusting SOI commanded by the designed PI controller. Initially the proportional and integral gains are obtained off-line by testing the controller on the plant model. The Zeigler-Nichol's closed-loop method [78] is used for tuning the PI gains. The operating range was selected based on the experimental steady-state data from FPGA. Also, a look up table was designed using this data. The operating condition is given in Table 6.7. The proportional and integral gains obtained are shown in Table 6.6 after tuning the controller on the plant model.

Table 6.6
Proportional(K_p) and Integral (K_i) gains for PI control of SOI

K_p	K_i
1	0.1

Table 6.7
Operating condition for PI control of CA50 through SOI

Parameter [Unit]	**Operating value**
PR [-]	20
T_{in} [°C]	40
m_{fuel} [mg/cyc]	18
λ	1.5
P_{in} [kPa]	96.5
IVO [CAD bTDC]	25.5
EVC [CAD bTDC]	22
Speed [RPM]	1000

The tracking performance of the designed controller tested on the off-line plant model

is shown in Fig. 6.6

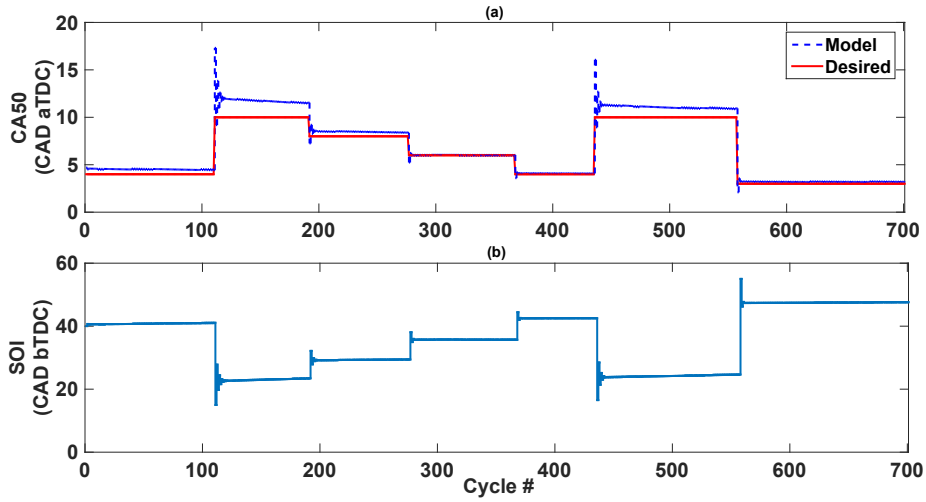

Figure 6.6: Control of CA50 by varying SOI using the plant model for operating conditions listed in Table 6.7

After getting PI gains from the off-line plant model, the gains are used in the same controller which is built in dSPACE MABx for the real time control of CA50 through SOI. The feedback CA50 of 3-cycle average is used for control rather than cyclic CA50. This is due to high cyclic fluctuations in CA50 that can make the controller unstable. Fig. 6.7 shows the experimental tracking results of cycle-to-cycle CA50 for the same operating conditions used for the testing the controller on off-line plant model. The results show that the controller is able to track the desired CA50 within 2-3 engine cycles with an average tracking error of 1 CAD.

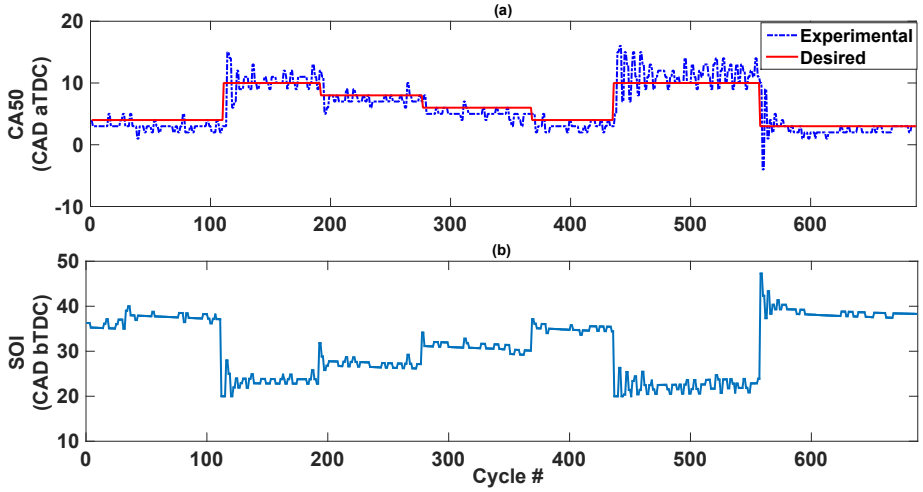

Figure 6.7: Control of real-time CA50 by varying SOI using gains from the off-line plant model

6.2.2 CA50 control by PR

Similarly, a PI controller is designed to adjust PR while maintaining desired CA50. The same procedure followed for SOI control is applied here as well. The operating conditions for control of PR are given in Table 6.9. A look-up table is designed based on the steady state data obtained at 40°C intake air temperature. The gains were tuned accordingly in order to track the desired combustion phasing and reduce the steady state error. The controller gains are shown in Table 6.8.

Table 6.8
Proportional(K_p) and Integral (K_i) gains for PI control of PR

K_p	K_i
2	0.1

Again, the gains were tuned using Zeigler-Nichol's closed-loop method [78]. The gains obtained were tested on the real engine and the results are shown in Fig. 6.9. As it can be seen from the experimental results that there is a delay between actual and desired response when there is a step change in CA50. This is due to the fuel transport dynamics in delivering PFI fuel (i.e., iso-octane). When there is a step change in desired CA50, the controller commands the required PR. Then, certain fuel quantity in the PFI rail should be injected. The injected fuel into intake ports will take time to enter into the cylinder. In addition, similar to SOI control the CA50 is controlled using 3-cycle average to avoid unstability of the PI combustion controller that does not have knowledge about dynamics causing combustion cyclic variability.

Table 6.9
Operating condition for PI control of CA50 through PR

Parameter [Unit]	**Operating value**
SOI [CAD bTDC]	30
T_{in} [°C]	40
m_{fuel} [mg/cyc]	15
λ	1.8
P_{in} [kPa]	96.5
IVO [CAD bTDC]	25.5
EVC [CAD bTDC]	22
Speed [RPM]	1000

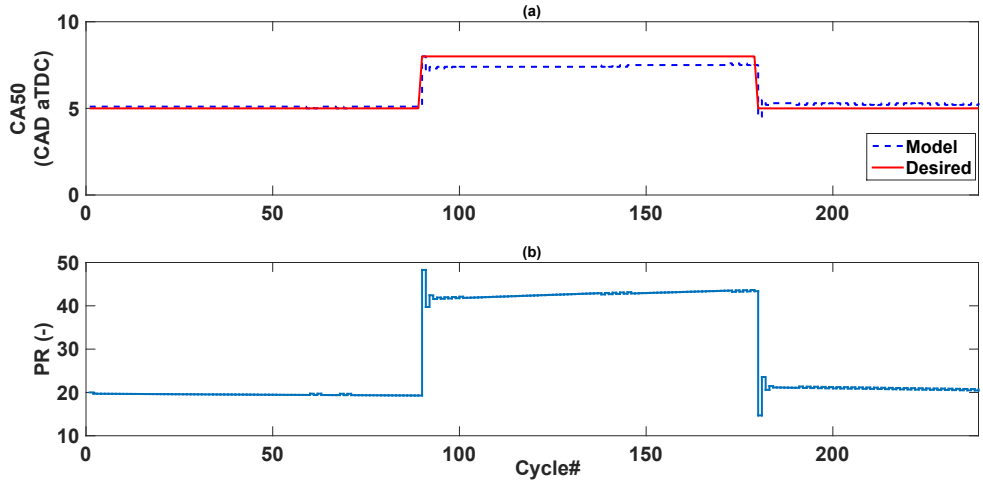

Figure 6.8: Control of CA50 by varying PR using plant model at 40°C intake temperature

The experimental results show that the desired CA50 is tracked within 4 engine cycles with an average tracking error of 2 CAD.

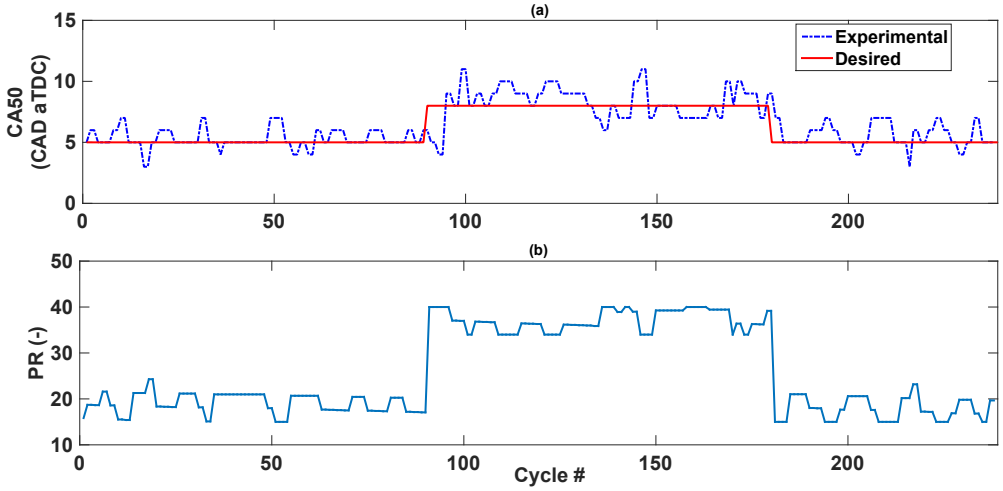

Figure 6.9: Control of real-time CA50 by varying PR using gains from the off-line plant model

The PI controller in this chapter is limited in removing engine disturbances and also addressing engine combustion cyclic variability. The dynamic RCCI model from Chapter 5 can be further enhanced by including actuator dynamics and also a model for combustion cyclic variability. The resulting model can be used for design of advanced model-based RCCI combustion controllers for optimum engine performance.

Chapter 7

Conclusion and Future Work

7.1 Conclusions

† An experimental study was done by operating 2.0L Ecotec Engine in RCCI mode under naturally aspirated conditions. The operating range of the engine was studied under different speed, load and intake temperature. It was seen that in order to operate at low speed and load, premixed ratio of PR-20 and intake temperature of 40°-80°C provides the best efficient region in terms of higher thermal efficiency and low specific fuel consumption. While to operate at higher speed and loads, fuel blend ratio of PR-40 with intake temperatures of 40°-60°C has provided higher thermal efficiency. Understanding the effect

of SOI and PR was the main focus of the study, since these parameters are the major control knobs for combustion phasing of RCCI engines. Effect of PR on IMEP, BMEP, ISFC, BSFC, $\eta_{the,ind}$, $\eta_{the,br}$ and exhaust gas temperature were studied at an intake temperature of 60°C. The operating conditions with minimum fuel consumption were identified through optimized maps. Maximum indicated thermal efficiency was observed to be 48.3% with minimum ISFC of 167.4 g/kWh. This was achieved at 1400 RPM and IMEP of 539 kPa with PR, SOI and T_{in} as 20, 60 CAD bTDC and 40°C respectively. Also, a parametric study was done for analyzing the experimental trends of the variation of SOI and PR and their effect on SOC and CA50. It was observed that with advancing SOI before TDC, CA50 and SOC advances initially but starts retarding with further advance. While with increase in PR, CA50 and SOC retards due to higher premixed fuel. A study was also done to characterize whether the heat release rate was happening in 2-stage or 1-stage. It was found that earlier the SOI and lower the PR, the probability for having two-stage heat release increases.

† A Mean Value Model for prediction of SOC and CA50 was developed. SOC was predicted using an MKIM model while CA50 was predicted using a fuel burn rate model. The equations were parametrized using the steady state experimental data acquired from the engine. SOC and CA50 were predicted for any given operating point with an average error of 1.5 CAD. In addition, the

validation results show that the model is able to track the experimental trends by changing engine variables. This proves that the developed mean value RCCI model can be used for predicting steady-state SOC and CA50.

† A complete physics-based dynamic model was developed to predict cycle-to-cycle combustion phasing for an RCCI engine. The model consists of different sub-models which can simulate the real engine plant from IVC to EVO events. The sub-models consist of equations based on thermodynamic laws and mean value models developed in Chapter 4. The dynamic model captures thermal coupling due to residual gases. The dynamic model was validated with experimental transient tests collected from the engine. The validation results show promising trends with minimal error($e_{CA50} < 2CAD$). The resulting dynamic model can be used for developing model-based RCCI controller for real-time applications.

† A PI controller was designed using the RCCI dynamic model as a virtual engine.Then, the PI controller was tested on a real engine. This approach significantly reduces the combustion controller calibration. The same PI gains from simulation were applied when testing the PI controller on the real engine. The results show that the controller can track the desired combustion phasing by varying the control outputs of either PR or SOI. Real-time testing results showed that the designed combustion controller can obtain the desired CA50 within 3-4 RCCI engine cycles.

7.2 Future Work

Future work may include:

† The compression ratio for the current engine is 9.2. This is very low for operating engine under RCCI mode as it restricts PR value to 60 only. The engine can be operated at higher loads with increase in PR values. This can be done by increasing the compression ratio to high values, e.g, by using the newly designed engine pistons to provide compression ratio of 12.1 [42].

† The developed dynamic model only captures residual gas dynamics from cycle-to-cycle. To improve accuracy of the model, other dynamics should be considered. These include port fuel rail dynamics which cause delay in injecting fuel from the port fuel injectors while varying PR and also fuel transport dynamics for transporting the fuel into the cylinder.

† In order to develop model based combustion controller, the model can be further simplified and formulated in state space representation. This will allow the model for use in common model-based controller design techniques such as state feedback controllers, sliding mode controllers etc.

† Once a model based controller is designed , it can be embedded in existing dSPACE Microautobox processor setup with FPGA board to control cycle-by-cycle CA50 for RCCI engines.

References

[1] D.A. Splitter, M.L. Wissink, D. DelVescovo, and R. D. Reitz. RCCI engine operation towards 60% thermal efficiency. SAE Technical Paper 2013-01-0279, 2013.

[2] U.S. White House Office of the Press Secretary. Obama Administration Finalizes Historic 54.5 MPG Fuel Efficiency Standards. https://www.whitehouse.gov/the-press-office/2012/08/28/obama-administration-finalizes-historic-545-mpg-fuel-efficiency-standard, 2012. Accessed on:2016-06-30.

[3] Environment Protection Agency. Regulations and Standards: Light-Duty. https://www3.epa.gov/otaq/climate/regs-light-duty.htm#2017-2025, 2012. Accessed on:2016-06-30.

[4] M. Robert. Engines of the Future. https://www.asme.org/engineering-topics/articles/energy/engines-of-the-future. Accessed on:2016-07-09.

[5] J.E. Dec. A conceptual model of DI diesel combustion based on laser-sheet imaging. SAE Technical Paper 970873, 1997.

[6] T. V. Johnson. Diesel emission control: 2001 in review. SAE Technical Paper 2002-01-0285, 2002.

[7] A. B. Dempsey. *Dual-fuel reactivity controlled compression ignition (RCCI) with alternative fuels*. PhD thesis, University Of Wisconsin-Madison, 2013.

[8] R. Stone. *Introduction to Internal Combustion Engines,Chapter-3*. Springer, 1999.

[9] S. L. Kokjohn. *Reactivity controlled compression ignition (RCCI) combustion*. PhD thesis, University Of Wisconsin-Madison, 2012.

[10] M. L.Wissink. *Direct injection for dual fuel stratification (DDFS): Improving the control of heat release in advanced IC engine combustion strategies*. PhD thesis, University Of Wisconsin-Madison, 2015.

[11] R. M. Hanson. *Experimental investigation of transient RCCI combustion in a light duty diesel engine*. PhD thesis, University Of Wisconsin-Madison, 2013.

[12] A. Paykani, A. Kakaee, P. Rahnama, and R. D. Reitz. Progress and recent trends in reactivity-controlled compression ignition engines. *International Journal of Engine Research*, 17(5):481–524, 2016.

[13] A. Widd, K. Ekholm, P. Tunestål, and R. Johansson. Physics-based Model Predictive Control of HCCI Combustion Phasing Using Fast Thermal Management and VVA. *IEEE Transactions on Control Systems Technology*, 20(3):688–699, 2012.

[14] M. Bidarvatan. *Physics-based modeling and control of powertrain systems integrated with Low Temperature Combustion engines.* PhD thesis, Michigan Technological University, 2015.

[15] N. Ravi, H-H. Liao, A.F. Jungkunz, A. Widd, and J.C. Gerdes. Model Predictive Control of HCCI Using Variable Valve Actuation and Fuel Injection. *Control Engineering Practice*, 20(4):421–430, 2012.

[16] N. Ravi, M. J. Roelle, Hsien-Hsin Liao, A. F. Jungkunz, C.F. Chang, S. Park, and J. C. Gerdes. Model-based control of HCCI engines using Exhaust recompression. *IEEE Transactions on Control Systems Technology*, 18(6):1289–1302, 2010.

[17] V. Tandra and N. Srivastava. Optimal Peak Pressure and Exhaust Temperature Tracking Control for a Two-zone HCCI Engine Model with Mean Burn Duration. SAE Technical Paper 2009-01-1130, 2009.

[18] N. Ravi, H-H. Liao, A.F. Jungkunz, C-F. Chang, H-H. Song, and J.C. Gerdes. Modeling and Control of an Exhaust Recompression HCCI Engine Using Split Injection. *ASME Journal of Dynamic Systems, Measurement, and Control*, 134(1), 2012.

[19] Y. Takeda, N. Keiichi, and N. Keiichi. Emission characteristics of premixed lean diesel combustion with extremely early staged fuel injection. SAE Technical Paper 961163, 1996.

[20] T. Hashizume, T. Miyamoto, A. Hisashi, and K. Tsujimura. Combustion and emission characteristics of multiple stage diesel combustion. SAE Technical Paper 2009-01-1130, 1998.

[21] M. Shahbakhti. *Modeling and experimental study of an HCCI engine for combustion timing control*. PhD thesis, University of Alberta, 2009.

[22] G. T. Kalghatgi, P. Risberg, and H. Angstrom. Partially pre-mixed auto-ignition of gasoline to attain low smoke and low NOx at high load in a compression ignition engine and comparison with a diesel fuel. SAE Technical Paper 2007-01-0006, 2007.

[23] C. Noehre, M. Andersson, B. Johansson, and A. Hultqvist. Characterization of partially premixed combustion. SAE Technical Paper 2006-01-3412, 2006.

[24] M. Tunér, K. Frojd, L. Seidel, and F. Mauss. Diesel-PPC engine: Predictive Full Cycle Modeling with Reduced and Detailed Chemistry. SAE Technical Paper 2011-01-1781, 2011.

[25] P. W. Bessonette, C. H. Schleyer, K. P. Duffy, W. L. Hardy, and M. P. Liechty. Effects of fuel property changes on heavy-duty HCCI combustion. SAE Technical Paper 2014-01-2679, 2007.

[26] S. L. Kokjohn, R. M. Hanson, D. A. Splitter, and R. D. Reitz. Experiments and modeling of dual-fuel HCCI and PCCI combustion using in-cylinder fuel blending. *SAE International Journal of Engines*, 2(2):24–39, 2009.

[27] K. Inagaki, T. Fuyuto, K. Nishikawa, K. Nakakita, and I. Sakata. Dual-fuel PCI combustion controlled by in-cylinder stratification of ignitability. SAE Technical Paper 2006-01-0028, 2006.

[28] Y. Yang, J. E. Dec, N. Dronniou, M. Sjöberg, and W. Cannella. Partial fuel stratification to control HCCI heat release rates: fuel composition and other factors affecting pre-ignition reactions of two-stage ignition fuels. *SAE International Journal of Engines*, 4(1):1903–1920, 2011.

[29] J. E. Dec, Y. Yang, and N. Dronniou. Boosted HCCI-controlling pressure-rise rates for performance improvements using partial fuel stratification with conventional gasoline. *SAE International Journal of Engines*, 4(1):1169–1189, 2011.

[30] S.L. Kokjohn and R.D. Reitz. Characterization of dual-fuel PCCI combustion in a light-duty engine. In *Proceedings of the International Multi-Dimensional Engine Modeling UserâĂŹs Group Meeting*, 2010.

[31] S.L. Kokjohn, R. Hanson, D.A. Splitter, J. Kaddatz, and R. D. Reitz. Fuel reactivity controlled compression ignition (RCCI) combustion in light-and heavy-duty engines. *SAE International Journal of Engines*, 4(1):360–374, 2011.

[32] S. Curran, R. Hanson, R. Wagner, and R.D. Reitz. Efficiency and emissions

mapping of RCCI in a light-duty diesel engine. SAE Technical Paper 2013-01-0289, 2013.

[33] Derek Splitter, Reed Hanson, Sage Kokjohn, Martin Wissink, and Rolf D Reitz. Injection effects in low load RCCI dual-fuel combustion. SAE Technical Paper 2011-24-0047, 2011.

[34] J. Benajes, S. Molina, A. García, E. Belarte, and M. Vanvolsem. An investigation on RCCI combustion in a heavy duty diesel engine using in-cylinder blending of diesel and gasoline fuels. *Applied Thermal Engineering*, 63(1):66–76, 2014.

[35] D.A Splitter, R.D. Reitz, and R.M. Hanson. High efficiency, low emissions RCCI combustion by use of a fuel additive. *SAE International Journal of Fuels and Lubricants*, 3(2):742–756, 2010.

[36] A. Dempsey, N.R. Walker, and R.D. Reitz. Effect of cetane improvers on gasoline, ethanol, and methanol reactivity and the implications for RCCI combustion. *SAE International Journal of Fuels and Lubricants*, 6(1):170–187, 2013.

[37] H. Wang, D. DelVescovo, M. Yao, and R.D. Reitz. Numerical study of RCCI and HCCI combustion processes using gasoline, diesel, iso-butanol and DTBP cetane improver. *SAE International Journal of Engines*, 8(2):831–845, 2015.

[38] J.H. Lim and R.D. Reitz. Improving the efficiency of low temperature combustion engines using a chamfered ring-land. *Journal of Engineering for Gas Turbines and Power*, 137(11):111509, 2015.

[39] K.K. Sadabadi. Modelling and Control of Combustion Phasing of an RCCI Engine. Master's thesis, Michigan Technological University, 2015.

[40] Y. Wu, R. Hanson, and R.D. Reitz. Investigation of Combustion Phasing Control Strategy During Reactivity Controlled Compression Ignition (RCCI) Multicylinder Engine Load Transitions. *Journal of Engineering for Gas Turbines and Power*, 136(9):091511, 2014.

[41] C. Bekdemir, R. Baert, F. Willems, and B. Somers. Towards control-oriented modeling of natural gas-diesel RCCI combustion. SAE Technical Paper 2015-01-1745, 2015.

[42] H. A. Saigaonkar. An Investigation of variable valve timing effects on HCCI Engine Performance. Master's thesis, Michigan Technological University, 2014.

[43] V. Thakkar. Modeling and Experimental setup of HCCI Engine. Master's thesis, Michigan Technological University, 2014.

[44] D. Kothari. Experimental Setup and Design for an RCCI Engine. Master's thesis, Michigan Technological University, 2014.

[45] K. Kannan. An Experimental investigation of Low Temperature Combustion (LTC) regimes in a light duty engine. Master's thesis, Michigan Technological University, 2016.

[46] National Center for Biotechnology Information. PubChem Compound Database.

https://pubchem.ncbi.nlm.nih.gov/compound/10907. Accessed on:2016-07-06.

[47] National Institure of Standards and Technology. Measurement Uncertainty. http://www.nist.gov/itl/sed/gsg/uncertainty.cfm. Accessed on:2016-07-06.

[48] B. N. Taylor and C. E. Kuyatt. *Guidelines for evaluating and expressing the uncertainty of NIST measurement results*. US Department of Commerce, Technology Administration, National Institute of Standards and Technology Gaithersburg, MD, 1994.

[49] F. Payri, A. Broatch, B. Tormos, and V. Marant. New methodology for in-cylinder pressure analysis in direct injection diesel enginesâĂŤapplication to combustion noise. *Measurement Science and Technology*, 16(2):540, 2005.

[50] N. J. Killingsworth, S. M. Aceves, D. L. Flowers, F. Espinosa-Loza, and M. Krstić. HCCI engine combustion-timing control: Optimizing gains and fuel consumption via extremum seeking. *Control Systems Technology, IEEE Transactions on*, 17(6):1350–1361, 2009.

[51] J. Chang, O. Güralp, Z. Filipi, D. Assanis, T. Kuo, P. Najt, and R. Rask. New heat transfer correlation for an HCCI engine derived from measurements of instantaneous surface heat flux. SAE Technical Paper 2004-01-2996, 2004.

[52] S. Tanaka, F. Ayala, J. C. Keck, and J. B. Heywood. Two-stage ignition in HCCI

combustion and HCCI control by fuels and additives. *Combustion and flame*, 132(1):219–239, 2003.

[53] G.M. Rassweiler and L. Withrow. Motion pictures of engine flames correlated with pressure cards. SAE Technical Paper 380139, 1938.

[54] J. B. Heywood. *Internal combustion engine fundamentals,Chapter-9*. Mcgraw-hill New York, 1988.

[55] J. B. Heywood. *Internal combustion engine fundamentals,Chapter-2*. Mcgraw-hill New York, 1988.

[56] J. C. Scott, M. H. Reed, and M. W. Robert. Reactivity controlled compression ignition combustion on a mutli-cylinder light-duty diesel engine. *International Journal of Engine Research*, 13(3):216–225, 2012.

[57] S. K. Chen and P. F. Flynn. Development of a single cylinder compression ignition research engine. SAE Technical Paper 650733, 1965.

[58] OMEGA. TJC36 Compact Series. `http://www.omega.com/pptst/TJC36.html`. Accessed on:2016-07-06.

[59] M. D. Firoozabadi, M. Shahbakhti, C.R. Koch, and S.A. Jazayeri. Thermodynamic control-oriented modeling of cycle-to-cycle exhaust gas temperature in an HCCI engine. *Applied Energy*, 110:236–243, 2013.

[60] J. Klimstra. The optimum combustion phasing angleâĂŤa convenient engine tuning criterion. SAE Technical Paper 852090, 1985.

[61] C. Cinar, A. Uyumaz, H. Solmaz, F. Sahin, S. Polat, and E. Yilmaz. Effects of intake air temperature on combustion, performance and emission characteristics of a HCCI engine fueled with the blends of 20% n-heptane and 80% isooctane fuels. *Fuel Processing Technology*, 130:275–281, 2015.

[62] R. D. Reitz and G. Duraisamy. Review of high efficiency and clean reactivity controlled compression ignition (RCCI) combustion in internal combustion engines. *Progress in Energy and Combustion Science*, 46:12–71, 2015.

[63] D. T. Klos and S. L. Kokjohn. Investigation of the effect of injection and control strategies on combustion instability in reactivity-controlled compression ignition engines. *Journal of Engineering for Gas Turbines and Power*, 138(1):011502, 2016.

[64] S.L. Kokjohn, R.D. Reitz, D.A. Splitter, and M. Musculus. Investigation of fuel reactivity stratification for controlling PCI heat-release rates using high-speed chemiluminescence imaging and fuel tracer fluorescence. *SAE International Journal of Engines*, 5(2):248–269, 2012.

[65] N. Mohammadreza and M. Shahbakhti. Modeling and analysis of fuel injection parameters for combustion and performance of an RCCI engine. *Applied Energy*, 165:135–150, 2016.

[66] R. Hanson, S. Kokjohn, D. Splitter, and R. D. Reitz. Fuel effects on reactivity controlled compression ignition (RCCI) combustion at low load. *SAE International Journal of Engines*, 4(1):394–411, 2011.

[67] J. Benajes, S. Molina, A. García, and J. Monsalve-Serrano. Effects of direct injection timing and blending ratio on RCCI combustion with different low reactivity fuels. *Energy Conversion and Management*, 99:193–209, 2015.

[68] R. Ebrahimi. Effect of specific heat ratio on heat release analysis in a spark ignition engine. *Scientia Iranica*, 18(6):1231–1236, 2011.

[69] J. Bengtsson, P. Strandh, R. Johansson, P. Tunestål, and B. Johansson. Closed-loop combustion control of homogeneous charge compression ignition (HCCI) engine dynamics. *International journal of adaptive control and signal processing*, 18(2):167–179, 2004.

[70] A.H. Kakaee, P. Rahnama, and A. Paykani. Numerical study of reactivity controlled compression ignition (RCCI) combustion in a heavy-duty diesel engine using 3D-CFD coupled with chemical kinetics. *International Journal of Automotive Engineering*, 4(3):792–804, 2014.

[71] U. Egüz, N.C.J. Maes, C.A.J. Leermakers, L.M.T. Somers, and L.P.H. De Goey. Predicting auto-ignition characteristics of RCCI combustion using a multi-zone model. *International Journal of Automotive Technology*, 14(5):693–699, 2013.

[72] J. Bengtsson, P. Strandh, R. Johansson, P. Tunestål, and B. Johansson. Hybrid

modelling of homogeneous charge compression ignition (HCCI) engine dynamic-sâĂŤa survey. *International journal of control*, 80(11):1814–1847, 2007.

[73] D.J. Rausen, A.G. Stefanopoulou, J.M. Kang, J.A. Eng, and T.W. Kuo. A mean-value model for control of homogeneous charge compression ignition (HCCI) engines. *Journal of Dynamic Systems, Measurement, and Control*, 127(3):355–362, 2005.

[74] N. Cavina, C. Siviero, and R. Suglia. Residual gas fraction estimation: Application to a GDI engine with variable valve timing and EGR. SAE Technical Paper 2004-01-2943, 2004.

[75] J. H. Chen, E. R. Hawkes, R. Sankaran, S. D. Mason, and H.G. Im. Direct numerical simulation of ignition front propagation in a constant volume with temperature inhomogeneities: I. Fundamental analysis and diagnostics. *Combustion and flame*, 145(1):128–144, 2006.

[76] J. B. Heywood. *Internal combustion engine fundamentals,Chapter-5*. Mcgraw-hill New York, 1988.

[77] J.K. Arora. Design of real-time combustion feedback system and experimental study of an RCCI engine for control. Master's thesis, Michigan Technological University, 2016.

[78] J.G. Ziegler and N.B. Nichols. Optimum settings for automatic controllers. *Journal of Dynamic Systems, Measurement, and Control*, 115(2B):220–222, 1993.

Appendix A

Experimental Data Summary

A.1 Experimental Data for RCCI Naturally Aspirated

Table A.1

Operating Conditions for RCCI Mapping Data - Naturally Aspirated

Exp #	T_{in} (°C)	P_{man} (kPa)	N (rpm)	λ (-)	SOI (CAD)	PR (-)	CA50 (CAD)	IMEP (kPa)	BMEP (kPa)	$T_{exhaust}$ (°C)	MPRR (bar)	COV (%)	$\eta_{ind,th}$ (%)	ISFC (g/kWh)
1	40	95	800	2.83	25	20	7	352.81	288.38	279.9	2.7	9.4	35.99	224.7
2	40	95	800	1.52	25	20	6	581.15	480.59	389.5	5.0	3.2	34.32	235.6
3	40	95	800	1.06	25	20	7	696.18	588.82	439.9	6.0	2.7	28.93	279.5
4	40	95	1000	3.19	35	20	10	312.01	277.94	280.2	1.3	8.0	35.01	231.0
5	40	95	1000	2.00	35	20	7	503.05	408.98	358.6	3.7	2.6	40.32	200.6
6	40	95	1000	1.49	35	20	7	615.43	509.09	432.3	4.2	3.3	36.35	222.5
7	40	95	1000	1.01	35	20	8	740.01	627.50	491.6	6.3	2.8	29.66	272.7
8	40	95	1200	2.40	50	20	8	506.99	410.27	367.3	2.8	4.4	47.41	170.6
9	40	95	1200	1.98	50	20	8	584.74	475.81	400.9	4.3	2.9	43.74	184.9
10	40	95	1200	1.51	50	20	5	674.07	556.98	460.7	6.4	2.6	39.81	203.1
11	40	95	1200	1.00	50	20	7	795.77	675.90	533.2	8.1	2.5	31.89	253.6
12	40	95	1400	2.41	60	20	9	538.14	433.65	385.6	2.8	3.7	48.31	167.4
13	40	95	1400	2.06	60	20	7	610.65	492.02	407.2	4.5	2.3	46.30	174.7
14	40	95	1400	1.87	60	20	5	653.20	530.27	424.6	6.5	2.9	44.42	182.0
15	40	94	1400	1.63	60	20	4	698.53	573.63	451.3	7.9	2.1	42.37	190.9
16	40	94	800	2.10	35	40	8	442.32	371.74	371.0	2.8	8.7	35.49	228.1
17	40	94	800	1.69	35	40	6	583.55	486.73	405.8	4.7	7.6	38.56	209.9
18	40	94	800	1.44	35	40	5	689.12	582.50	441.5	6.7	2.1	38.70	209.1
19	40	94	800	1.27	35	40	5	734.79	626.26	471.8	6.8	1.8	35.88	225.6
20	40	94	800	1.04	35	40	7	784.32	674.49	483.1	7.1	1.9	31.46	257.3
21	40	94	1000	2.06	40	40	8	468.18	391.54	402.9	2.7	8.5	37.56	215.5
22	40	94	1000	1.66	40	40	6	625.14	519.60	437.0	5.3	6.2	41.30	196.0
23	40	94	1000	1.43	40	40	5	708.12	596.11	475.7	6.9	2.3	39.77	203.5

continued on next page...

Exp #	T_{in} (°C)	P_{man} (kPa)	N (rpm)	λ (-)	SOI (CAD)	PR (-)	CA50 (CAD)	IMEP (kPa)	BMEP (kPa)	$T_{exhaust}$ (°C)	MPRR (bar)	COV (%)	$\eta_{ind,th}$ (%)	ISFC (g/kWh)
24	40	94	1000	1.21	40	40	5	767.00	652.95	508.8	7.8	2.0	35.90	225.5
25	40	94	1000	1.03	40	40	7	809.19	694.42	523.1	7.0	1.4	32.46	249.4
26	40	94	1200	1.90	50	40	9	587.47	489.96	450.3	3.2	9.6	41.24	196.3
27	40	94	1200	1.66	50	40	7	699.54	583.64	484.4	5.6	5.2	41.35	195.7
28	40	95	1200	1.47	50	40	6	775.64	656.34	513.5	7.3	2.0	39.60	204.4
29	40	94	1200	1.26	50	40	8	825.99	706.00	541.6	8.1	1.8	35.68	226.8
30	40	94	1200	1.01	50	40	13	853.27	734.67	544.9	5.8	1.2	30.92	261.8
31	40	94	1400	1.95	60	40	10	652.16	537.53	461.3	3.5	8.1	44.94	180.1
32	40	94	1400	1.71	60	40	9	753.20	629.75	484.6	6.0	2.2	44.53	181.8
33	40	94	1400	1.52	60	40	7	811.99	685.75	500.3	7.6	1.7	41.46	195.2
34	40	94	1600	1.85	60	40	14	729.71	614.60	547.6	3.2	4.5	43.14	187.6
35	40	94	1600	1.60	60	40	14	796.66	675.10	580.3	3.9	3.5	40.67	199.0
36	40	94	1600	1.37	60	40	14	838.46	715.58	604.4	3.0	3.7	37.67	214.9
37	40	94	800	1.71	40	60	9	679.02	583.14	457.6	4.2	8.0	39.15	207.0
38	40	93	800	1.43	40	60	8	751.24	644.46	479.5	5.8	2.7	38.39	211.0
39	40	93	800	1.04	40	60	10	853.29	742.42	502.0	7.7	1.3	33.08	244.9
40	40	93	1000	1.98	45	60	7	708.31	597.79	462.5	4.7	6.7	41.92	193.3
41	40	93	1000	1.64	45	60	8	784.93	671.07	488.4	5.6	2.9	40.12	202.0
42	40	93	1000	1.42	45	60	7	846.54	730.01	511.6	7.7	1.6	38.07	212.8
43	40	93	1000	1.25	45	60	8	874.97	757.29	515.6	8.9	1.2	35.14	230.6
44	40	94	1000	1.03	45	60	18	860.44	753.08	510.0	3.7	1.6	29.32	276.4
45	60	94	800	3.91	20	20	6	276.27	235.08	247.7	2.3	5.6	34.44	234.8
46	60	94	800	3.11	20	20	6	306.53	253.62	276.7	2.8	6.9	34.05	237.4
47	60	94	800	2.09	20	20	7	443.55	365.13	340.2	3.6	2.7	38.28	211.2
48	60	94	800	1.53	20	20	7	544.63	455.63	407.2	4.0	3.1	33.03	244.8
49	60	95	800	1.27	20	20	8	608.25	513.41	437.5	4.2	3.1	31.02	260.7

continued on next page...

Exp #	T_{in} (°C)	P_{man} (kPa)	N (rpm)	λ (-)	SOI (CAD)	PR (-)	CA50 (CAD)	IMEP (kPa)	BMEP (kPa)	$T_{exhaust}$ (°C)	MPRR (bar)	COV (%)	$\eta_{ind,th}$ (%)	ISFC (g/kWh)
50	60	94	800	1.03	20	20	10	664.94	566.33	462.4	4.2	2.6	27.63	292.6
51	60	94	1000	3.73	25	20	6	290.51	243.18	284.0	2.3	4.9	36.22	223.3
52	60	94	1000	3.12	25	20	6	314.85	262.35	295.1	2.3	6.4	35.33	228.9
53	60	94	1000	2.05	25	20	7	454.27	372.84	361.6	3.2	2.8	39.21	206.2
54	60	94	1000	1.54	25	20	8	548.74	457.40	431.2	3.3	3.2	34.21	236.4
55	60	94	1000	1.26	25	20	9	623.22	524.37	476.4	3.6	3.0	31.79	254.4
56	60	94	1000	1.02	25	20	10	677.33	575.51	506.5	3.9	2.8	28.15	287.3
57	60	94	1200	3.16	35	20	6	326.94	264.12	324.2	2.3	7.9	36.68	220.4
58	60	94	1200	2.08	35	20	7	471.08	380.75	383.7	3.3	2.7	40.66	198.9
59	60	95	1200	1.63	35	20	7	554.99	454.41	467.3	3.7	4.0	36.63	220.7
60	60	94	1200	1.26	35	20	8	649.14	540.47	529.4	4.1	4.3	33.11	244.2
61	60	94	1200	1.03	35	20	8	709.92	597.66	556.9	4.5	3.3	29.50	274.1
62	60	94	1400	2.78	45	20	6	360.92	283.65	365.9	2.3	8.9	36.82	219.6
63	60	94	1400	2.33	45	20	6	452.97	356.25	385.4	2.9	7.5	42.36	190.9
64	60	94	1400	2.03	45	20	5	486.78	382.17	422.5	3.8	5.3	39.01	207.3
65	60	94	1400	1.61	45	20	6	592.09	478.54	479.7	4.6	4.1	36.91	219.1
66	60	94	1400	1.31	45	20	7	668.27	550.33	552.0	4.9	3.9	34.08	237.2
67	60	94	1400	1.01	45	20	7	741.19	619.55	587.5	5.2	3.7	30.80	262.5
68	60	94	1600	1.01	50	20	10	473.74	386.21	410.8	2.2	6.9	44.30	182.5
69	60	94	1600	2.04	50	20	9	501.83	400.54	442.2	3.1	4.0	40.22	201.0
70	60	93	1600	1.59	50	20	9	603.66	490.23	527.7	3.7	3.7	37.63	214.9
71	60	93	1600	1.31	50	20	10	678.59	559.83	593.2	4.2	4.3	34.61	233.6
72	60	93	1600	1.02	50	20	11	745.47	623.20	641.2	4.4	4.0	29.87	270.7
73	60	93	1800	2.28	60	20	6	515.07	394.90	433.2	4.2	4.2	46.24	174.9
74	60	94	1800	2.14	60	20	5	536.79	412.42	451.5	5.1	5.1	43.02	188.0
75	60	93	1800	1.70	60	20	4	657.27	525.25	518.8	7.2	3.0	40.97	197.4

continued on next page...

Exp #	T_{in} (°C)	P_{man} (kPa)	N (rpm)	λ (-)	SOI (CAD)	PR (-)	CA50 (CAD)	IMEP (kPa)	BMEP (kPa)	$T_{exhaust}$ (°C)	MPRR (bar)	COV (%)	$\eta_{ind,th}$ (%)	ISFC (g/kWh)
76	60	94	1800	1.42	60	20	5	716.58	583.90	585.8	7.1	3.5	38.29	211.2
77	60	94	1800	1.09	60	20	8	794.93	661.16	631.3	6.8	3.3	33.04	244.8
78	60	94	2000	1.97	70	20	6	616.16	479.77	476.1	6.1	3.2	44.61	181.3
79	60	94	2000	1.72	70	20	4	699.94	559.60	516.8	9.0	2.7	42.45	190.5
80	60	93	800	2.52	25	40	7	383.33	324.58	334.0	2.6	9.1	34.45	235.0
81	60	93	800	2.11	25	40	6	422.12	352.36	366.5	3.2	7.0	33.87	239.0
82	60	93	800	1.58	25	40	7	563.98	474.30	423.5	4.4	5.8	35.19	230.0
83	60	93	800	1.26	25	40	8	676.73	579.91	472.1	4.7	2.9	33.05	244.9
84	60	93	800	1.03	25	40	10	739.80	638.05	483.9	4.8	1.6	29.68	272.7
85	60	94	1000	2.36	30	40	7	414.88	345.00	380.8	2.9	8.4	35.85	225.8
86	60	94	1000	1.95	30	40	7	469.03	388.86	414.7	3.3	7.9	35.12	230.5
87	60	94	1000	1.53	30	40	7	595.22	497.48	467.7	4.6	5.1	36.14	224.0
88	60	94	1000	1.25	30	40	7	703.51	597.11	499.4	5.3	3.0	34.36	235.6
89	60	94	1000	1.01	30	40	8	762.43	652.26	516.3	5.4	1.6	30.59	264.7
90	60	94	1200	1.78	40	40	7	559.99	461.44	467.2	3.8	7.5	39.31	205.9
91	60	94	1200	1.51	40	40	7	645.83	538.22	516.4	4.7	4.2	38.18	212.0
92	60	94	1200	1.23	40	40	8	740.40	627.14	564.5	5.3	2.7	35.39	228.7
93	60	94	1200	1.03	40	40	10	782.94	668.60	578.3	4.9	2.0	31.98	253.1
94	60	94	1400	1.75	47	40	8	596.52	488.13	498.5	4.0	7.5	40.61	199.3
95	60	94	1400	1.51	47	40	7	678.31	562.20	544.4	5.1	4.3	39.07	207.2
96	60	94	1400	1.25	47	40	8	768.41	648.31	603.1	5.5	2.7	35.96	225.1
97	60	94	1400	1.01	47	40	11	825.55	704.27	618.1	5.6	2.2	31.98	253.1
98	60	94	1600	1.93	60	40	7	626.78	506.37	497.2	4.3	8.1	44.00	184.0
99	60	94	1600	1.67	60	40	6	707.38	580.04	543.2	6.0	6.3	41.82	193.6
100	60	94	1600	1.43	60	40	6	781.80	652.33	569.3	7.9	2.1	41.82	193.6
101	60	94	1800	1.83	65	40	7	688.89	556.56	532.2	6.3	4.4	45.52	177.8

continued on next page...

Exp #	T_{in} (°C)	P_{man} (kPa)	N (rpm)	λ (-)	SOI (CAD)	PR (-)	CA50 (CAD)	IMEP (kPa)	BMEP (kPa)	$T_{exhaust}$ (°C)	MPRR (bar)	COV (%)	$\eta_{ind,th}$ (%)	ISFC (g/kWh)
102	60	94	1800	1.60	65	40	6	763.09	628.43	571.6	8.0	2.9	42.86	188.9
103	60	94	800	1.65	30	60	10	638.13	553.20	475.2	3.8	7.6	36.79	220.2
104	60	94	800	1.47	30	60	9	693.05	599.34	487.2	4.9	3.2	37.11	218.4
105	60	94	800	1.29	30	60	9	751.82	648.56	505.2	5.0	2.6	35.22	230.0
106	60	94	800	1.02	30	60	10	812.05	703.03	507.3	5.9	1.3	31.48	257.4
107	60	94	1000	1.65	35	60	8	668.49	571.15	490.0	3.9	7.7	37.96	213.4
108	60	93	1000	1.41	35	60	8	732.24	626.36	509.9	4.8	2.6	37.42	216.5
109	60	93	1000	1.22	35	60	8	785.15	672.42	528.9	5.7	1.9	35.31	229.5
110	60	94	1000	1.01	35	60	10	834.95	721.00	531.1	5.8	1.1	32.37	250.3
111	60	94	1200	1.68	50	60	10	724.41	615.36	526.0	3.8	9.2	39.73	203.9
112	60	94	1200	1.54	50	60	10	801.23	684.63	546.7	5.1	2.9	39.17	206.9
113	60	94	1200	1.28	50	60	11	859.38	740.41	567.5	6.0	1.8	35.79	226.4
114	60	95	1200	1.05	50	60	15	872.21	755.02	553.8	5.1	0.9	31.64	256.1
115	60	95	1400	1.69	55	60	15	718.04	622.55	553.7	2.4	12.0	37.55	215.8
116	60	95	1400	1.52	55	60	13	832.35	713.61	581.1	3.9	4.0	38.99	207.8
117	60	95	1400	1.29	55	60	16	875.14	757.47	606.4	3.8	2.8	35.14	230.6
118	60	94	1400	1.02	55	60	23	867.61	777.97	597.9	2.0	4.0	29.56	274.1
119	80	94	800	3.62	23	20	4	262.49	216.61	254.5	2.6	8.2	32.01	252.6
120	80	94	800	3.09	23	20	4	264.19	215.43	268.2	2.8	5.5	29.06	278.2
121	80	94	800	2.04	23	20	2	441.02	349.86	327.8	5.6	4.5	38.97	207.5
122	80	94	800	1.51	23	20	2	544.35	442.82	382.1	6.0	2.9	33.93	238.3
123	80	94	800	1.22	23	20	1	606.30	499.86	414.0	7.3	2.7	30.92	261.5
124	80	94	800	1.00	23	20	2	657.91	549.49	433.8	8.3	2.1	27.86	290.3
125	80	94	1000	3.08	25	20	5	286.09	235.34	307.5	2.3	6.8	32.10	251.9
126	80	95	1000	2.01	25	20	6	436.84	353.67	374.5	3.8	3.7	39.21	206.2
127	80	95	1000	1.49	25	20	7	534.60	441.22	431.1	4.0	3.1	33.33	242.6

continued on next page...

Exp #	T_{in} (°C)	P_{man} (kPa)	N (rpm)	λ (-)	SOI (CAD)	PR (-)	CA50 (CAD)	IMEP (kPa)	BMEP (kPa)	$T_{exhaust}$ (°C)	MPRR (bar)	COV (%)	$\eta_{ind,th}$ (%)	ISFC (g/kWh)
128	80	95	1000	1.20	25	20	8	603.05	504.33	460.2	4.0	3.2	30.76	262.9
129	80	96	1000	1.01	25	20	9	651.48	549.18	496.0	4.4	2.7	28.12	287.6
130	80	96	1200	3.27	30	20	5	298.19	240.17	319.5	2.3	8.1	35.22	229.6
131	80	96	1200	2.11	30	20	6	419.44	337.47	382.9	3.1	3.9	39.22	206.2
132	80	96	1200	1.49	30	20	9	534.20	442.08	469.0	3.2	3.7	33.30	242.8
133	80	96	1200	1.20	30	20	10	601.87	503.50	519.6	3.3	3.7	30.70	263.4
134	80	96	1200	1.02	30	20	11	649.98	548.37	551.4	3.4	3.6	28.05	288.3
135	80	96	1400	3.11	37	20	4	314.39	239.50	346.4	2.5	6.5	35.28	229.2
136	80	96	1400	2.02	37	20	6	455.18	357.35	417.4	3.4	4.0	39.29	205.8
137	80	96	1400	1.52	37	20	7	549.87	444.86	509.0	3.4	3.5	34.28	235.9
138	80	96	1400	1.24	37	20	8	622.35	512.40	559.4	3.6	4.0	31.74	254.7
139	80	96	1400	1.06	37	20	9	666.83	554.23	585.8	3.7	3.6	29.34	275.6
140	80	96	1600	2.62	42	20	5	365.40	280.53	390.3	2.5	8.3	37.27	216.9
141	80	96	1600	2.04	42	20	7	460.49	362.98	435.9	3.1	4.1	39.75	203.4
142	80	95	1600	1.54	42	20	10	549.58	446.87	536.4	2.8	4.1	34.26	236.0
143	80	95	1600	1.25	42	20	10	626.80	516.72	610.4	3.2	4.0	31.97	252.9
144	80	95	1600	1.08	42	20	12	668.06	556.55	643.4	3.2	4.1	29.40	275.1
145	80	95	1800	2.19	53	20	5	471.50	359.95	450.2	3.4	4.7	44.09	183.4
146	80	95	1800	2.02	53	20	5	504.36	388.55	461.7	3.8	3.0	43.53	185.7
147	80	95	1800	1.54	53	20	7	604.08	481.41	552.2	4.3	4.1	37.66	214.7
148	80	95	1800	1.26	53	20	8	680.28	553.34	619.7	4.6	3.6	34.70	233.1
149	80	95	1800	1.07	53	20	9	730.36	601.40	651.8	4.9	4.1	31.52	256.5
150	80	96	2000	2.24	57	20	5	468.26	350.96	448.9	3.2	4.8	43.79	184.7
151	80	96	2000	2.08	57	20	6	505.42	385.54	462.6	3.2	3.6	43.62	185.4
152	80	95	2000	1.56	57	20	7	605.12	477.25	568.9	3.9	4.1	37.72	214.4
153	80	95	2000	1.27	57	20	9	669.38	539.21	639.1	3.9	4.1	34.14	236.8

continued on next page...

Exp #	T_{in} (°C)	P_{man} (kPa)	N (rpm)	λ (-)	SOI (CAD)	PR (-)	CA50 (CAD)	IMEP (kPa)	BMEP (kPa)	$T_{exhaust}$ (°C)	MPRR (bar)	COV (%)	$\eta_{ind,th}$ (%)	ISFC (g/kWh)
154	80	95	2000	1.09	57	20	10	711.70	580.59	670.7	3.9	3.5	30.71	263.3
155	80	95	2200	2.26	65	20	8	471.08	357.49	482.8	2.7	8.1	44.05	183.6
156	80	95	2200	2.08	65	20	7	521.68	397.78	488.5	3.4	4.3	45.03	179.6
157	80	96	2200	1.61	65	20	7	618.90	482.31	569.4	4.7	3.3	40.85	197.9
158	80	96	800	3.20	16	40	5	316.44	276.99	299.9	2.5	5.9	37.41	216.3
159	80	96	800	3.08	16	40	7	313.51	275.08	295.2	2.3	11.8	34.52	234.5
160	80	96	800	2.10	16	40	8	379.57	327.96	354.4	2.9	6.2	30.45	265.8
161	80	96	800	1.55	16	40	8	546.18	461.49	420.7	4.4	4.7	34.08	237.5
162	80	96	800	1.26	16	40	7	649.17	553.97	456.4	5.3	2.5	33.14	244.2
163	80	96	800	1.03	16	40	9	706.43	605.84	473.2	5.4	1.5	29.39	275.4
164	80	96	1000	2.68	25	40	7	361.92	306.44	351.3	2.4	8.0	35.35	229.0
165	80	59	1000	2.12	25	40	7	402.56	347.13	389.8	2.5	7.1	33.49	241.7
166	80	95	1000	1.51	25	40	9	568.19	478.22	460.5	3.9	3.9	35.46	228.3
167	80	94	1000	1.24	25	40	9	656.43	559.45	499.5	4.5	3.2	33.51	241.5
168	80	96	1000	1.04	25	40	10	714.26	613.61	516.7	4.5	2.1	30.27	267.4
169	80	81	1200	2.62	35	40	6	387.25	319.67	367.9	2.4	7.5	37.18	217.7
170	80	95	1200	2.12	35	40	7	424.69	349.48	404.7	2.8	6.9	35.34	229.1
171	80	96	1200	1.52	35	40	7	588.48	489.10	488.0	3.9	4.6	36.72	220.4
172	80	96	1200	1.24	35	40	7	678.28	571.40	543.5	4.8	3.3	34.63	233.7
173	80	96	1200	1.04	35	40	9	742.07	631.16	568.5	4.6	2.3	31.45	257.3
174	80	95	1400	2.62	40	40	8	396.25	324.34	386.1	2.0	9.1	37.09	218.2
175	80	91	1400	2.08	40	40	8	438.19	359.09	446.4	2.5	7.2	34.42	235.2
176	80	95	1400	1.58	40	40	9	582.57	480.20	523.8	3.4	5.1	36.35	222.7
177	80	95	1400	1.29	40	40	9	684.92	572.84	581.5	4.3	3.7	34.97	231.5
178	80	99	1400	1.10	40	40	10	745.61	630.63	614.4	4.3	3.0	32.21	251.3
179	80	96	1600	2.44	52	40	8	459.00	371.40	437.4	2.4	9.2	39.66	204.1

continued on next page...

Exp #	T_{in} (°C)	P_{man} (kPa)	N (rpm)	λ (-)	SOI (CAD)	PR (-)	CA50 (CAD)	IMEP (kPa)	BMEP (kPa)	$T_{exhaust}$ (°C)	MPRR (bar)	COV (%)	$\eta_{ind,th}$ (%)	ISFC (g/kWh)
180	80	96	1600	2.01	52	40	9	495.29	405.83	489.5	2.3	8.9	37.59	215.3
181	80	95	1600	1.58	52	40	7	646.12	528.16	547.9	4.4	5.3	40.32	200.8
182	80	95	1600	1.30	52	40	9	733.18	611.37	605.7	4.8	2.9	37.43	216.2
183	80	95	1600	1.11	52	40	11	774.82	653.38	635.6	4.9	2.4	33.47	241.8
184	80	95	1800	2.31	60	40	7	514.26	406.45	465.0	2.8	7.4	42.79	189.2
185	80	95	1800	2.06	60	40	8	560.71	448.16	498.6	3.1	8.2	41.99	192.8
186	80	95	1800	1.42	60	40	7	741.09	609.00	582.2	6.2	2.5	41.62	194.5
187	80	95	1800	1.30	60	40	6	775.19	641.66	618.4	6.6	2.2	39.58	204.5
188	80	95	2000	2.02	70	40	9	587.17	467.57	514.5	2.6	8.9	41.22	196.4
189	80	95	2000	1.86	70	40	7	639.96	507.13	528.4	4.3	7.5	42.28	191.4
190	80	95	800	1.83	16	60	10	557.25	483.86	434.2	3.6	9.9	35.80	226.3
191	80	94	800	1.53	16	60	10	649.33	565.61	468.4	4.7	3.7	36.50	222.0
192	80	94	800	1.22	16	60	9	729.29	623.98	488.5	5.3	1.4	34.17	237.2
193	80	94	800	1.03	16	60	9	766.02	657.31	484.8	6.1	1.2	30.76	263.4
194	80	94	1000	1.74	29	60	9	602.51	517.53	487.3	3.8	8.2	36.62	221.3
195	80	95	1000	1.52	29	60	8	661.60	570.67	504.5	4.3	3.0	37.19	217.8
196	80	95	1000	1.22	29	60	9	734.72	634.02	520.2	4.5	2.0	34.42	235.4
197	80	95	1000	1.02	29	60	9	796.17	684.01	523.1	5.5	1.2	31.97	253.4
198	80	92	1200	1.67	42	60	7	667.39	564.88	520.7	3.9	6.9	39.08	207.3
199	80	91	1200	1.48	42	60	7	705.57	597.44	538.3	4.2	3.7	38.70	209.4
200	80	94	1200	1.20	42	60	7	777.36	661.06	568.2	5.1	2.0	35.68	227.1
201	80	95	1200	1.01	42	60	9	826.25	707.92	560.2	5.3	1.3	32.60	248.6
202	80	83	1400	1.64	52	60	6	708.59	593.06	547.6	4.1	8.3	39.84	203.4
203	80	80	1400	1.43	52	60	5	758.27	638.25	580.5	4.7	3.0	38.75	209.1
204	80	80	1400	1.26	52	60	7	823.34	699.07	606.1	5.8	2.4	37.03	218.8
205	80	85	1400	1.05	52	60	8	873.88	748.47	599.8	6.9	1.4	34.48	235.0

continued on next page...

Exp #	T_{in} (°C)	P_{man} (kPa)	N (rpm)	λ (-)	SOI (CAD)	PR (-)	CA50 (CAD)	IMEP (kPa)	BMEP (kPa)	$T_{exhaust}$ (°C)	MPRR (bar)	COV (%)	$\eta_{ind,th}$ (%)	ISFC (g/kWh)
206	80	84	1600	1.69	60	60	9	744.41	619.95	589.7	4.0	6.4	40.83	198.5
207	80	95	1600	1.52	60	60	9	802.94	674.67	619.2	4.6	2.4	39.25	206.4
208	80	95	1600	1.31	60	60	8	851.82	722.23	649.5	5.8	2.5	36.84	220.0
209	80	48	1600	1.02	60	60	11	885.97	755.46	654.1	7.0	0.8	32.13	252.2
210	80	26	1800	1.56	70	60	14	783.24	659.06	632.7	2.7	5.2	40.03	202.4
211	80	94	1800	1.43	70	60	13	839.88	708.00	651.1	4.1	3.1	39.35	205.9
212	80	94	1800	1.20	70	60	13	887.36	753.76	659.7	4.5	1.6	35.63	227.4
213	80	95	1800	1.02	70	60	14	893.90	759.79	612.3	5.8	1.1	32.42	249.9
214	100	95	800	3.13	15	20	5	272.98	234.47	288.6	2.7	7.6	30.63	264.0
215	100	95	800	2.02	15	20	6	395.45	327.67	342.3	3.8	5.9	34.13	236.9
216	100	95	800	1.50	15	20	6	492.27	409.87	416.4	4.7	3.2	30.69	263.5
217	100	94	800	1.21	15	20	8	557.24	468.09	442.0	4.7	3.3	28.42	284.5
218	100	94	800	1.01	15	20	9	611.13	516.88	466.9	5.3	2.3	26.37	306.6
219	100	94	1000	2.92	20	20	7	286.84	248.26	335.1	1.9	8.0	31.25	258.8
220	100	94	1000	2.00	20	20	9	403.71	343.24	380.0	2.5	5.2	34.85	232.1
221	100	95	1000	1.47	20	20	11	487.41	418.26	447.5	2.8	3.5	30.38	266.1
222	100	95	1000	1.20	20	20	12	544.41	470.99	494.0	2.8	3.7	27.77	291.2
223	100	99	1000	1.00	20	20	14	594.02	516.32	530.2	2.9	2.6	25.64	315.4
224	100	95	1200	2.79	28	20	5	310.54	253.75	362.2	2.3	7.5	32.57	248.3
225	100	95	1200	2.01	28	20	7	413.13	338.96	417.2	2.7	5.9	36.50	221.5
226	100	95	1200	1.48	28	20	9	503.31	418.90	484.1	3.0	4.2	31.38	257.7
227	100	95	1200	1.20	28	20	10	570.17	479.48	547.9	3.1	4.3	29.08	278.1
228	100	95	1200	1.01	28	20	11	618.17	525.35	565.3	3.1	3.7	26.68	303.1
229	100	95	1400	2.65	33	20	4	331.73	263.62	388.6	2.4	8.3	33.24	243.3
230	100	95	1400	2.06	33	20	7	416.13	334.83	430.1	2.6	5.7	35.92	225.1
231	100	95	1400	1.52	33	20	9	511.33	420.23	513.7	2.8	3.8	31.88	253.7

continued on next page...

Exp #	T_{in} (°C)	P_{man} (kPa)	N (rpm)	λ (-)	SOI (CAD)	PR (-)	CA50 (CAD)	IMEP (kPa)	BMEP (kPa)	$T_{exhaust}$ (°C)	MPRR (bar)	COV (%)	$\eta_{ind,th}$ (%)	ISFC (g/kWh)
232	100	95	1400	1.23	33	20	10	579.89	482.74	574.4	2.8	3.5	29.58	273.4
233	100	95	1400	1.04	33	20	9	625.85	530.41	611.4	3.0	3.7	27.01	299.4
234	100	95	1600	2.22	40	20	0	394.50	313.72	450.4	2.9	8.2	36.89	219.2
235	100	95	1600	2.01	40	20	-6	436.98	349.61	457.3	3.1	6.2	37.72	214.4
236	100	81	1600	1.51	40	20	7	531.28	434.28	549.9	3.1	4.1	33.12	244.2
237	100	93	1600	1.22	40	20	10	600.21	495.20	609.2	3.1	4.6	30.61	264.1
238	100	94	1600	1.04	40	20	10	641.41	536.67	647.6	3.0	4.1	27.68	292.1
239	100	94	1800	2.18	47	20	5	415.55	316.34	462.7	2.7	7.9	38.86	208.1
240	100	8	1800	2.04	47	20	4	451.64	354.39	472.7	2.9	5.8	40.22	201.0
241	100	63	1800	1.53	47	20	7	557.83	445.28	562.2	3.4	4.7	34.77	232.5
242	100	93	1800	1.25	47	20	9	623.03	506.21	628.9	3.4	5.0	31.78	254.5
243	100	94	1800	1.05	47	20	10	670.37	551.07	666.8	3.6	5.2	28.93	279.5
244	100	94	2000	2.06	53	20	5	429.45	324.44	487.2	2.7	9.2	35.69	226.5
245	100	94	2000	1.54	53	20	7	561.97	441.62	573.6	3.2	4.2	35.03	230.8
246	100	94	2000	1.25	53	20	8	627.87	503.61	643.2	3.5	5.2	32.02	252.5
247	100	95	2000	1.09	53	20	9	661.60	537.21	679.1	3.4	4.2	28.55	283.2
248	100	95	800	2.67	17	40	5	338.94	289.32	320.8	3.4	7.0	34.61	233.9
249	100	95	800	2.00	17	40	6	397.55	334.57	362.2	3.9	6.6	33.08	244.7
250	100	94	800	1.48	17	40	6	575.93	487.18	417.8	5.4	2.8	35.94	225.2
251	100	94	800	1.22	17	40	6	586.56	497.59	455.5	4.8	18.2	29.95	270.3
252	100	94	800	1.07	17	40	8	684.95	584.57	446.2	5.3	1.8	29.59	273.5
253	100	94	1000	2.65	24	40	7	343.43	298.32	355.8	2.4	11.3	34.44	235.0
254	100	94	1000	1.99	24	40	8	413.56	351.99	391.3	3.0	6.0	34.16	237.0
255	100	95	1000	1.44	24	40	9	552.25	468.20	480.5	3.8	3.6	34.46	234.9
256	100	95	1000	1.04	24	40	11	686.73	593.51	523.8	3.8	2.2	29.67	272.8
257	100	94	1200	2.48	32	40	6	380.58	316.94	382.8	2.6	5.5	36.54	221.5

continued on next page...

Exp #	T_{in} (°C)	P_{man} (kPa)	N (rpm)	λ (-)	SOI (CAD)	PR (-)	CA50 (CAD)	IMEP (kPa)	BMEP (kPa)	$T_{exhaust}$ (°C)	MPRR (bar)	COV (%)	$\eta_{ind,th}$ (%)	ISFC (g/kWh)
258	100	94	1200	1.98	32	40	6	425.91	352.98	428.5	3.0	6.1	34.67	233.5
259	100	94	1200	1.46	32	40	8	567.90	474.66	505.3	3.9	3.9	35.44	228.4
260	100	94	1200	1.20	32	40	9	652.53	552.84	549.7	4.3	3.5	33.32	243.0
261	100	95	1200	1.03	32	40	10	703.39	600.77	567.4	4.1	2.1	30.39	266.4
262	100	94	1400	2.56	39	40	6	393.44	318.76	389.6	2.4	7.2	36.83	219.8
263	100	94	1400	2.03	39	40	7	430.76	349.63	439.5	2.8	6.7	34.56	234.2
264	100	94	1400	1.53	39	40	7	563.86	463.48	522.5	3.7	5.0	35.19	230.0
265	100	94	1400	1.26	39	40	8	669.53	559.81	581.9	4.3	3.5	34.18	236.8
266	100	94	1400	1.08	39	40	9	724.41	611.58	615.9	4.3	2.8	31.30	258.6
267	100	94	1600	2.47	49	40	7	428.52	346.55	424.8	2.2	13.2	37.90	213.6
268	100	94	1600	2.07	49	40	8	450.03	367.94	469.4	2.2	7.8	36.11	224.2
269	100	94	1600	1.55	49	40	7	605.87	495.04	548.6	3.9	5.9	37.81	214.1
270	100	94	1600	1.27	49	40	9	691.75	575.98	610.2	4.2	3.1	35.32	229.2
271	100	94	1600	1.08	49	40	12	735.43	621.27	637.4	4.0	3.1	31.77	254.8
272	100	94	1800	2.02	58	40	7	503.00	400.93	498.3	2.7	6.9	40.36	200.6
273	100	94	1800	1.55	58	40	7	643.05	520.30	560.2	4.3	6.1	40.13	201.7
274	100	94	1800	1.28	58	40	7	739.64	608.80	624.2	5.7	2.5	37.76	214.3
275	100	93	1800	1.18	58	40	7	766.60	634.42	652.4	6.0	2.2	35.88	225.6
276	100	94	2000	1.79	65	40	8	538.77	428.15	544.3	2.4	7.6	37.82	214.0
277	100	94	2000	1.59	65	40	6	653.18	520.41	569.6	4.6	6.5	40.76	198.6
278	100	95	800	1.79	15	60	10	550.56	482.41	453.0	3.8	9.4	36.41	222.5
279	100	95	800	1.71	15	60	10	576.59	505.87	460.5	4.1	8.0	36.63	221.2
280	100	95	800	1.47	15	60	11	635.46	558.35	487.3	4.5	3.1	35.72	226.8
281	100	94	800	1.17	15	60	10	711.13	608.39	497.9	5.4	1.7	33.32	243.2
282	100	95	1000	1.72	29	60	9	592.02	508.47	490.4	3.7	8.6	36.98	219.1
283	100	95	1000	1.43	29	60	9	661.82	570.03	512.8	4.4	2.8	36.30	223.2

continued on next page...

Exp #	T_{in} (°C)	P_{man} (kPa)	N (rpm)	λ (-)	SOI (CAD)	PR (-)	CA50 (CAD)	IMEP (kPa)	BMEP (kPa)	$T_{exhaust}$ (°C)	MPRR (bar)	COV (%)	$\eta_{ind,th}$ (%)	ISFC (g/kWh)
284	100	95	1000	1.21	29	60	9	720.49	616.00	525.7	4.3	1.4	33.75	240.0
285	100	95	1000	1.02	29	60	8	768.95	656.42	521.6	5.5	1.0	31.44	257.7
286	100	94	1200	1.65	40	60	7	640.02	542.09	525.7	3.5	6.6	37.88	213.9
287	100	94	1200	1.41	40	60	7	696.88	590.04	548.8	4.1	2.7	37.31	217.2
288	100	95	1200	1.22	40	60	8	743.44	631.34	566.0	3.9	1.8	34.83	232.6
289	100	95	1200	1.02	40	60	8	788.54	671.30	557.4	4.9	1.1	32.36	250.4
290	100	94	1400	1.63	52	60	7	674.15	559.75	552.6	3.6	8.7	38.28	211.7
291	100	94	1400	1.42	52	60	5	732.54	610.92	576.3	4.6	2.4	38.31	211.5
292	100	94	1400	1.27	52	60	6	783.32	659.72	598.1	5.2	1.5	35.95	225.4
293	100	94	1400	1.06	52	60	7	836.77	711.91	588.4	5.8	1.3	33.60	241.1
294	100	94	1600	1.47	58	60	14	695.71	596.29	596.7	2.3	6.4	37.25	217.5
295	100	94	1600	1.26	58	60	14	774.17	663.29	616.0	2.7	2.6	35.53	228.1
296	100	94	1600	0.98	58	60	16	849.10	729.40	584.2	3.5	1.9	31.82	254.6
297	100	93	1800	1.47	70	60	15	723.70	613.43	613.6	2.1	9.8	38.75	209.1
298	100	93	1800	1.29	70	60	16	789.97	672.83	630.9	2.3	2.2	37.01	218.9
299	100	93	1800	1.05	70	60	15	859.05	730.35	606.3	3.5	1.8	34.50	234.9
300	100	94	2000	1.33	80	60	18	792.64	675.57	654.5	2.0	3.7	38.75	209.1
301	100	94	2000	1.08	80	60	14	877.45	739.57	643.5	4.6	1.8	36.54	221.7

A.2 Experimental Data for Model Parametrization

Table A.2
Operating Conditions for Model Parametrization - MKIM,BD and CA50 models

Exp #	T_{in} (°C)	P_{man} (kPa)	N (rpm)	λ (-)	m_{fuel} ($\frac{mg}{cyc}$)	SOI (CAD)	PR (-)	$CA10_{main}$ (CAD)	CA50 (CAD)	IMEP (kPa)	$T_{exhaust}$ (°C)	MPRR (bar)	COV (%)	η_{comb} (%)
1	40	102	989	2.13	14.0	100	20	0	3	523.4	336.0	4.8	7.6	89.57
2	40	101	988	1.89	15.5	100	20	-2	0	555.2	335.2	9.6	3.9	92.30
3	40	101	988	1.70	17.0	100	20	-3	-1	557.5	330.1	11.1	3.7	93.32
4	40	101	988	2.28	13.0	80	20	1	3	492.1	324.4	3.2	10.8	91.62
5	40	101	989	1.96	15.0	80	20	-1	1	551.7	330.9	7.4	3.3	89.75
6	40	101	988	1.71	17.0	80	20	-2	-1	569.2	334.1	9.3	4.2	90.33
7	40	101	988	2.27	13.0	60	20	-2	0	482.0	325.5	5.2	7.8	84.96
8	40	101	988	1.96	15.0	60	20	-2	-1	540.6	334.8	7.8	3.4	83.01
9	40	102	988	1.70	17.0	60	20	-3	-2	568.4	348.4	9.7	3.4	75.67
10	40	102	988	1.60	18.0	60	20	-3	-2	586.8	353.8	11.0	4.3	75.43
11	40	102	988	2.26	13.0	50	20	-2	0	487.2	340.1	6.3	6.5	85.47
12	40	102	988	1.95	15.0	50	20	-2	-1	541.5	363.1	7.9	4.3	81.11
13	40	102	988	1.72	17.0	50	20	-4	-2	587.2	381.3	8.6	3.5	78.34
14	40	102	988	1.52	19.0	50	20	-4	-3	623.0	408.2	10.1	3.0	74.78
15	40	102	988	1.31	22.0	50	20	-5	-3	678.8	440.6	12.3	2.7	69.67
16	40	102	988	2.22	13.2	40	20	-1	1	470.0	350.3	5.6	5.3	81.13
17	40	102	988	1.96	15.0	40	20	-1	1	517.5	379.5	6.0	4.0	77.65
18	40	101	988	1.62	18.0	40	20	-1	1	586.1	423.3	6.4	3.9	73.27
19	40	102	988	1.32	22.0	40	20	-1	1	661.5	475.4	7.6	3.6	68.74
20	40	102	988	0.99	29.0	40	20	0	2	741.9	494.9	9.6	2.2	58.11
21	40	96	988	2.35	12.5	30	20	4	7	442.4	361.6	3.4	5.9	61.49
22	40	96	988	1.95	15.0	30	20	3	6	503.1	388.9	3.9	3.6	73.97

continued on next page...

Exp #	T_{in} (°C)	P_{man} (kPa)	N (rpm)	λ (-)	m_{fuel} ($\frac{mg}{cyc}$)	SOI (CAD)	PR (-)	$CA10_{main}$ (CAD)	CA50 (CAD)	IMEP (kPa)	$T_{exhaust}$ (°C)	MPRR (bar)	COV (%)	η_{comb} (%)
23	40	96	988	1.72	17.0	30	20	3	6	543.4	415.9	4.2	3.9	70.38
24	40	96	988	1.54	19.0	30	20	3	6	584.0	445.4	4.4	3.3	67.40
25	40	96	988	1.32	22.0	30	20	3	6	638.1	476.4	5.0	3.2	63.00
26	40	96	988	1.00	29.0	30	20	4	7	725.8	500.9	5.3	3.0	54.52
27	40	96	988	2.26	13.0	20	20	9	13	431.6	393.2	1.7	3.2	74.58
28	40	96	988	1.95	15.0	20	20	10	15	469.2	414.9	1.6	3.6	70.45
29	40	96	988	1.72	17.0	20	20	10	15	505.1	444.4	1.7	3.0	66.43
30	40	96	988	1.33	22.0	20	20	11	16	585.9	510.1	1.9	3.4	61.04
31	40	96	988	1.04	28.0	20	20	13	18	645.1	551.6	1.8	3.0	53.55
32	40	96	989	1.88	16.0	100	30	3	5	593.7	355.0	4.6	7.0	86.19
33	40	96	988	1.64	18.0	100	30	2	4	649.5	364.7	7.4	2.9	85.32
34	40	96	988	2.14	14.0	80	30	4	10	494.1	349.8	1.5	18.6	82.56
35	40	96	988	1.74	17.0	80	30	2	4	637.0	373.6	8.1	2.9	86.69
36	40	96	988	1.54	19.0	80	30	1	3	660.5	380.1	8.3	3.5	86.86
37	40	96	988	2.20	13.5	60	30	1	5	501.5	352.1	3.1	9.2	81.51
38	40	96	988	1.98	15.0	60	30	1	3	576.4	362.6	5.7	6.0	85.67
39	40	96	988	1.73	17.0	60	30	0	2	622.8	372.8	8.6	3.0	80.61
40	40	96	988	1.53	19.0	60	30	0	1	654.1	384.5	10.5	3.2	76.61
41	40	96	988	2.27	13.0	50	30	1	4	463.8	361.1	3.4	9.4	77.65
42	40	96	988	1.97	15.0	50	30	0	2	574.0	378.1	6.1	6.6	82.85
43	40	96	988	1.73	17.0	50	30	-1	1	634.9	403.4	7.8	2.5	82.10
44	40	96	988	1.54	19.0	50	30	-2	0	675.3	420.8	10.0	2.5	76.60
45	40	96	988	1.32	22.0	50	30	-2	-1	719.1	444.7	11.7	2.2	71.75
46	40	96	988	2.37	12.5	40	30	3	6	402.8	352.5	2.7	7.5	70.17
47	40	96	988	1.96	15.0	40	30	2	4	555.3	381.5	5.2	5.8	80.67
48	40	96	988	1.73	17.0	40	30	1	3	605.0	417.6	6.4	3.5	78.47

continued on next page...

Exp #	T_{in} (°C)	P_{man} (kPa)	N (rpm)	λ (-)	m_{fuel} ($\frac{mg}{cyc}$)	SOI (CAD)	PR (-)	$CA10_{main}$ (CAD)	CA50 (CAD)	IMEP (kPa)	$T_{exhaust}$ (°C)	MPRR (bar)	COV (%)	η_{comb} (%)
49	40	96	988	1.46	20.0	40	30	1	3	670.0	457.5	6.4	3.1	74.17
50	40	96	988	1.21	24.0	40	30	1	3	732.5	496.5	7.6	2.3	66.35
51	40	96	988	1.03	28.0	40	30	2	4	776.9	505.6	8.7	1.9	60.89
52	40	96	988	2.36	12.5	30	30	5	9	388.1	367.9	2.1	7.3	67.85
53	40	96	988	1.96	15.0	30	30	5	9	523.4	397.6	3.2	4.8	76.14
54	40	96	988	1.72	17.0	30	30	5	8	567.4	428.2	3.7	3.6	72.71
55	40	96	988	1.46	20.0	30	30	5	8	629.1	464.1	4.1	3.3	69.91
56	40	96	988	1.22	24.0	30	30	4	8	701.9	495.5	4.9	3.4	65.13
57	40	96	988	1.04	28.0	30	30	5	8	757.2	509.8	5.2	2.1	59.92
58	40	96	988	2.27	13.0	20	30	12	17	412.9	409.2	1.1	8.1	71.39
59	40	96	988	1.96	15.0	20	30	13	19	461.6	421.9	1.0	5.8	71.11
60	40	96	989	1.72	17.0	20	30	13	19	510.0	455.2	1.2	3.8	68.14
61	40	96	992	1.76	17.0	100	40	3	5	663.4	378.7	6.6	3.9	89.86
62	40	97	989	1.55	19.0	100	40	2	4	669.0	368.7	11.9	3.5	85.92
63	40	97	992	2.16	14.0	80	40	4	8	547.3	359.8	2.5	13.7	92.40
64	40	97	989	2.02	15.0	80	40	4	7	595.1	365.3	3.3	6.9	92.43
65	40	97	990	1.75	17.0	80	40	1	3	649.2	370.0	7.0	3.1	90.95
66	40	97	988	2.24	13.5	60	40	3	7	518.0	353.5	2.6	14.2	88.32
67	40	97	990	1.63	18.0	60	40	0	2	660.4	397.1	9.9	3.3	83.34
68	40	97	988	2.23	13.3	40	40	3	6	480.4	364.4	3.7	8.2	83.38
69	40	97	990	1.47	20.0	40	40	0	2	719.2	479.7	7.9	2.1	82.61
70	40	97	987	0.97	30.0	40	40	4	6	843.8	503.1	9.0	1.3	63.94
71	40	97	987	0.72	40.0	40	40	12	15	848.7	530.5	4.1	1.6	50.42
72	40	97	988	2.28	13.0	20	40	13	19	382.0	379.9	0.8	6.2	72.46
73	40	97	988	1.46	20.0	20	40	12	17	577.7	503.1	1.6	3.2	70.83
74	40	97	988	0.98	30.0	20	40	13	19	751.4	592.5	2.0	2.4	63.58

continued on next page...

Exp #	T_{in} (°C)	P_{man} (kPa)	N (rpm)	λ (-)	m_{fuel} ($\frac{mg}{cyc}$)	SOI (CAD)	PR (-)	$CA10_{main}$ (CAD)	CA50 (CAD)	IMEP (kPa)	$T_{exhaust}$ (°C)	MPRR (bar)	COV (%)	η_{comb} (%)
75	40	97	988	0.88	33.0	20	40	14	21	772.1	577.6	1.9	1.9	59.76
76	40	97	988	2.39	12.5	30	40	5	9	411.2	357.3	2.4	5.9	76.22
77	40	97	988	1.59	18.5	30	40	4	7	631.9	455.1	4.8	3.6	80.54
78	40	97	987	1.19	24.5	30	40	4	7	756.9	504.1	5.7	1.9	71.03
79	40	96	987	0.82	35.5	30	40	9	12	837.5	522.8	5.1	1.2	55.75
80	40	96	987	0.78	37.5	30	40	14	19	819.9	154.4	2.9	1.7	54.83
81	40	96	988	1.37	20.0	40	60	3	8	630.8	453.6	4.1	4.6	75.73
82	40	96	988	1.24	22.0	40	60	4	8	672.4	467.1	4.6	1.6	74.42
83	40	96	988	1.13	24.0	40	60	4	7	727.8	490.2	5.6	1.3	72.32
84	40	96	988	1.04	26.0	40	60	4	7	757.4	510.0	5.5	1.1	69.92
85	40	96	988	0.96	28.0	40	60	5	8	782.9	523.3	6.0	1.1	67.10
86	40	96	989	1.46	19.0	60	60	4	9	602.6	430.9	2.4	5.0	75.40
87	40	96	988	1.39	20.0	60	60	5	9	666.1	440.5	3.7	1.9	78.94
88	40	96	988	1.24	22.0	60	60	6	9	694.6	456.9	4.4	0.8	76.97
89	40	96	988	1.08	25.0	60	60	7	9	770.7	490.6	6.2	0.8	74.66
90	40	96	989	1.39	20.0	80	60	6	11	659.4	450.4	2.3	3.1	80.39
91	40	96	988	1.24	22.0	80	60	7	13	665.9	468.1	2.0	11.5	76.85
92	60	97	988	2.46	11.0	40	20	5	9	213.4	245.8	0.9	4.7	46.45
93	60	97	988	2.25	12.0	40	20	1	4	279.3	264.3	2.4	3.9	54.52
94	60	97	988	1.91	14.0	40	20	0	2	356.9	297.7	4.0	3.3	60.23
95	60	97	988	1.66	16.0	40	20	-1	1	446.7	347.3	5.2	2.3	66.99
96	60	97	988	1.40	19.0	40	20	-2	0	503.5	391.9	6.7	3.2	65.04
97	60	97	988	1.15	23.0	40	20	-2	-1	566.0	439.1	7.6	2.8	59.87
98	60	97	987	0.94	28.0	40	20	-2	0	628.3	472.0	8.6	2.5	55.10
99	60	97	988	2.35	11.7	60	20	-2	2	285.2	263.6	1.5	5.3	57.01
100	60	97	988	2.28	12.0	60	20	-3	1	311.3	269.4	1.9	4.7	60.95

continued on next page...

Exp #	T_{in} (°C)	P_{man} (kPa)	N (rpm)	λ (-)	m_{fuel} ($\frac{mg}{cyc}$)	SOI (CAD)	PR (-)	$CA10_{main}$ (CAD)	CA50 (CAD)	IMEP (kPa)	$T_{exhaust}$ (°C)	MPRR (bar)	COV (%)	η_{comb} (%)
101	60	97	988	2.02	13.5	60	20	-4	-2	373.6	297.3	3.5	4.2	64.92
102	60	97	988	1.58	17.0	60	20	-6	-5	478.0	338.3	8.7	2.8	73.18
103	60	97	988	2.14	12.8	80	20	-1	3	362.6	294.3	1.7	2.8	68.56
104	60	97	988	1.95	14.0	80	20	-3	0	393.5	306.4	3.1	6.0	68.15
105	60	97	987	1.80	15.0	80	20	-6	-4	443.1	322.8	7.3	3.7	74.03
106	60	97	988	1.67	16.0	80	20	-7	-5	444.3	324.3	8.8	3.7	86.39
107	60	97	988	2.00	13.5	30	40	1	3	347.7	316.7	3.1	3.7	61.28
108	60	97	988	1.72	15.5	30	40	1	4	385.8	338.6	3.3	3.4	59.97
109	60	97	988	1.56	17.0	30	40	0	3	426.1	371.6	4.0	3.4	61.03
110	60	97	988	1.32	20.0	30	40	1	3	532.0	426.9	5.2	4.1	64.48
111	60	97	988	1.14	23.0	30	40	0	3	596.6	473.1	5.3	2.6	62.60
112	60	100	987	0.94	28.0	30	40	2	5	676.6	498.2	5.4	1.8	59.58
113	60	97	988	2.00	13.5	40	40	-3	0	375.2	333.7	3.7	3.8	65.31
114	60	97	988	1.74	15.5	40	40	-2	0	428.0	347.6	4.6	3.6	65.43
115	60	97	988	1.53	17.5	40	40	-2	0	485.7	379.0	5.2	2.9	65.47
116	60	97	988	1.34	20.0	40	40	-3	0	587.4	419.4	6.5	2.8	69.66
117	60	97	987	0.95	28.0	40	40	0	2	709.8	481.8	8.7	1.6	59.84
118	60	97	988	2.11	13.0	60	40	-2	2	419.4	348.8	2.3	3.4	74.67
119	60	97	988	1.76	15.5	60	40	-3	0	488.0	351.2	4.2	1.9	74.37
120	60	97	988	1.55	17.5	60	40	-3	-1	531.8	369.5	5.9	1.9	71.55
121	60	97	987	1.32	20.3	60	40	-2	-1	613.0	399.4	9.9	2.5	71.28
122	60	97	988	2.08	13.3	80	40	3	9	431.8	337.6	1.2	4.3	78.49
123	60	97	988	1.83	15.0	80	40	1	5	480.5	349.2	2.3	2.1	77.15
124	60	97	988	1.70	16.0	80	40	-1	2	508.7	361.1	4.2	1.8	76.77
125	60	97	988	1.50	18.0	80	40	-2	0	541.7	375.0	8.2	2.0	75.38
126	60	97	987	1.33	20.0	80	40	-2	0	573.5	382.5	10.6	3.1	77.24

continued on next page...

Exp #	T_{in} (°C)	P_{man} (kPa)	N (rpm)	λ (-)	m_{fuel} ($\frac{mg}{cyc}$)	SOI (CAD)	PR (-)	$CA10_{main}$ (CAD)	CA50 (CAD)	IMEP (kPa)	$T_{exhaust}$ (°C)	MPRR (bar)	COV (%)	η_{comb} (%)
127	60	97	988	1.39	19.3	30	60	2	8	555.0	457.3	3.3	3.9	71.34
128	60	97	988	1.27	21.0	30	60	2	8	611.4	476.1	3.7	2.1	72.21
129	60	97	987	1.10	24.0	30	60	3	8	687.0	507.3	4.5	1.2	69.71
130	60	97	988	0.91	29.0	30	60	5	9	758.1	534.3	4.9	1.1	63.60
131	60	97	988	1.40	19.0	40	60	-2	2	595.5	451.2	4.6	4.2	75.32
132	60	97	988	1.26	21.0	40	60	-2	2	651.8	468.0	5.7	1.2	73.95
133	60	97	988	1.10	24.0	40	60	-1	2	703.4	497.1	6.3	1.1	69.89
134	60	97	987	0.90	29.0	40	60	0	3	769.3	522.2	7.5	1.0	62.50
135	60	97	988	1.40	19.0	60	60	-1	3	590.5	432.7	4.0	4.5	74.08
136	60	97	989	1.27	21.0	60	60	0	3	661.8	449.9	7.0	1.4	74.99
137	60	97	1078	0.96	25.0	60	60	1	3	746.8	487.7	9.6	1.5	71.28
138	60	97	1118	1.25	19.3	80	60	3	8	609.2	434.2	2.9	5.0	74.96
139	60	97	1103	1.21	20.0	80	60	3	7	641.4	440.3	3.8	2.4	75.35
140	60	97	1116	1.11	21.5	80	60	5	8	672.7	455.1	4.3	1.2	75.62
141	60	97	1101	1.06	23.0	80	60	7	11	709.0	479.2	4.0	1.5	76.14
142	80	96	927	2.54	10.0	20	20	1	3	217.3	256.2	2.2	3.8	51.34
143	80	96	928	2.29	11.0	20	20	2	4	222.4	256.0	2.4	2.6	47.95
144	80	96	935	1.67	14.7	20	20	3	5	351.4	345.4	3.3	3.1	57.27
145	80	96	939	1.25	19.5	20	20	4	6	443.5	423.8	3.7	4.0	55.11
146	80	96	947	0.89	27.0	20	20	6	9	544.8	488.9	3.5	3.7	49.22
147	80	96	931	2.52	10.0	30	20	-6	-4	218.5	244.8	3.6	3.3	51.80
148	80	96	926	2.29	11.0	30	20	-6	-4	226.6	245.4	3.3	2.3	49.08
149	80	96	936	2.00	12.3	30	20	-5	-3	275.4	271.3	4.0	4.1	53.48
150	80	100	938	1.67	14.6	30	20	-5	-3	354.0	316.1	5.5	4.8	59.84
151	80	96	943	1.23	19.5	30	20	-5	-3	473.7	395.0	6.1	3.5	59.96
152	80	96	951	0.88	27.0	30	20	-3	-1	586.4	448.7	7.0	2.6	52.09

continued on next page...

Exp #	T_{in} (°C)	P_{man} (kPa)	N (rpm)	λ (-)	m_{fuel} ($\frac{mg}{cyc}$)	SOI (CAD)	PR (-)	$CA10_{main}$ (CAD)	CA50 (CAD)	IMEP (kPa)	$T_{exhaust}$ (°C)	MPRR (bar)	COV (%)	η_{comb} (%)
153	80	96	933	2.50	10.0	40	20	-8	-7	211.5	263.0	3.8	4.3	50.25
154	80	96	931	2.27	11.0	40	20	-8	-6	223.0	246.4	4.0	2.8	47.78
155	80	96	939	1.99	12.4	40	20	-8	-6	288.1	272.4	5.2	5.1	55.14
156	80	96	940	1.67	14.6	40	20	-9	-7	360.8	309.4	6.0	4.9	60.45
157	80	96	948	1.23	19.5	40	20	-8	-7	486.1	381.3	7.7	2.9	61.64
158	80	96	948	0.86	27.5	40	20	-7	-6	588.7	461.0	9.9	2.8	53.87
159	80	96	947	2.37	10.5	60	20	-7	-3	211.9	239.8	1.4	5.4	48.31
160	80	96	939	2.11	11.8	60	20	-8	-4	261.9	254.6	2.1	4.3	53.21
161	80	96	940	1.96	12.6	60	20	-8	-6	326.2	281.4	3.3	5.3	61.65
162	80	96	944	1.68	14.6	60	20	-9	-8	373.8	305.3	6.1	4.3	62.91
163	80	96	943	1.27	19.0	60	20	-9	-8	461.5	339.4	11.0	3.9	69.30
164	80	96	945	1.91	13.0	80	20	-5	-2	351.4	288.0	2.6	2.4	64.54
165	80	96	941	1.77	14.0	80	20	-6	-4	368.5	298.5	3.7	4.5	64.95
166	80	96	941	1.64	15.0	80	20	-8	-6	404.4	313.0	7.1	3.4	76.44
167	80	96	940	1.44	17.0	80	20	-8	-7	427.8	320.3	10.3	3.9	81.62
168	80	96	938	1.90	13.0	20	40	5	8	301.0	322.4	2.1	4.1	55.77
169	80	96	939	1.64	15.0	20	40	5	9	334.6	330.5	2.2	3.6	54.36
170	80	96	949	1.26	19.0	20	40	6	9	433.4	397.4	2.7	4.0	55.94
171	80	96	957	0.85	28.0	20	40	8	12	631.8	491.2	3.2	2.5	56.65
172	80	96	940	1.91	13.0	30	40	-3	0	329.2	308.1	3.5	4.2	59.35
173	80	96	949	1.60	15.2	30	40	-3	-1	377.6	336.1	4.2	2.9	59.53
174	80	96	955	1.24	19.3	30	40	-3	0	521.5	400.4	5.9	3.3	64.48
175	80	96	958	0.84	28.0	30	40	-1	2	668.4	457.7	6.5	1.8	56.52
176	80	96	951	1.83	13.3	40	40	-7	-4	372.9	329.5	4.3	3.3	66.35
177	80	96	951	1.60	15.2	40	40	-7	-4	422.7	340.9	5.1	3.0	67.03
178	80	96	955	1.24	19.3	40	40	-7	-5	539.7	395.5	7.6	2.5	68.25

continued on next page...

Exp #	T_{in} (°C)	P_{man} (kPa)	N (rpm)	λ (-)	m_{fuel} ($\frac{mg}{cyc}$)	SOI (CAD)	PR (-)	$CA10_{main}$ (CAD)	CA50 (CAD)	IMEP (kPa)	$T_{exhaust}$ (°C)	MPRR (bar)	COV (%)	η_{comb} (%)
179	80	96	958	0.84	28.0	40	40	-5	-3	672.9	468.1	9.8	1.7	60.51
180	80	96	966	1.82	13.3	60	40	-7	-4	396.9	331.8	3.3	4.4	70.99
181	80	96	953	1.58	15.3	60	40	-7	-5	442.6	343.1	4.8	1.6	70.75
182	80	99	955	1.23	19.3	60	40	-6	-5	531.9	371.9	9.1	2.8	79.49
183	80	96	979	1.79	13.3	80	40	-5	-1	397.5	333.1	3.0	5.0	70.70
184	80	96	976	1.70	14.0	80	40	-5	-2	418.7	334.3	3.7	1.7	71.89
185	80	96	969	1.50	15.8	80	40	-6	-4	451.6	350.4	6.3	1.8	69.76
186	80	96	956	1.28	18.5	80	40	-6	-5	491.8	362.5	9.0	2.9	81.64
187	80	100	978	1.18	19.5	30	60	-4	3	555.7	434.0	3.9	5.0	70.42
188	80	96	972	1.13	20.5	30	60	-4	2	596.9	451.4	4.8	1.3	70.11
189	80	96	970	0.94	24.5	30	60	-3	1	661.7	485.6	5.9	1.1	63.85
190	80	96	977	0.80	28.5	30	60	-1	2	708.2	497.4	6.4	1.4	58.89
191	80	96	975	1.19	19.5	40	60	-6	-2	572.5	437.4	4.9	3.3	70.26
192	80	96	976	1.13	20.5	40	60	-5	-2	609.0	446.2	6.3	1.2	70.98
193	80	96	979	0.94	24.5	40	60	-4	-2	674.6	477.1	6.9	1.3	65.97
194	80	96	985	0.81	28.5	40	60	-3	0	728.4	497.8	7.6	1.3	60.39
195	80	96	992	1.20	19.5	60	60	-2	2	567.3	407.6	3.7	5.6	69.09
196	80	96	994	1.13	20.5	60	60	-1	1	612.7	425.1	5.7	3.4	70.64
197	80	96	994	1.03	22.5	60	60	0	2	669.3	447.8	8.5	1.1	70.78
198	80	96	992	0.92	25.5	60	60	0	1	730.7	478.3	10.2	1.5	67.27
199	80	96	1015	1.18	19.5	80	60	0	4	561.4	418.2	3.1	8.8	69.65
200	80	96	1009	1.11	20.5	80	60	0	4	605.9	421.0	4.4	3.3	70.44
201	80	96	1004	1.02	22.5	80	60	2	5	652.4	438.3	5.9	2.3	69.92
202	80	96	989	0.91	25.5	80	60	2	4	710.2	459.0	10.6	2.2	67.53
203	80	96	965	1.16	20.4	20	60	6	13	520.2	478.3	2.7	3.8	65.25
204	80	96	967	1.09	21.5	20	60	6	14	557.0	500.3	2.8	3.2	66.08

continued on next page...

Exp #	T_{in} (°C)	P_{man} (kPa)	N (rpm)	λ (-)	m_{fuel} ($\frac{mg}{cyc}$)	SOI (CAD)	PR (-)	$CA10_{main}$ (CAD)	CA50 (CAD)	IMEP (kPa)	$T_{exhaust}$ (°C)	MPRR (bar)	COV (%)	η_{comb} (%)
205	80	96	969	0.98	24.0	20	60	7	14	626.1	526.0	3.1	1.6	66.03
206	80	96	975	0.83	28.0	20	60	9	15	690.2	547.8	2.8	1.2	61.82

A.3 FPGA Experimental Data

A.3.1 Intake Temperature - 40°C

Table A.3
Operating Conditions FPGA Experimental Data-40°C

Exp #	SOC (CAD)	CA50 (CAD)	EOC (CAD)	BD (CAD)	PR (-)	SOI (CAD bTDC)	m_{fuel} ($\frac{mg}{cyc}$)	m_{iso} ($\frac{mg}{cyc}$)	m_{nhep} ($\frac{mg}{cyc}$)	IMEP (kPa)	MAP (kPa)	λ (-)	N (rpm)
1	-5	9	49	54	20	30	21	4.23	16.77	604.13	96.54	1.36	986.48
2	-7	5	49	56	20	40	21	4.23	16.77	666.34	96.61	1.35	985.88
3	-9	1	17	26	20	50	21	4.23	16.77	701.46	96.15	1.35	985.77
4	-5	8	53	58	20	30	19	3.83	15.17	566.69	95.79	1.51	986.61
5	-7	4	39	46	20	40	19	3.83	15.17	623.93	96.11	1.49	987.69
6	-9	1	17	26	20	50	19	3.83	15.17	669.17	96.39	1.51	988.45
7	-6	7	41	47	20	30	15	3.02	11.98	455.45	96.60	1.97	986.24
8	-8	2	33	41	20	40	15	3.02	11.98	529.83	97.07	1.89	987.01
9	-10	1	20	30	20	50	15	3.02	11.98	557.16	96.60	1.93	986.76
10	-5	12	53	58	40	30	21	8.46	12.54	646.75	96.17	1.32	984.46
11	-6	8	45	51	40	40	21	8.46	12.54	721.82	96.29	1.30	986.30
12	-8	4	22	30	40	50	21	8.46	12.54	753.61	96.21	1.31	986.08
13	-5	9	51	56	40	30	19	7.65	11.35	587.20	96.56	1.46	987.86
14	-7	5	38	45	40	40	19	7.65	11.35	671.93	96.81	1.41	987.01
15	-9	3	19	28	40	50	19	7.65	11.35	697.89	96.74	1.43	986.53
16	-5	10	44	49	40	30	16	6.44	9.56	409.43	95.99	1.91	989.56
17	-6	7	43	49	40	40	16	6.44	9.56	465.85	95.81	1.85	987.54
18	-9	6	38	47	40	50	16	6.44	9.56	518.62	96.62	1.88	987.44

Appendix B

Program and Data Files Summary

B.1 Chapter 1

Table B.1
Figure Files

File name	File Description
LTC_comparison_new.png	Figure1.1
LTC_evolution.png	Figure1.2
RCCIresearchStudies.pdf	Figure1.3
ThesisOrganization_RCCI.pdf	Figure1.4

Table B.2
Visio Files

File name	File Reference
RCCI_research_studies.vsdx	Figure1.3
ThesisOrganization_RCCI.vsdx	Figure1.4

B.2 Chapter 2

Table B.3
Figure Files

File name	File Reference
ExperimentalTestSetup.pdf	Figure2.1
Exp_RCCI_2.jpg	Figure2.2
HRR_order_comp.eps	Figure2.3
Frequency_spectrum.eps	Figure2.4
Pressure_trace.eps	Figure2.5
HRR_1stage_2stage.eps	Figure2.6
HRR_explained.eps	Figure2.7
FMEP_model.eps	Figure2.8
Thermocouple_before_TF.eps	Figure2.9
Thermocouple_after_TF.eps	Figure2.10

Table B.4
Matlab fig files

File name	File Reference
HRR_order_comp.fig	Figure2.3
Frequency_spectrum.fig	Figure2.4
Pressure_trace.fig	Figure2.5
HRR_1stage_2stage.fig	Figure2.6
FMEP_model.fig	Figure2.8
Thermocouple_before_TF.fig	Figure2.9
Thermocouple_after_TF.fig	Figure2.10

Table B.5
Visio File

File name	File Reference
ExperimentalTestSetup_RCCI.vsdx	Figure2.1

Table B.6
Matlab script and simulink model files

File name	File Description
HRR_plots.m	Matlab code for plots in Figures 2.3,2.4,2.5,2.6 and 2.7
FMEP_model.m	Matlab code for FMEP Flynn-Chenn Model parametrization(Figure2.8) This uses excel file **Test_copy.xlsx** to extract experimental data.
Thermocouple_Lagmodel.slx	Simulink file for thermocouple delay model.Need to load **Thermocouple_simulink_workspace.mat** file before running.
Thermocouple_plots.m	Matlab code for plots in Figure2.9 and 2.10

B.3 Chapter 3

Table B.7
Figure Files

File name	File Reference
RCCI_NA_40C_Operatingmap.eps	Figure3.1a
RCCI_NA_60C_Operatingmap.eps	Figure3.1b
RCCI_NA_80C_Operatingmap.eps	Figure3.1c
ISFC_PR20.eps,ISFC_PR40.eps,ISFC_PR60.eps	Figure3.2a,3.2b,3.2c
BSFC_PR20.eps,BSFC_PR40.eps,BSFC_PR60.eps	Figure3.3a,3.3b,3.3c
ITE_PR20.eps,ITE_PR40.eps,ITE_PR60.eps	Figure3.4a,3.4b,3.4c
BTE_PR20.eps,BTE_PR40.eps,BTE_PR60.eps	Figure3.5a,3.5b,3.5c
T_exh_PR20.eps,T_exh_PR40.eps,T_exh_PR60.eps	Figure3.6a,3.6b,3.6c
RCCI_NA_ISFC.eps	Figure3.7a
RCCI_NA_BSFC.eps	Figure3.8a
RCCI_NA_ITE.eps	Figure3.7b
RCCI_NA_BTE.eps	Figre3.8b
RCCI_NA_T_exh.eps	Figure3.9
SOI_PR20T40_HRR.eps	Figure3.10
SOI_PR20T40_CA50.eps	Figure3.11
SOI_PR20T40_IMEP.eps	Figure3.12
PR_SOI60_T40_HRR.eps	Figure3.13
PR_SOI60_T40_CA50.eps	Figure3.14
PR_SOI60_T40_IMEP.eps	Figure3.15
SOI40_PR40_HRR.eps	Figure3.16
SOI40_PR40_CA50.eps	Figure3.17
Tin_Pres_Vol.eps	Figure3.18
SOI40_PR40_IMEP.eps	Figure3.19
Diff_T40.eps,Diff_T60.eps,Diff_T80.eps	Figure3.20a,3.20b,3.20a
CA50_T40.eps,CA50_T60.eps,CA50_T80.eps	Figure3.21a,3.21b,3.21c

Table B.8
Matlab fig file

File name	File Reference
Tin_Pres_Vol.fig	Figure3.18

Table B.9
Origin Pro Project Files

File name	File Description
RCCI_NA_Operating Maps.opj	Project file which consists of raw data points and plots for NA Operating Regions at different Temperatures(Figure3.1a,3.1b3.1c).
RCCI_NA_Performance Maps.opj	This project file contains separate folders **Brake Maps** & **Indicated Maps** which consists plots for all Performance Maps explained in Section3.2.2
RCCI NA Optimized Maps.opj	This project file consists of separate folders for **Optimized Brake** & **Optimized Indicated** maps at different speeds and loads(Figure3.7a,3.8a,3.7b,3.8b,3.9)
RCCI_Parametricstudy.opj	This project file contains different subfolders for Parametric study of SOI, PR and T_{intake} explained in Section3.3.
RCCI_dualstage and CA50_maps.opj	This file consists of plots for Dual stage heat release(Figure3.20a,3.20b,3.20a) and combustion phasing maps(Figure3.21a,3.21b,3.21c) explained in Section3.3.4 and Section3.3.5

Table B.10
Exp Data files

Folder name	Sub-folders and Description
RCCI_NA_Exp_Data	**EXP_18.rar & EXP_19.rar** - Contains ACAP,dSPACE,LabVIEW data files for all Naturally Aspirated tests alongwith their respective post processing code in each rar file
RCCI_Parametric_Exp_Data	**EXP_15.rar, EXP_17.rar, EXP_26.rar & EXP_27.rar** - Contains all ACAP,dSPACE,LabVIEW data files for Model Parametrization with their respective post processing code in each rar file.

Table B.11
Matlab Workspace Files

File name	File Description
RCCI_NaturallyAspirateddata.mat	Workspace file containing all the experimental data points for RCCI Naturally Aspirated Tests
RCCI_Parametricdata.mat	Workspace file containing all the experimental datapoints for RCCI Parametric Study
Effect of SOI.mat	Matlab workspace file containing datapoints for Parametric study of SOI explained in Section3.3.1
Effect of PR.mat	Matlab workspace file containing datapoints for Parametric study of PR explained in Section.3.3.2
Effect of Tin.mat	Matlab workspace file containing datapoints for Parametric study of Intake temperature explained in Section3.3.3.

B.4 Chapter 4

Table B.12
Figure Files

File name	File Reference
Autoignitionreview.pdf	Figure.4.1
ModelschematicMVM.pdf	Figure.4.2
P_ivc_est.eps	Figure4.3
P_ivc_val.eps	Figure4.4
MKIM_SOC_est.eps	Figure4.5
MKIM_SOC_val.eps	Figure4.6
MKIM_CA50_est.eps	Figure4.7
MKIM_CA50_val.eps	Figure4.8
Individual_parameter_effect.eps	Figure4.9

Table B.13
Visio Files

File name	File Description
Autoignition lit review_MVM.vsdx	Visio file for Figure4.1
Model schematic_MVM.vsdx	Visio file for Figure.4.2

Table B.14
Matlab Fig Files

File name	File Reference
P_ivc_est.fig	Figure4.3
P_ivc_val.fig	Figure4.4
MKIM_SOC_est.fig	Figure4.5
MKIM_SOC_val.fig	Figure4.6
MKIM_CA50_est.fig	Figure4.7
MKIM_CA50_val.fig	Figure4.8
Individual_parameter_effect.fig	Figure4.9

Table B.15
Matlab Script Files

File path name	File Description
Pivc Correlation\ P_IVC_estimation.m	M-file for estimation and validation of P_{ivc} correlation shown in Equation.4.5. This file uses experimental data from Sheet1 of **Pivc_corr.xlsx** file.
Model_pred_val.m	M-file for estimation and validation of MKIM and CA50 models to calculate SOC and CA50 for steady state data. This file uses experimental data from **RCCI_paramet.xlsx** file. Estimation data from **RCCI_est** Sheet and Validation data from **RCCI_val** Sheet.
Individual_parameter_effect.m	M-file for plotting the trends of the effect of individual parameter on SOC and CA50 which was discussed in Section.4.4.

B.5 Chapter 5

Table B.16
Figure Files

File name	File Reference
Exhaust_gas_Estimation.eps	Figure5.1
Exhaust_gas_Validation.eps	Figure5.2
DynamicModel.pdf	Figure5.3
Transient_SOI_ACAP.eps	Figure5.5
Transient_PR_ACAP.eps	Figure5.4

Table B.17
Visio File

File name	File Reference
DynamicModelSchematic.vsdx	Figure5.3

Table B.18
Matlab Fig Files

File name	File Reference
Exhaust_gas_Estimation.fig	Figure5.1
Exhaust_gas_Validation.fig	Figure5.2
Transient_SOI_ACAP.fig	Figure5.5
Transient_PR_ACAP.fig	Figure5.4

Table B.19
Matlab script and simulink model Files

File path name	File Description
Exhaust_gas_estimation.m	M-file for estimation and validation of Exhaust gas residual temperature shown in Section.5.1.5. This file uses **RCCI_est.xlsx** for estimation and **RCCI_val.xlsx** for validation.
Engine_data_analysis_transient_ACAP.m	This file is used for post-processing the transient data in which Pressure trace is logged from ACAP.
RCCI_dyn.m	This file represents the whole dynamic model of RCCI engine from IVC to EVO explained in Chapter5
RCCI_dyn_model.slx	Simulink file used for running offline transient tests using the above dynamic model. Input should be either SOI-step from **RCCI_TR_tests_SOI.mat** file or PR-step **RCCI_TR_tests_PR.mat** file.
plots.m	Used for plotting transient experimental and model results which are shown in Figure5.5 and 5.4

B.6 Chapter 6

Table B.20
Figure Files

File name	File Reference
FPGA_MKIM_T40.eps	Figure6.1
FPGA_CA50_T40.eps	Figure6.2
FPGA_Transient_PR.eps	Figure6.3
FPGA_Transient_SOI.eps	Figure6.4
ControlModelSchematic.pdf	Figure6.5
PI_SOI_Cntrl_Model.eps	Figure6.6
PI_SOI_Cntrl_Exp.eps	Figure6.7
PI_PR_Cntrl_Model.eps	Figure6.8
PI_PR_Cntrl_Exp.eps	Figure6.9

Table B.21
Visio File

File name	File Reference
Control Model Schematic.vsdx	Visio file for Figure6.5

Table B.22
Matlab Fig Files

File name	File Reference
FPGA_MKIM_T40.fig	Figure6.1
FPGA_CA50_T40.fig	Figure6.2
FPGA_Transient_PR.fig	Figure6.3
FPGA_Transient_SOI.fig	Figure6.4
PI_SOI_Cntrl_Model.fig	Figure6.6
PI_SOI_Cntrl_Exp.fig	Figure6.7
PI_PR_Cntrl_Model.fig	Figure6.8
PI_PR_Cntrl_Exp.fig	Figure6.9

Table B.23
Matlab script and simulink model Files

File path name	File Description
Engine_data_analysis_steady_FPGA.m	Steady State processing code for the data logged from FPGA. Uses dSPACE files from folders **dSPACE_FPGA_T40** and **dSPACE_FPGA_T60**
RCCI_dyn.m	Dynamic transient model code with respect to FPGA data.
RCCI_dyn_FPGA.slx	Simulink file for running offline transient tests using above dynamic model. This file uses **FPGA_TR_PR.mat** for step change in PR and **FPGA_TR_SOI.mat** for step change in SOI.
RCCI_dyn_control_PR.slx	Simulink file for running PI control of CA50 by varying PR
RCCI_dyn_control_SOI.slx	Simulinnk file for running PI control of CA50 by varying SOI

Appendix C

MS Publication

C.1 Conference Paper

1. A. Solouk, M. Shakiba, K. Kannan, H. Solmaz, M. Bidarvatan, **N. T. Kondipati**, P. Dice, M. Shahbakhti,"Fuel Economy Benefits of Integrating a Multi-Mode Low Temperature Combustion (LTC) Engine in a Series Extended Range Electric Powertrain", *SAE 2016 International Powertrains, Fuels & Lubricants Conference*, 15 pages, 16FFL-0277, October 24-26, 2016, Baltimore, Maryland, USA. (Approved for Publication in June 2016)

Appendix D

Letter of Permission

D.1 Permission for Figure1.1 and Figure1.2

Below shown is the permission from corresponding publisher to re-use the Figure1.1 and Figure1.2 which were originally used in [12]

Figure D.1: Letter of Permission